Embedded Wireless Intracranial Pressure Monitoring Implant at Microwave Frequencies

A Thesis

Submitted to the Faculty

of

Drexel University

by

Usmah Kawoos

in partial fulfillment of the

requirements for the degree

of

Doctor of Philosophy

June 2009

Dedications

To my mother, who believes in me and has supported me all the way,

and

in loving memory of my father and grandfather (Aba), who taught me to dream.

Acknowledgements

Words will do no justice in expressing my gratitude towards my advisor and mentor, Dr. Arye Rosen. He has constantly widened the ambits of my education that I have received under his tutelage. Dr. Rosen always maintains an aura of optimism around him which has been my constant source of encouragement during my stay at Drexel. The lessons that I have learnt here will stay with me for my life. I cannot thank him enough for his mentorship.

I am indebted to Dr. Mohammad Tofighi, whose expertise and enthusiasm were instrumental to the success of my project and Dr. Frank Kralick, a neurosurgeon, who created magic while implanting the ICP implants in animals, both of who have been always available for discussions, have given me priceless feedback, and have encouraged me to diversify my skills. Their invaluable suggestions have refined my work and at the same time steered it in an excellent direction. I am also grateful to Dr. Peter Herczfeld who not only introduced me to Dr. Rosen, but has also been very supportive of my work in many ways. Thank you, Dr. Herczfeld for your countless inputs during many stages, especially the final compilation, of this research work. I am thankful to Dr. Afshin Daryoush for sharing his laboratory with our project group. Dr. Daryoush has boosted my confidence at many occasions that include technical talks and exams. I am fortunate to have known Late. Dr. Samuel Neff who taught me to tackle a problem by breaking it into small parts.

I thank the members of my candidacy and final examination committees, which include Dr. Kambiz Pourrezaei, Dr. Chang Chang, Dr. Ryszard Lec, Dr. Hazem Maragah, Dr. Rahamim Seliktar, and Dr. Sam Goldwasser for their advice and support. I am thankful to Dr. Wei Sun who was kind to provide his feedback, on a short notice. I would like to express my gratitude to Dr. Banu Onaral for her endless encouragement and support. I would also like to thank Dr.

David Yoo and Dr. Tom Neal for believing in our research and constantly promoting its importance. The constructive criticism that I received from Dr. Zafar Khan cannot go unrecognized.

I appreciate the support that I received from Dr. Richard Huneke, Janet, Andrea, and Kim, that made it easy for me to take up new challenges. Thank you, Kim for being a wonderful teacher and a friend. I am also thankful to Carlton, Craig, and Sean for helping me with the animal studies. During the course of my research work, the professional expertise and support of the following have been instrumental in attaining the desired outcomes: Dr. Moses Noh, Temi, Dr. Peter Oelkers, Dr. Allen Katz, Mike Umbro, Dr. Timothy Zhou, Andreaa Dimofti, Dr. Anthony Lowman, John, and Walter Janton.

I was fortunate to have wonderful colleagues and labmates: Giri, Ruchi, Xu, Yifei, Liming, David (now Dr. Yoo), Ryan, Nikhil, Gabor, Milad, David, Nick, Ding, Rupa, Khushali, who made learning a pleasant experience. I am especially thankful to Gabor for helping me prepare for my most crucial exam- Ph.D defense. I acknowledge the inputs on my work that I received from our Star students: Kathreen, Cathreen, and John. I value the friendliness of our Biomed staff- Lisa, Danielle, Aylin, Natalia, Susan, and Frank. Life without friends would not have been easy. I am glad to have friends like Arun, Nihad, Huda, Ali, Ajarat, Priyanka, Rabi, Ruchi, Piyush, Surbhi, Manju, and Raj who have stood by me through the thick and thin. I cannot forget how Renee and Bernie have always been there for me, Thank you!

Most importantly, I express my perpetual gratitude to my mother Firdos, my brother Irfan, my sister-in-law Ibtisam, and the rest of the family for having faith in me. I would not have been here if it was not for their constant support and unconditional love. I am thankful to Anwar who has always inspired me and supported me in pursuing my dreams.

Table of Contents

List of Tables

List of Figures

Abstract

Embedded Wireless Intracranial Pressure Monitoring Implant at Microwave Frequencies
Usmah Kawoos
Dr. Arye Rosen, Ph.D

Intracranial Pressure (ICP) monitoring is a significant tool that aids in the management of neurological disorders like hydrocephalus, head trauma, tumors, colloid cysts, cerebral hematomas etc. ICP is the pressure exerted on the rigid, bony skull by its constituents that are brain, cerebrospinal fluid, and the cerebral blood. Increased ICP can lead to brain damage, disability, and death. Various modalities have been developed for the monitoring of ICP in hospitals and in ambulatory conditions. Currently, only catheter based systems have made it to the clinical practice. The catheter based systems can only be used in a hospital setting, and have a limited useful life due to drift and risk of infection.

The motivation for this research was the intent to develop a completely implantable, wireless ICP monitoring implant that can provide long-term monitoring of the pressure in ambulatory conditions. The uniqueness of this work is accentuated by the ability of the implant to transmit at 2.4 GHz. These implants have undergone a battery of tests in the *in-vitro* and *in-vivo* (canine) studies during which the feasibility of microwave transmission through scalp was established. Long-term animal studies were conducted to determine the integrity, biocompatibility, and the performance of the implant in a biological environment. Animal studies for long durations with epidural implants showed a thickening of the dura mater under sensor area. Therefore, the effect of dural thickness on the sensitivity of pressure sensing mechanism was simulated. The histo-pathological examination of the tissue specimens that were excised at the termination of an animal study showed the presence of lymphocytes, and

fibrous tissue which is a normal immunological reaction to a foreign body. These tests did not reveal any toxicity due to the presence of the implant. In the animal studies that were conducted with sub-dural implants, a correlation coefficient of 0.94 and better was determined between the gold standard for ICP monitoring and our implant. In our latest animal study a sub-dural implant has been successfully tested in an animal for a duration of one month, thus proving the reliability of the implant packaging and its performance for a long-duration ICP monitoring application. This study also underscores the applicability of our ICP implant for monitoring of traumatic brain injuries, among other applications.

1. Motivation and Introduction

For more than two centuries the concepts of physics have been applied to the intracranial contents. It was in 1783, Alexander Monro - a Scottish anatomist published his findings in a monogram [1] that form the basis of many hypotheses and principles described thereafter. The key points made by Monro were:

i) Skull is a non-expandable rigid case,

ii) The brain matter is nearly incompressible,

iii) The volume of blood in a cranial cavity is essentially constant, and

iv) There has to be a continuous outflow of venous blood from the cranial cavity to make room for the inflow of arterial blood.

Thus, for the first time it appeared in the literature that the volume of blood circulating in the cranium remains constant at all times. Monro's doctrine was later confirmed by Kelly and Abercrombie [2] and is popularly known as "Monro-Kelly Hypothesis" or "Monro-Abercrombie Doctrine''. However, all of them ignored the presence of cerebrospinal fluid (CSF) and assumed that the volume of the cerebral blood swung between the venous and the arterial side while the total volume remained constant. It was Francois Magendie, a French Physiologist of the 19th century who recognized the significance of CSF and its contribution towards the total intracranial volume [3]. He demonstrated a communication between the fourth ventricle and the sub-arachnoid space (SAS) through a foramen that became to be known as "Foramen of Magendie".

Considering that the skull is a rigid vault, with a slightly compressible brain matter and an almost fixed volume of blood at any given time, any increase in the volume of CSF is a significant factor leading to an elevation of the intracranial pressure (ICP). CSF is constantly being produced and absorbed in the cranial system, and it also maintains a circulatory system through the ventricles of the brain, SAS, and the spinal canal [4]. An abnormality in the volume of CSF can arise due to- i) an imbalance between its production and absorption or ii) an

obstruction in its circulatory pathway. The consequences of an elevated ICP can range from mild (headache, nausea, vomiting) to severe (brain damage, disability, death) [5].

A direct motivation to the development of a completely implantable ICP monitoring device came from Late. Dr. Samuel Neff, a pediatric neurosurgeon, who experienced a lack of a long-term ICP monitoring technique for hydrocephalic children in his clinical practice. He collaborated with a team at Drexel University, led by Dr. Arye Rosen and Dr. Mohammad Reza Togighi that took up an initiative to work towards the development of an implantable, wireless ICP device.

In the present clinical practices, ICP is monitored by a catheter system in hospital settings. A most typical example of such a system is Camino catheter manufactured by Integra Life Sciences Inc. A catheter system is a direct and invasive method for the monitoring of ICP that presents the risks of infection, patient discomfort, dislodgement of the catheter, and tissue damage. It also restricts patient mobility and keeps him/her attached to external monitors. On the contrary, an implantable, wireless ICP monitoring device would provide the means of taking non-invasive ICP measurements once the device is implanted by a surgical procedure. The patients in need of ICP monitoring undergo a surgical procedure for the treatment of any underlying cause of abnormal ICP. The ICP device can be implanted as a part of the surgery, thus demanding no exclusive preparation for its implantation. In addition to the ease of ICP monitoring by non-invasive method, this implantation procedure also offers monitoring of ICP in ambulatory conditions along with providing patient comfort.

This thesis primarily focuses on:

i) The development of an ICP implant at microwave frequencies,
ii) Evaluating the biocompatibility of the implant,
iii) Devising various protocols for experimental testing of the implant in laboratory settings,
iv) Conducting proof-of-concept and long-term studies in animal models, and

v) Performing finite element analysis of the interaction of dura mater with pressure sensing membrane.

As we progressed through this research initiative, various generations of the ICP implant were built. The information gathered from each generation was utilized in improving the next one. The details of each generation along with the procedures undertaken to ensure the biocompatibility of the devices are detailed in Chapter 4 of this thesis. The methods and materials, protocols, and results related to *in-vitro* and *in-vivo* experimentation are presented in Chapter 5 and Chapter 6, respectively. A finite element analysis of the interaction between dura mater, scar tissue and the pressure sensing membrane is documented in Chapter 7. Throughout the various developmental stages of this work, it has received a tremendous inflow of constructive criticism and inputs from within the team as well as various collaborators and reviewers. This has led to the opening of a realm of diverse applications of ICP monitoring as diagnostic, therapeutic, and research tool. A brief note of such applications as well as the contribution of this thesis is presented in Chapter 8. Chapter 8 also broaches the envisioned future work that can be undertaken with the latest generation of the implant. For the sake of completeness, a brief account of neuroanatomy that is directly relevant to the CSF circulation, and the pathophysiology of ICP elevation has been included in the beginning of this thesis as a separate chapter.

2. Neuroanatomy in Relation to Intracranial Pressure

An understanding of the central nervous system (CNS) relevant to various aspects responsible for the build-up and maintenance of ICP is pivotal to the development of an ICP monitoring modality. This chapter presents a description of the ventricular system, cerebrospinal fluid, meninges of the brain, and the pathophysiology of intracranial hypertension (ICH).

2.1 Ventricular system

The CNS contains a series of interconnecting chambers and channels that develop from the lumen of the embryonic neural tube. The ventricular system has four ventricles: two lateral ventricles, third, and fourth ventricle [6]. The lateral ventricles are relatively large, somewhat 'C-shaped' and are located within the cerebral hemisphere, one on each side. A lateral ventricle has four distinct regions, i.e., anterior horn towards the frontal end, body, posterior horn towards the occipital end, and inferior horn towards the temporal end. The lateral ventricles communicate with the third ventricle via interventricular foramen or foramen of Monro. The third ventricle is a narrow slit-like cavity in the mid brain whose lateral walls are formed by thalamus and hypothalamus on either side. The third and fourth ventricles communicate via cerebral aqueduct. The fourth ventricle is a wide and shallow, rhomboid-shaped depression which is located in the hind brain on the dorsal surface of the brain stem beneath the cerebellum. On each side of the fourth ventricle a lateral recess extends towards the lateral side of the brain stem and is in continuity with the SAS through a lateral aperture. Figure 2.1, shows a resin cast model of the ventricular system where as ventricles with respect to the surface of brain are shown in Figure 2.2. A number of foramena (holes) interconnect the ventricles and connect the ventricles to the SAS. Table 1.1 lists the foramena along with their alternate names and the connections that they make.

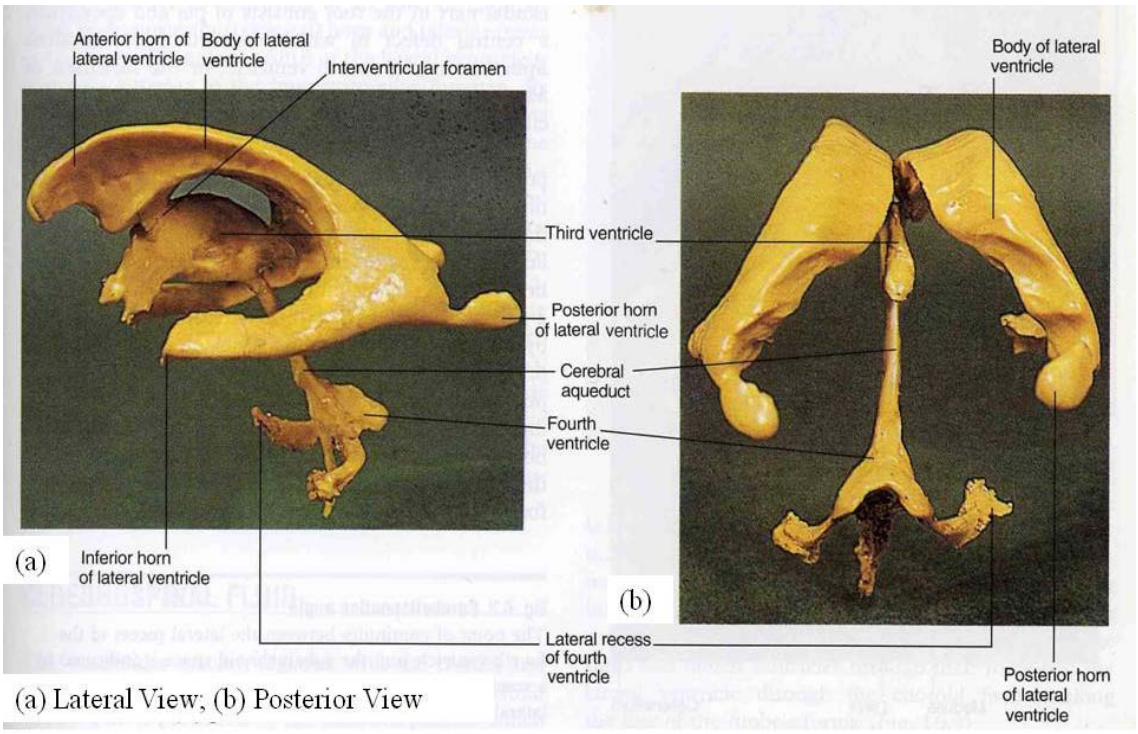

Figure 2.1. Resin cast of the ventricular system [6].

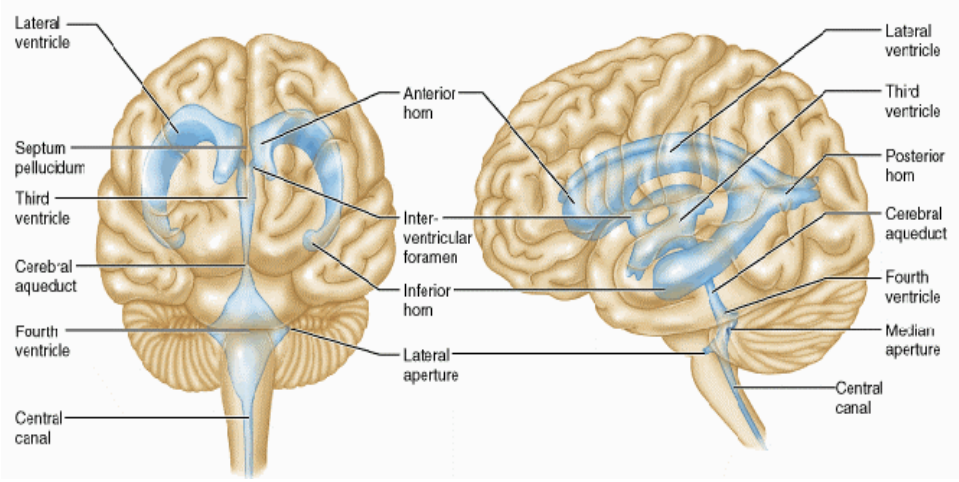

Figure 2.2. The position of ventricles with respect to the surface of the brain [7].

Table 1.1. The foramena of brain.

Name	Alternate Name	Connection/Role
Interventricular Foramen	Foramen of Monro	Lateral ventricles to the third ventricle
Cerebral Aqueduct	Foramen of Sylvia	Third ventricle to the fourth ventricle
Median Aperture	Foramen of Magendie	Fourth ventricle to cisterna magna
Lateral Apertures (right and left)	Foramen of Lushka	Fourth ventricle to SAS

2.2 Cerebrospinal fluid

Cerebrospinal fluid (CSF) fills the ventricles, SAS and the spinal canal of the CNS. In humans, the volume of CSF is about 150 ml most of which is contained in the lateral ventricles and has a production rate of 20ml/hour [7]. It forms a liquid cushion in and around the brain and spinal cord and gets constantly absorbed and replaced. It also provides buoyancy to brain, thus preventing it from crushing against its own weight. It has been estimated that 60-70% of the CSF is produced by the choroid plexus that are located in the ventricles [8]. The remainder of the volume is secreted around blood vessels and ventricular walls. The choroid plexus is formed by invagination of vascular pia mater (outer-most meninge of the brain) into the ventricular lumen where it assumes a highly convoluted, sponge-like appearance. The choroid plexus enters the third and fourth ventricle through their roofs and the lateral ventricles through choroid fissures.

The CSF flows through the interventricular foramen from the lateral ventricles to the third ventricle and continues to the fourth ventricle via cerebral aqueduct. The CSF leaves the fourth ventricle through the median and the two lateral apertures to enter cistern magna and SAS, respectively. Figure 2.3 depicts the flow of CSF in relation to the SAS and the circulation of CSF is indicated by arrows. Some CSF also flows into the spinal canal. Figure 2.4 shows the circulation of CSF in CNS. The majority of CSF flows superiorly over the brain to the site of reabsorption, i.e., arachnoid villi. CSF is absorbed in to the venous system by passing into the

dural venous sinuses (superior sagittal sinus). Arachnoid villi are located along the lumen of the sinuses and are formed by the invagination of arachnoid mater through the dural layer and into the lumen of the sinuses. A depiction of arachnoid villi is presented in Figure 2.5.

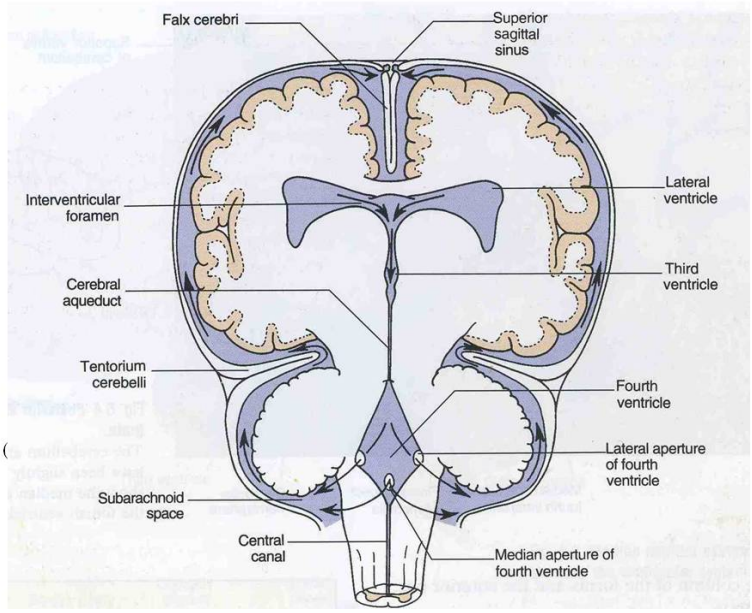

Figure 2.3. The relationship of cerebral ventricular system with the subarachnoid space [6].

The venous sinuses are the sites of reabsorption because of two reasons:

i) the hydrostatic pressure in SAS is higher than that of the venous sinuses, and

ii) the colloid osmotic pressure of blood is greater than that of the CSF. As age progresses, the arachnoid villi form arachnoid granulations due to hypertrophy.

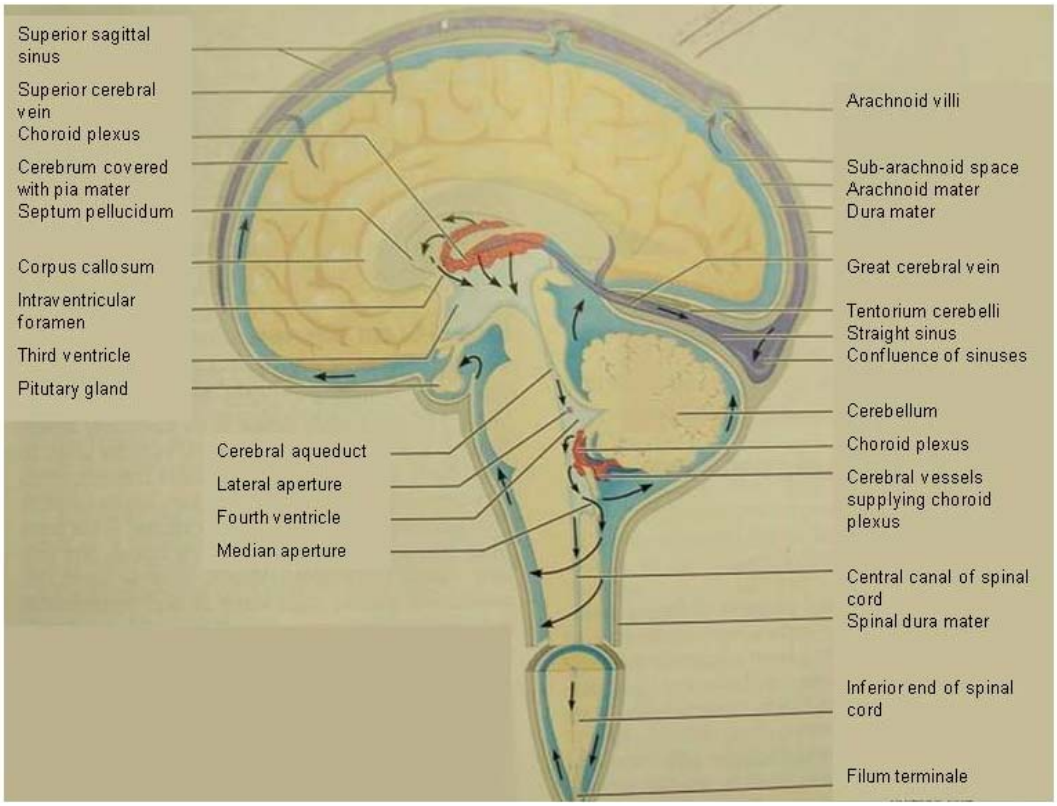

Figure 2.4. Circulation of CSF in the ventricles, subarachnoid space and the spinal canal [7].

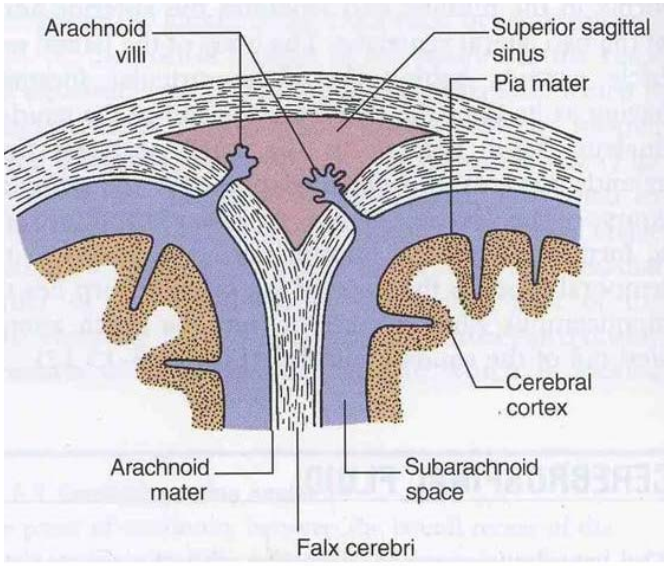

Figure 2.5. Presence of arachnoid villi in the venous sinus for reabsorption of cerebrospinal fluid [6].

2.3 Meninges of brain

The brain and the spinal cord are enveloped by three concentric membranes, also called meninges, within the bony cranial vault. The outermost membrane is dura mater, arachnoid mater being the middle layer, and pia mater is the innermost membrane that runs along the brain parenchyma. The organization of the meninges is described in Figure 2.6. Dura mater is a tough, fibrous membrane that is separated from the skull by a narrow extradural space except in certain regions like the midline of cranial roof where dura tightly adheres to the skull. Falx cerebri and tentorium cerebelli are two large reflections of dura that occupies the fissures separating major components of the brain. Falx cerebri lies in the longitudinal fissure, separating the two cerebral hemispheres. Tentorium cerebella is a horizontal shelf of dura that lies in the transverse cerebral fissure between the cerebral hemispheres and cerebellum. Dura mater is made of two layers that adhere to each other in most places except at dural venous sinuses. At the venous sinus the two dural layers let a formation a space that is rich in venous blood. These sinuses drain into the internal jugular vein through a series of interconnecting channels.

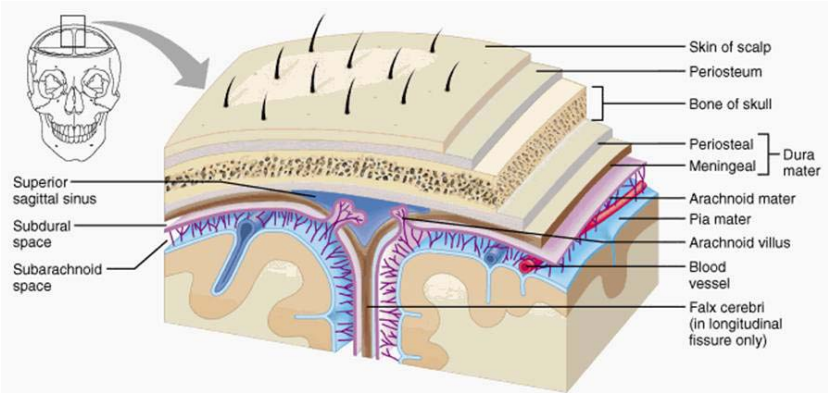

Figure 2.6. The meninges of brain [7].

Arachnoid mater is a soft translucent membrane that loosely envelopes the brain. It is separated from dura by a narrow subdural space that contains veins en route to the venous sinuses. The innermost layer-pia mater is a highly vascular, microscopic membrane that closely adheres to the brain while following all of its concavities and convexities. The space between pia mater and arachnoid mater is the subarachnoid space (SAS). The SAS contains a filamentous network of connective tissue strands called trabeculae, is transvered by blood vessels, and contains CSF. Since the pia mater is closely adherent to the brain and arachnoid mater is like a loose fitting bag, the depth of SAS is non-uniform and varies greatly over different regions of the brain. Subarachnoid cisterns like cistern magna are formed at regions where significant fissures are spanned by arachnoid mater. CSF flows from the fourth ventricle into cistern magna.

2.4 Physiology of intracranial pressure and intracranial hypertension

ICP is the pressure exerted by the components of the cranial vault. Figure 2.7 is a pictorial expression of ICP. Under normal conditions, CSF is the most significant contributor to ICP. Any imbalance in the volume of CSF can lead to an abnormality in the ICP. As per Monro-Kelly doctrine [1], the volume of blood, CSF, and brain in the cranium at a given time must be relatively constant. The cerebral vessels are compressed whenever there is an increase in ICP. An elevation of ICP for a short duration of time results in ischemia due to a reduction in the cerebral blood flow which in turn stimulates the vasomotor area, increasing the systemic blood pressure (i.e. Cushing reflex) [8]. Stimulation of vagal outflow results in bradycardia and hypoventilation. The Cushing reflex helps to maintain cerebral blood flow. However this is not true for a prolonged period of intracranial hypertension (ICH). Over a certain range, the systemic blood pressure rises proportionaly with the rise in ICP. During extended periods of ICH , a point is reached where ICP exceeds arterial blood pressure and thus ceasing cerebral blood circulation which results in ischemia. Thus, an immediate homeostatic response comes

into action to counter ICH. The efficacy of compensatory response depends on the rate at which the cranial volume increases. The brain can cope with ICH to a certain extent after which a slight increase in the cerebral volume results in a rapid rise of ICP [9] as indicated in Figure 2.8.

Figure 2.7. Pictoral presentation of intracranial pressure.

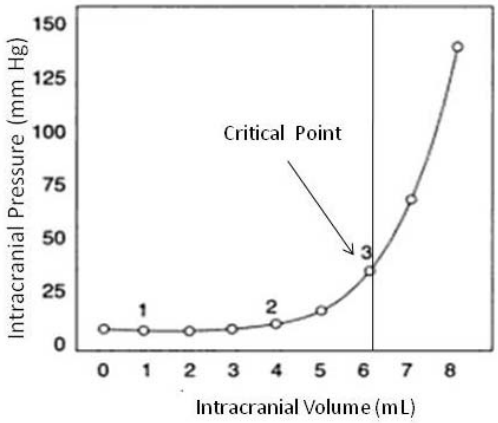

Figure 2.8. Effect of intracranial volume on intracranial pressure [9].

As per the idealized pressure-volume curve, a small change in the cranial volume can be compensated by insignificant changes in ICP (up till point 1 of the curve). At this stage, the intracranial contents are not tightly packed in the cranium and there is a bit more room for an increase in the intracranial volume. A critical stage is reached at point 2 of the curve where a slight volume increase results in an elevation of the ICP. The intracranial compliance fails after point 3 when the pressure-volume curve assumes a steep form. An incremental rise in the volume leads to a rapid increase in the pressure.

2.4.1 Causes of ICH

Any factor leading to an increase in the cranial volume could contribute to ICH. Few of the disorders that lead to an ICH are, but are not limited to, hydrocephalus, brain tumors, traumatic brain injury (TBI), brain aneurysms, sub-arachnoid hemorrhage, colloid cysts, meningitis, and Reye's Syndrome. Head injuries can be closed or penetrating causing the skull to be fractured and depressed, tearing the meninges, and the brain itself. Displacement and torsion of the brain lead to contusion and intracranial hematoma, causing concussion, neurological deficits, and post traumatic epilepsy. The tearing of a middle meningeal artery causes bleeding into extradural space i.e. extradural hematoma. An expansion in the size of a blood clot compresses the brain thus causing ICH. Sub-dural hematomas are caused by bleeding and seepage of blood from the veins stretching across subdural space. Meningitis, inflammation of the meninges, from fungal or bacterial source damages cranial nerves and the brain. If left untreated can lead to ICH followed by brain herniation and death. Once meningeal pathogens enter the subarachnoid space, host defense mechanisms are generally inadequate to control the infection [8,10]. Hydrocephalus (Figure 2.9) is the most commonly recognized cause of ICH. It can be of communicating or non-communicating type. In communicative type the reabsorptive capability of the arachnoid villi is impaired or there is an over production of CSF by choroid plexus. The balance between the filtration and reabsorption of CSF leads to an increase to the

intracranial volume which results in ICH. CSF also accumulates in the ventricles (Figure 2.9 [11]) when the foramena of Luschka or Magendie are blocked or there is an obstruction in the ventricular system, giving rise to non-communicating hydrocephalus [12, 13]. Few other classifications of hydrocephalus are adapted- i) internal and external [14], ii) active and passive, iii) acute, sub-acute, and chronic, and iv) normal pressure and elevated pressure [15, 16]. Colloid cysts are benign tumors that are found in the anterior third ventricle [17, 18]. They are epithelium lined cysts which cause morbidity and occasional mortality due to their location. Their presence in the third ventricle might present an obstruction to the flow of CSF into the fourth ventricle, leading to obstructive hydrocephalus, ICH, and sometimes intracystic hemorrhage. With the imaging tools like CT and MR colloid cysts are generally identified without any evidence of hydrocephalus on the scans. Figure 2.10 presents a case study of 35 year old patient with the diagnosis of colloid cysts in the third ventricle.

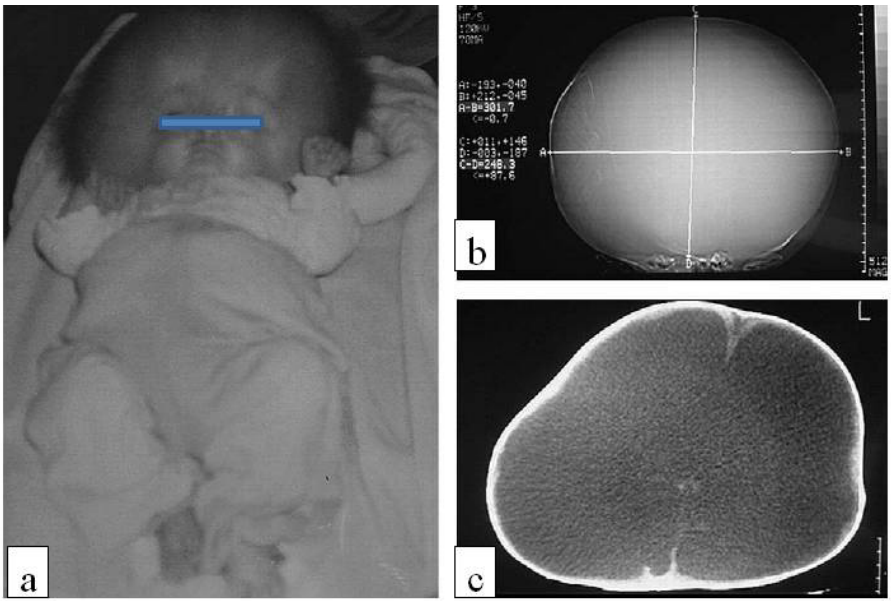

Figure 2.9. Appearance of a hydrocephalic infant and its CT images. a)The head circumference is nearly 70cm at the age of 3 months, b) CT scan has estimated the coronal (AB) and sagittal (CD) diameters of enlarged skull as 301.7 and 248.3mm, respectively , c) severe atrophy of cerebral parenchyma and huge ventriculomegaly [11].

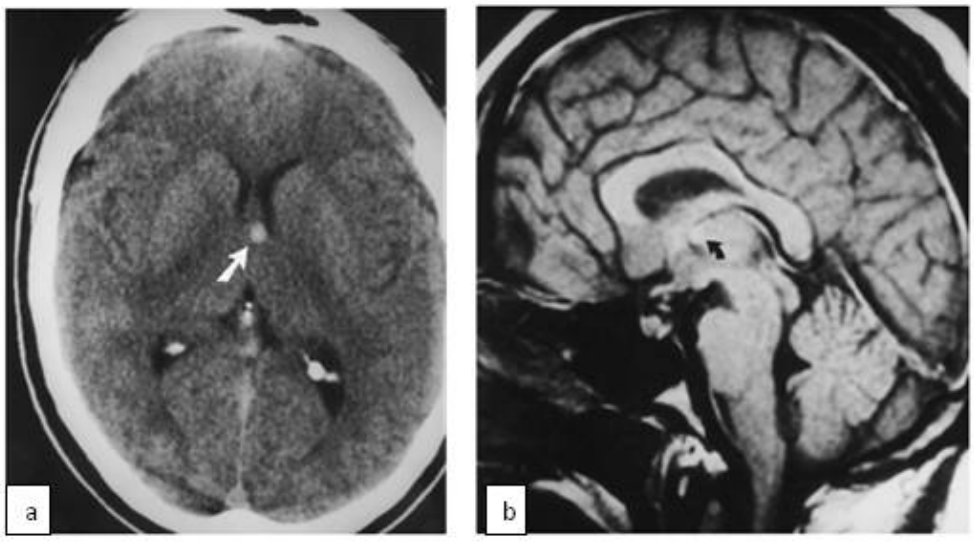

Figure 2 10. Images of a patient diagnosed with colloid cysts. a) Axial unenhanced CT scan shows a high attenuation colloid cyst, b)Sagittal MR image shows the colloid cyst (arrow) [19].

Any space occupying lesion (tumor, hematoma, or abscess) distorts the brain and displaces it downwards, in the direction of foramen of magnum due to ICH. The symptoms are headache, drowsiness, vomiting, and blurring of vision. A benign type of ICH is a result of any generalized swelling of the brain in absence of a focal space occupying lesion. It is often found in women, resenting symptoms of a tumor and is also known as pseudo tumor cerebri.

A significant reason for death and long term disability due to head injuries and pathological conditions is an elevation in the ICP. ICP > 20mmHg is considered a significant threshold and demands an immediate control measure [32].

3. Literature Review

ICP monitoring can assist in the management of patients with a variety of brain diseases. The technique has proven valuable, indeed often lifesaving, in the acute care of traumatic brain injury (TBI) [14], hydrocephalus [20], drowning [21], inflammatory and related cerebral diseases such as Reye's syndrome [22], hepatic failure [23], intracranial hemorrhage [24-26], and postoperative suboccipital brain tumors [27]. There is a conspicuous need for a wireless, implantable ICP monitoring system, as several chronic diseases are associated with intracranial hypertension (ICH). Conditions for which chronic ICP monitoring are useful include cerebral malignancies (annual incidence 16/100,000 population) [28], obstructive hydrocephalus (5/100,000) [29], multiple and complex aneurysms and vascular malformations (4/100,000) [30], benign ICH or pseudotumor cerebri (1/100,000) [31], and TBI [32]. Most of these patients have headaches and other symptoms suggestive (but not always indicative) of raised ICP; continuous access to ICP levels would greatly facilitate their management. In the United States alone, these diseases represent approximately 70,000 new cases per year and an estimated prevalence of more than 500,000. As per 2006 Center for Disease Control and Prevention (CDC) report [33], atleast 1.4 million TBIs occur in the United States each year. Yet the incidence of TBI in the active and returning military population is understandably much higher [34]. In fact, it has been estimated that approximately 30 percent of those evacuated from the battlefield to Walter Reed Army Medical Center have TBI [35]. It is well known that blast injuries are a leading cause of open and closed head injuries (including TBI), shell shock, and Post Traumatic Stress Disorder (PTSD).In the aforementioned cases of neurological disorders, an implant placed during surgery for tumor, hydrocephalus or vascular disease would be a useful adjunct to patient care. A burr hole to insert an implant in patients with benign ICH could also be justified.

The development of a medical device encompasses a wide range of technologies to

ensure the feasibility of its use in a biological environment. In this work, the attributes that were reviewed for the ICP implant are broadly categorized into-i) features of the implant and ii) the materials used to build the implant. The first category outlines the selection of frequency for wireless transmission, size of the implant, site of implantation, and the methods of measurement (invasive vs. non-invasive). The second category focuses on the interaction of the implant with biological tissue. It is critical to thoroughly weigh our options in determining the material characteristics of the implant to ascertain the survivability of the implant in a hostile biological environment.

The ICP implant in discussion is designed to operate in microwave frequency range. For this reason, it is important to have a good understanding of the biological effects of microwave frequencies. A section on the biological effects of microwaves is also presented here.

3.1 Implant features

Therapeutic and diagnostic applications of radio frequency (RF) and microwave in medicine have been a subject of extensive studies in the past [36]-[38]. Medical implants for transfer of information at these non-ionizing frequencies have been developed [39]. The research accomplishments of using data communication links at microwave frequencies between a medical implant and an external unit have been reported by many researchers. The resonance characteristics of implanted antennas operating at a frequency band of 402-405 MHz and their radiation pattern outside the body have been shown to be favorable for short-range medical implants [40]. Poon and co-workers demonstrated that the optimal frequency for power transmission in biological media is in the GHz range [41]. Gosalia and his colleagues [42] demonstrated a novel approach of establishing a data telemetry link between an implant and an external unit at 1.45 and 2.45 GHz band, for retinal prosthesis. Such medical implants are basic components for the success of telemedicine, which refers to the utilization of

telecommunication technologies in health care. Telemedicine not only facilitates medical treatment and care, but is also gaining increasing popularity in post-hospital patient care [43]. It provides expert consultation in remote understaffed locations and advanced emergency care via modern telecommunication techniques [44]. Mobile patient monitoring systems using wireless implants have been developed to maintain records of patient's vital signs and history [45], [46]. These systems are useful during intra-hospital patient transport, intra-operative procedures, or post hospital management of patients.

The core of our active implantable device for ICP measurement is an oscillator operating at the Industrial-Scientific-Medical (ISM) band of 2.4000-2.4835 GHz. The sensing component is a MEMS piezoresistive or MEMS capacitive sensor, whose variation with the ICP changes the oscillation frequency of an oscillator. The oscillator output is coupled to an antenna and can be displayed by an external monitoring unit. There are a number of reasons for choosing an oscillator- based implantable unit operating at microwave frequencies. Firstly, the oscillation frequency of a well-designed oscillator is very sensitive to the change of its tank capacitor if a capacitive sensor is used as part of the tank circuit. Secondly, the microwave signal transmitted by a small antenna inside the implant can be detected from a significant distance outside the patient. Thirdly, the microwave frequency of 2.4 GHz is high enough to be efficiently radiated by a small antenna, but is low enough to avoid significant absorption by the implant package and skin [38]. In contrast, the passive (battery-less) Bio-MEMS operating at MHz range (e.g. 10-20 MHz [47] or 330 MHz [48]) require transcutaneous inductive links [47], [48] for monitoring of the pressure. Since the inductive links operate at near-field, pressure monitoring receiver must be placed on the surface of the body (i.e., no remote monitoring is possible). Moreover, such an implant would require large inductors (e.g., 3.7 μH [47] and 150-200 nH [48]), which would make it MRI incompatible.

An implantable, wireless method for continuous or intermittent monitoring of ICP aids

the management of patients with brain disorders or trauma. Accurate monitoring of the ICP following a neurosurgical procedure is a basic requirement for an adequate treatment [49]-[51]. Since the intracranial contents exist within a rigid vault (skull), direct ICP measurements require neurosurgical intervention, with their attendant risks.

The pioneering work in ameliorating ICH was done by a machinist out of Philadelphia, John W. Holter [52] who developed a one way shunt valve for the treatment of hydrocephalus. With further modifications, the valve was later known as Holter-Spitz valve, named after its inventors- John Holter and Eugene Spitz. This valve did not measure ICP, but created a one way diversion for excessive cerebrospinal fluid (CSF).

In the past, various techniques have been developed for estimating the ICP. These include lumbar puncture, intra-ventricular catheter, sub-arachnoid screw (Richmond bolt), fiber optic transducer tip catheters, and acoustic apparatus. In lumbar puncture, a catheter is placed in the spinal sub-arachnoid space, estimating the CSF pressure. This CSF pressure at the lumbar level does not give an accurate estimate of ICP. Intraventricular catheters provide more accurate pressure transduction, but are erroneous if the catheter is dislodged or occluded. The opening of the sub-arachnoid screw is placed right under the arachnoid membrane by penetrating the skull and dura mata. The bolt can get easily dislodged and restricts the patient to ICU. The above examples outline various modalities of ICP measurement based on the site of pressure sensing, such as intra-parenchymal (i.e., within the tissue), sub-dural (i.e., below the dura mata, which is the outermost protective layer surrounding the brain), and epidural (i.e., above the dura mata). These examples also lack accuracy, and simplicity [53], [54]. The utilization of a fluid filled manometer and an external strain gage has been the gold standard for ventricular (ventricles are the fluid filled cavities inside the brain) ICP measurement and treatment. However, cannulating (i.e., introducing a tube into) the ventricle in cases of brain edema may not be feasible, and it is the most invasive method of ICP monitoring that can result in infection and brain injury. Epidural pressure monitoring is an attractive alternative to the ventricular approach, since the

brain or the CSF are not exposed to the external environment, thus presenting fewer complications [54]. Studies have been carried out in the past to gauge the reliability of various epidural pressure monitors [53]-[58] and at the same time comparing them with ventricular or intra-parenchymal monitors. Sub-dural pressure monitoring appears to be a good compromise between the risks encountered in ventricular pressure sensing and the reliability limitations posed by epidural pressure sensing (Powell and Crockard [56]). In addition, Powell and Crockard [56] also observed a stable and linear relationship between sub-dural and ventricular pressure measurements with no drift over time. Pressure in the higher range (>30 mmHg) was accurately measured by the sub-dural approach. Along with the invasive approaches delineated above various efforts have been made to monitor ICP in a non-invasive fashion. For example, by using ultrasound or near- infrared spectroscopy (NIRS) [59-62]. In one instance, 23 case studies were conducted to evaluate the utility of measuring the optic nerve sheath diameter in children with shunted hydrocephalus, who were suspected of having raised ICP [59]. Lin et.al [60] have described the role of NIRS in the evaluation of ICP. Their work is based on the principle that the intensity of diffuse reflection light is proportional to the thickness of CSF, resulting in a correlation between ICP and diffuse reflection light.

Existing clinical ICP monitoring relies on catheter based systems to record the ventricular pressure. This technique restricts the patient to hospital settings, accompanied by risks, patient discomfort, and expense. ICP can also be inferred indirectly from neuroimaging like computer tomography (CT) and magnetic resonance imaging (MRI) scans [63]. However, these methods lack sensitivity and represent only one moment in time during which the scan is performed. They also require transportation of the patient out of the intensive care unit (ICU) and exposure to ionizing radiation in the case of CT scan. Therefore, neuroimaging and in-hospital monitoring are unrealistic options for long term and recurring symptoms.

All the current methods of ICP monitoring have limitations that require wires, cables, or catheters emanating from the patient's head. These tethers are frequently dislodged by the

patient's movement. Wired devices can also cause patient discomfort and risk of infection at the site of implantation. The widely used Camino catheters (Integra Life Sciences, CA), Figure 3.1, for ICP measurement have been extensively studied [64]-[67].

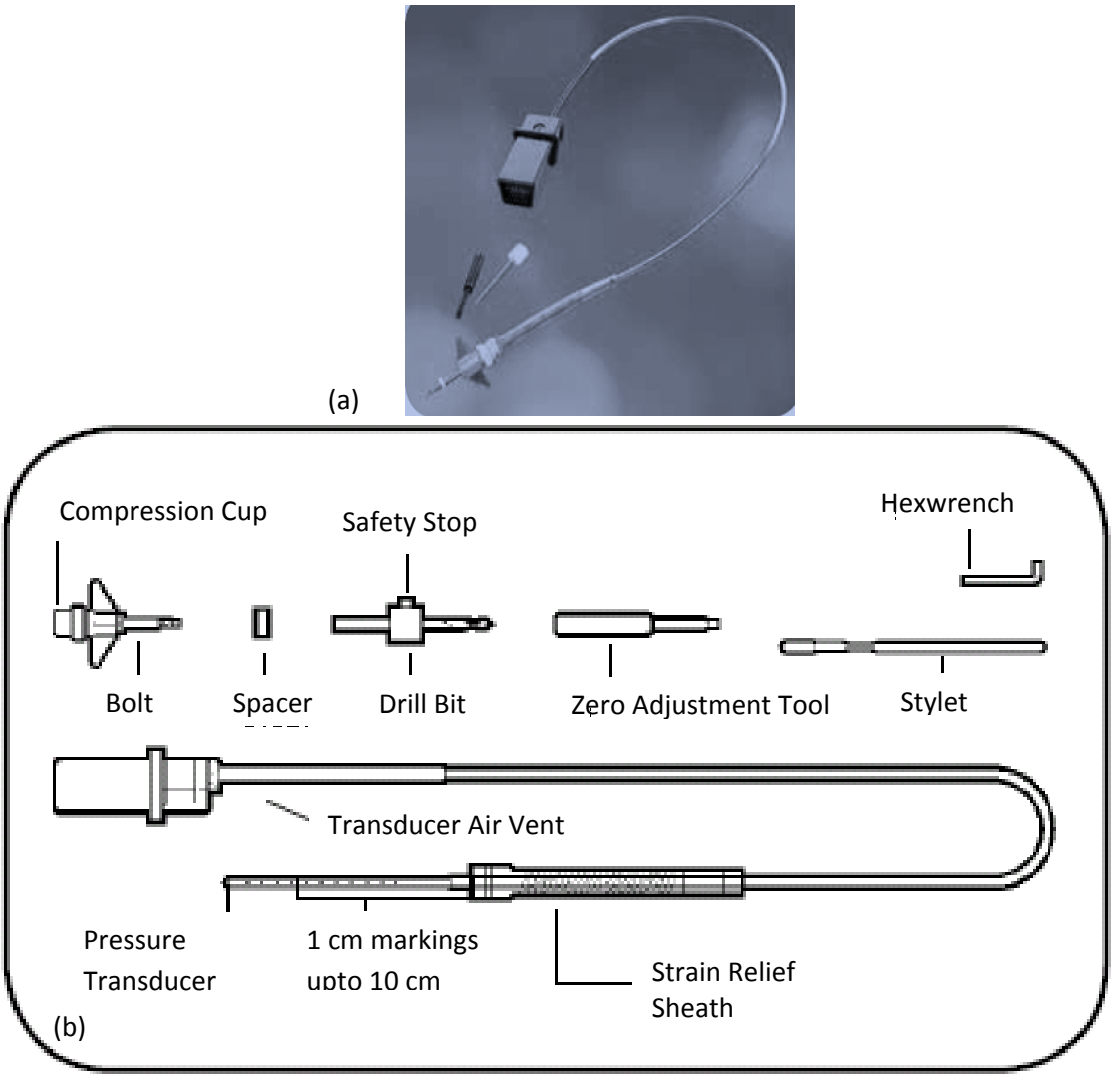

Figure 3.1. Camino ICP catheter (model 110-4B). a) Photograph of the catheter, and b) Mechanical drawing of catheter along with auxiliary tools [68].

Table 3.1, presents a comparison between few of the techniques that are used for ICP monitoring and the approach that has been adopted for the development of our ICP implant.

Table 3.1. Comparison of intracranial pressure monitoring modalities.

Factors	**Methods**			
	Catheters	CSF Drainage Systems	Low Frequency Implants (kHz-MHz)	Our ICP Implant (GHz)
Long Term ICP Implantation	NO	NO	YES	YES
Complete Implantation	NO	NO	YES	YES
Wireless Implantation	NO	YES	YES	YES
Distant Wireless Reader Range	NO	NO	NO (< few inches)	YES (up to 0.8m)
MRI Compatibility	NO	NO	NO	YES
Patient Comfort	NO	NO	YES	YES

CSF stands for cerebrospinal fluid

3.2 Implant materials

The safety of a medical device in a biological medium begins with the choice of materials that are used in building an implant. In January 2000, National Institutes of Health (NIH) reported that 8-10% Americans have some type of implant in their body [69]. The surface of an implant that comes in contact with body should be composed of biomaterials. Metals like stainless steel, aluminum, titanium, gold, cobalt-based alloys, nickel-titanium alloys have long been used as biomaterials are also approved by the Food and Drug Administration (FDA) for use in medical implants[70-73]. Polymeric materials [70] like Ploymethyl siloxane (silicone rubber, silastics) has been used in joint replacement, polymethyl methacrylate as cement (grout), polyurethane in hip joints, etc. Silicones are applicable at a wide range of temperatures (-50 ^{o}C to 260 ^{o}C) and can mechanically adhere to a wide range of materials. They have low tensile and surface peel strengths which indicates that silicones are suitable as structural sealants

than structural adhesives. Typical silicone applications include bonding and sealing of silicone based assemblies, coating of components to minimize rough edges, and coating of highly flexible assemblies such as endotrachial tubes [74], [75]. Cyanoacrylates (crazy glue) and epoxies are known to be effective adhesives and bond well with many materials. In considering materials for a medical implant, several factors are of significance. The material should be:

i) non-toxic and non-carcinogenic, cause no or little foreign body reaction, and chemically stable,
ii) able to handle stresses in corrosive body environment, and
iii) able to be fabricated into the desired form.

Polymeric coatings are applied to medical devices for a variety of reasons which include enhancing biocompatibility and biostability, thromboresistance, antimicrobial action, dielectric strength and lubricity [70]. Parylene (Poly xylylene or its derivatives) is a vapor deposited polymer that is heavily used in medical device industry. The process does not use any solvents, plasticizers or surface enhancers and is carried out at room temperature. Parylene coatings are completely conformal, produce uniform thickness, and are pinhole free. The advantage of this process is that the coating forms from a gaseous monomer without an intermediate liquid stage. As a result, component configurations with sharp edges, points, flat surfaces, crevices or exposed internal surfaces are coated uniformly without voids [76]. Parylene coatings can resist chemical attack from organic solvents, inorganic reagents, and acids and also offers high dielectric strength. It can be coated on a diverse types of surfaces like metals, glass, paper, plastics, ceramics, silicon etc. A properly formulated Parylene is pure, has no foreign impurities, and thus does not change the surface properties of the base material. Parylene coatings are transparent, have very low thrombogenic properties, and exhibit a potential for triggering an immune response [70]. These coatings are also deemed to be resistant to the damaging effects of corrosive body fluids, proteins, enzymes, electrolytes, and lipids. The coating also acts as a barrier to the passage of any contaminants from the coated surface to the

external environment. Out of the four variants of Parylene (Parylene C, D, N, and HT), Parylene C and Parylene N are widely used in the coating of medical devices. Further details on the chemistry and the deposition process of Parylene are presented in Chapter 4.

Parylene coatings have been proven effective in coating electronic circuits and silicon (micro electro mechanical systems, MEMS) in medical devices. Chen et al. [77], have described a microfabricated Parylene based implantable intra-ocular pressure sensor for glaucoma. The biocompatibility of their implant was successfully verified in a six-month long animal study. In another study carried out by Wasielewski and his colleagues, an intra-operative pressure monitoring device was used in total knee arthoplasty in a group of 38 patients [78]. The packaging applications of Parylene in the fabrication of medical devices have also been elucidated in [79] and [80].

3.3 Biological effects of microwaves

Although microwaves are non-ionizing radiations, yet their interaction with biological media is usually quantified in terms of its (thermal) absorption in the tissue. The thermal effects of microwave depend on the external field as well as the dielectric field inside the body [38]. The properties of internal field are affected by a number of factors that include:

i) Frequency, intensity, and polarization of the external field,
ii) Dimensions and dielectric properties of the biological tissue under consideration,
iii) Spatial configuration of the source in relation to the tissue that is receiving the electromagnetic energy, and
iv) Presence of other objects in the surroundings for multipath effects.

A biological medium is an inhomogeneous and lossy dielectric with complex shape or dimensions. Since a number of parameters are involved in the characterization of the biological effects of microwave, it becomes a highly complex problem to model the effects of each parameter at the same time. Consequently, simplified models are designed to analyze the problem.

As microwaves pass through a biological tissue, most or all of its electromagnetic energy is converted to thermal energy and the extent of conversion is determined by the dielectric properties of the medium and the frequency of the source. The dosimetric measure of the energy conversion is defined by specific absorption rate (SAR) which is the rate of energy deposited per unit mass of the tissue and is expressed in the units of Watt/kg. SAR can be expressed as one 0f the following equations [38]:

$$\text{SAR} = \left(\frac{d}{dt}\right)\left(\frac{dW}{dm}\right) = \left(\frac{d}{dt}\right)\left(\frac{dW}{\rho dV}\right) \tag{3.1}$$

where, *dW* is the incremental energy absorbed by the tissue, *dm* is the incremental mass of the tissue, *dV* is the total volume of the tissue, and ρ is the density of the tissue.

$$\text{SAR} = \left(\frac{\sigma}{2\rho}\right)|\bar{E}_\iota|^2 = \left(\frac{\omega\varepsilon_o\varepsilon^{"}}{2\rho}\right)|\bar{E}_\iota|^2 \tag{3.2}$$

where, $\bar{E}\iota$ is the peak value of the internal electric field , ε_o is the permittivity of free space, $\varepsilon^{"}$ is the imaginary part of permittivity of tissue, and σ is the conductivity of tissue.

SAR is averaged over the whole body (average SAR) or localized to a small volume (local SAR) of 1 g or 10 g of tissue. It is used to quantify the energy absorbed due to the use of mobile phones, medical devices, and MRI scans. In United States, Federal Communications Commission (FCC) directs 1.6 W/kg to be the upper limit for local SAR when averaged over 1g of tissue [36].

4. Intracranial Pressure Monitoring Implants

The ideal specifications of an intracranial pressure (ICP) monitoring system have been defined in [81]. The system should:

i) be simple, reliable, and able to function efficiently over a long period of time and under a variety of conditions, either continuously or intermittently,

ii) cause no significant discomfort or risk to the patient,

iii) minimize trauma or irritation of intracranial structures,

iv) cause no leakage through the link between the ventricle or the point of interest and the monitoring apparatus,

v) allow for ease of disconnecting the patient to permit other investigational procedures or possibility of recording pressure measurements during various diagnostic or therapeutic procedures, and

vi) provide maximum information about variations in the ICP.

The implants for the monitoring of ICP that are designed by our group are small enough to be inserted in a burr hole and also have the following characteristics:

i) Small: can be implanted by a common neurosurgical procedure, which can be performed either during primary surgery or through a burr hole.

ii) Stable: produce an insignificant drift over the usage time of the device. The device should have a maximum error of +/- 2 mmHg in the range of 0-20 mmHg or +/- 10% of the full scale in the range of 20-100 mmHg, as per American National Standard Institute (ANSI) specifications [82].

iii) Compatible with imaging systems: no damage to the device with minimal impact on image quality from modern investigational procedures including MRI, CT, and ultrasound.

iv) Biocompatible: no adverse effects over the lifetime of the device.

v) Rugged: likely to survive any non-fatal injury.

vi) Inexpensive and patient comfort: The cost of the device must be reasonable compared to the cost of competing clinical options. An X-ray or CT scan exposes the patient to enough radiation to increase lifetime cancer risk by a fraction of 1%. An MRI study involves no ionizing radiation, but may require sedation and monitoring.

vii) Others: wireless, simple, rapid and painless interrogation procedure.

Over the duration of this research effort, a variety of ICP monitoring implants were developed, mainly based on three factors i.e., the method of pressure sensing, the site of pressure sensing, and the ease of implantation procedure. There are two methods of pressure sensing and hence two electronic different designs. An additional factor of classification, i.e., the type of animal model for conducting *in-vivo* studies, was also introduced that only affected the size and shape of the implant packaging. The aforementioned classifications are enumerated and detailed in this chapter. This chapter also describes the process of measurement from pressure transduction to wireless transmission. The last section of this chapter elaborates on the selection of various materials in the fabrication of these implants from the point of view of biocompatibility.

4.1 Packaging concept of implant

The implants are contained in a cylindrical metallic casing to be implanted in a burr hole in the skull. The casing has a fixed/adjustable flange or four tabs on the top side which is screwed to the skull for a tight fit. The sensor, electronics, and the antenna are assembled on printed circuit boards, PCB (FR4, 30 mil thickness). The numbers of PCBs used in a design vary as per the size and shape of the implant casing for a desired type of study. In total three configurations were developed as the designs evolved. In all the configurations, the sensor is placed at the bottom surface of the implant and the antenna is mounted on the top surface. Figure 4.1 shows one of the implants with a two layer design, forming a cage shaped cylindrical structure, the side legs of which provide stability as well as electrical connections.

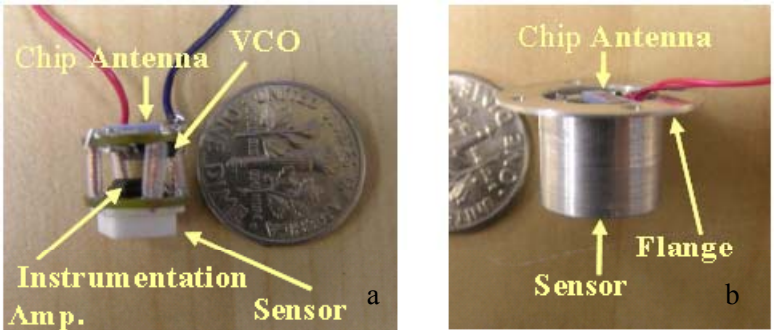

Figure 4.1. An implant is shown; a) without the case and b) mounted in the stainless steel metallic case (12 mm diameter and 9 mm height).

4.2 Various classifications of the implant

For a good understanding of the implant characterization and references to various types of implants in the upcoming description and discussion, the ICP implants have been categorized based on:

i) The method of pressure sensing,

ii) The site of pressure sensing,

iii) The size of burr hole, and

iv) The nature of intended study.

4.2.1 Method of pressure sensing

The choice of a pressure sensor was mainly influenced by its commercial availability as the primary focus was to conduct a proof-of-concept study (*in-vitro* and *in-vivo*) with an implant that was designed and fabricated with commercially available components. The important issues of ICP monitoring with the implant i.e., biocompatibility, implant sealing, integrity, pressure sensitivity, temperature sensitivity, trans-scalp wireless transmission, scar tissue formation (histo-pathology) at the implant and sensor site, and trans-dural versus sub-arachnoid pressure sensing were addressed. To perform initial *in-vitro* and *in-vivo* tests, a PZR sensor was used because of the unavailability of microelectromechanical systems (MEMS) capacitive pressure

sensors with the desirable features of size and frequency response over the pressure range of interest at the time. At a later stage, implants based on capacitive MEMS sensors were developed. Figure 4.2 shows a photograph of the PZR and capacitive pressure sensors. A (MEMS) capacitive pressure sensing element is a preferred choice of pressure transduction. The PZR sensor has the advantages of availability and lower cost. However, there were major disadvantages that were noted in our study and are as follows:

i) Poor performance repeatability (due to large sensor tolerance, for example, a standard deviation of 3 mV for a 69 mV sensor output voltage at room pressure, or 4.5%),

ii) High sensitivity to temperature variations, and

iii) Requirement of larger number of components and a signal conditioning circuit that increase the power consumption and contribute to poor performance repeatability and temperature sensitivity. On the other hand capacitive pressure sensors are small in size; operate over a wider range of temperature; and exhibit good linearity and compatibility to CMOS signal conditioning [83].

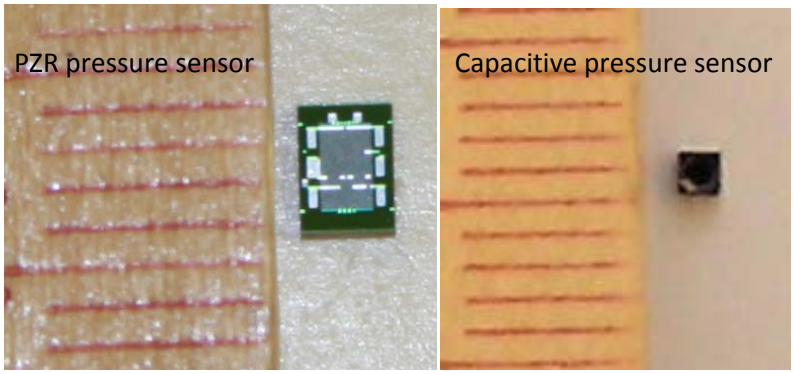

Figure 4.2. Photograph of a) PZR pressure sensor, and b) capacitive MEMS pressure sensors

The PZR absolute pressure sensor, model 3000 series that was used in the initial studies was acquired from Merit Sensor Systems, South Jordan, UT. Surface mount and die versions of this sensor were obtained for a pressure range of 0-5 PSI, resistance of 3500 Ω. The capacitive absolute MEMS pressure sensors, model number SCB10H series were obtained from VTI Technologies, Finland. Table 4.1 lists few of the parameters of the PZR and the capacitive pressure sensors. The governing equations of the sensor model used in our latest ICP implant, are described below [84]. The details of capacitive sensors are emphasized here as the latest prototypes of the implant are built with this type of sensor.

4.2.1.1 Capacitive sensor model

The governing equation of the capacitance as a function of pressure is

$$Cmodel\,(p) = Coo + rCo + \frac{Co}{1 - \left(\frac{Co}{k}\right)p} + \frac{aCo}{1 - \left(\frac{Co}{bk}\right)p} \tag{4.1}$$

where, *Co, Coo*, and *k* are statistical variables that are independent of each other and vary from batch to batch and unit to unit with the standard deviations, *a, b,* and *r* are constants for a given type of sensor, and *p* is the applied absolute pressure.

Functions α (t) and β(t) are described for temperature dependency at constant pressure (p=p_{ref}) and temperature dependency of sensitivity, respectively.

$$\alpha(t) = \propto_1 (T - Tref) + \propto_2 (T - Tref)^2 \tag{4.2}$$

$$\beta(t) = \beta_1(T - Tref) + \beta_2(T - Tref)^2 \tag{4.3}$$

where, p_{ref} = 760 mmHg, T*ref*= 25^{o}C, α_1 is the temperature coefficient of offset (TCO), and β_1 is temperature coefficient of sensitivity (TCS).

Table 4.1: Characteristics of the PZR and capacitive MEMS pressure sensor.

PZR Sensor (0-5PSI, 0-258.33 mmHg)		
Parameter	**Value**	**Units**
Excitation input	3; 5(Nominal)	V
Impedance (input/output)	3500	Ω
Operating temperature	-40 to 150	C
Linearity	0+/- 0.2	%FSO
Pressure hysteresis	0+/- 0.1	%FSO
Thermal hysteresis	0+/- 0.2	%FSO
Full Scale Output (FSO)	75+/-12.5 at 5V excitation	mV
Capacitive Pressure Sensor (30-120 kPa, 225-900 mmHg, absolute)		
Size (length, width, thickness)	1.4, 1.4, 0.85 (+/- 0.05)	mm
Lowest mechanical resonance frequency of diaphragm	450	kHz

The temperature dependency of the sensor can be calculated by the following equation:

$$\frac{\partial p}{\partial T} = \frac{\partial\left(\propto (t)\right)}{\partial T} + \frac{\partial\left(\beta(t)\right)}{\partial T}(p - p_{ref}) \tag{4.4}$$

Based on equations 4.1 to 4.4, and the parameters listed in Table 4.2, the change in capacitance for a full range of pressure, i.e ΔC (C_{at} 120 kPa- C_{at} 30kPa) has a minimum value of 2.7pF and a maximum value of 6.8pF.

Table 4.2: Capacitance-pressure characteristics and parameters for capacitance calculations.

Capacitance-Pressure Characteristics		
Parameter	**Nominal Value**	**Units**
A	0.657	
B	1.477	
C_{oo}	0.82+/- 0.22	pF
C_o	3.64+/- 0.22	pF
K	864 + 200/-164	kPa*pF
Sensitivity dC/dP	59 +41/-21	fF/kPa
Non-linearity	0.028	kPa

4.2.2 Site of pressure sensing

The type of implant falls into two classifications (epidural and sub-dural) based on the site of pressure sensing. An epidural (ED) implant measures pressure as function of the dural deflection. A PZR pressure sensor rests on the dura mater and transduces pressure to voltage. In a sub-dural (SD) implant, the pressure sensor is exposed to the CSF in the sub-arachnoid space (SAS). Figure 4.3 depicts the position of the pressure sensor in epidural and sub-dural spaces. Irrespective of the epidural or sub-dural nature of pressure sensing, the implant is designed to be placed in a burr hole drilled in the skull. The types of burr holes are detailed in the next sub-section.

4.2.3 Size of hole drilled in the skull for implant placement

The initial prototypes are housed in cylindrical cases of approximately 10-12 mm diameter. This design was modified to allow for implantation in a smaller burr hole in the skull. The second type of hole is 3-4 mm in diameter and is designed to provide access to the CSF in the SAS. It must be noted that the sensor and its electronics are contained inside the casing. The

small hole (S) in the skull contains a part of the casing whereas the large hole (L) accommodates the entire casing. Figure 4.4 shows the two sizes of hole drilled in the skull along with their respective implant casings. Figure 4.5 is a representation of the placement of implants in small and large holes.

4.2.4 Nature of intended study

The *in-vivo* studies conducted in this research work were performed in a big animal model (swine or canine). However, the casing was later redesigned to accommodate any possibility of performing studies on rodent models in any future endeavors. Figure 4.6 shows the two types of casings. Casing 'C' is symmetric and is intended to be placed in a skull that is comparable to a pediatric skull. The symmetry ensures a snug fit of the implant in a burr hole and is a good candidate for canine studies. Casing 'R' has an asymmetric orientation of the nozzle due to a limited availability of space in a rodent skull model. The bulk of the device rests posteriorly on the skull leaning more toward the back of the rodent.

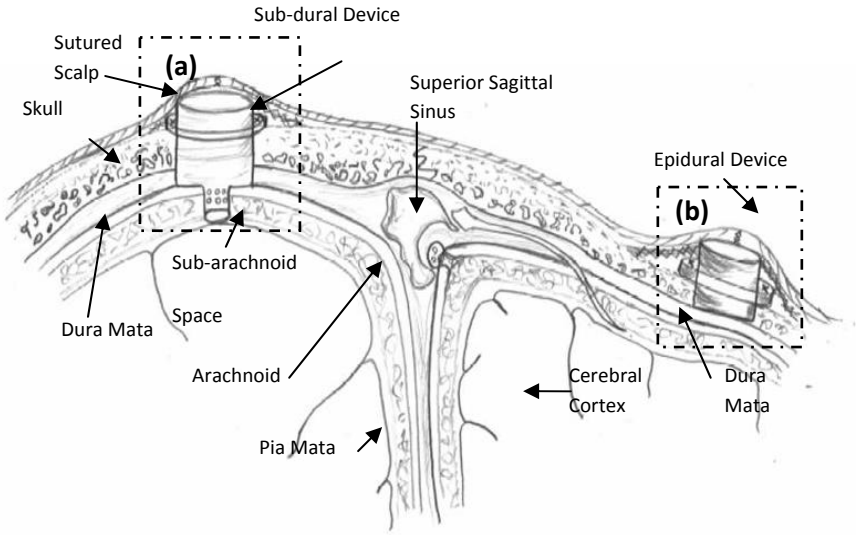

Figure 4.3. . Diagrammatic representation of the device placement in skull; a) sub-dural device implantation and b) epidural device in contiguous sections of the meninges. The sensor is exposed to the cerebral spinal fluid in sub-arachnoid space for sub-dural pressure detection. In epidural detection, the sensor maintains a contact with the dura mata and relies on dural deflection.

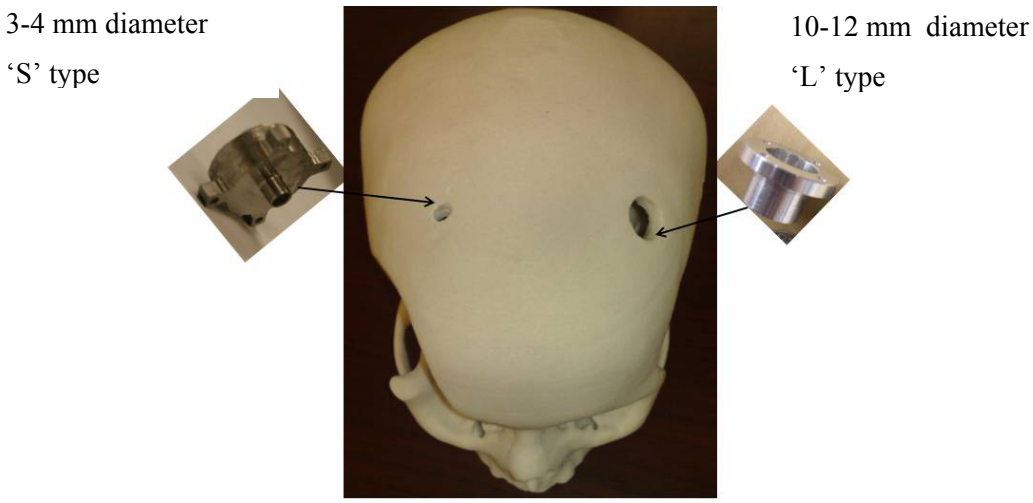

Figure 4.4. Two types of implants based on the size of burr hole in the skull for the placement of implant.

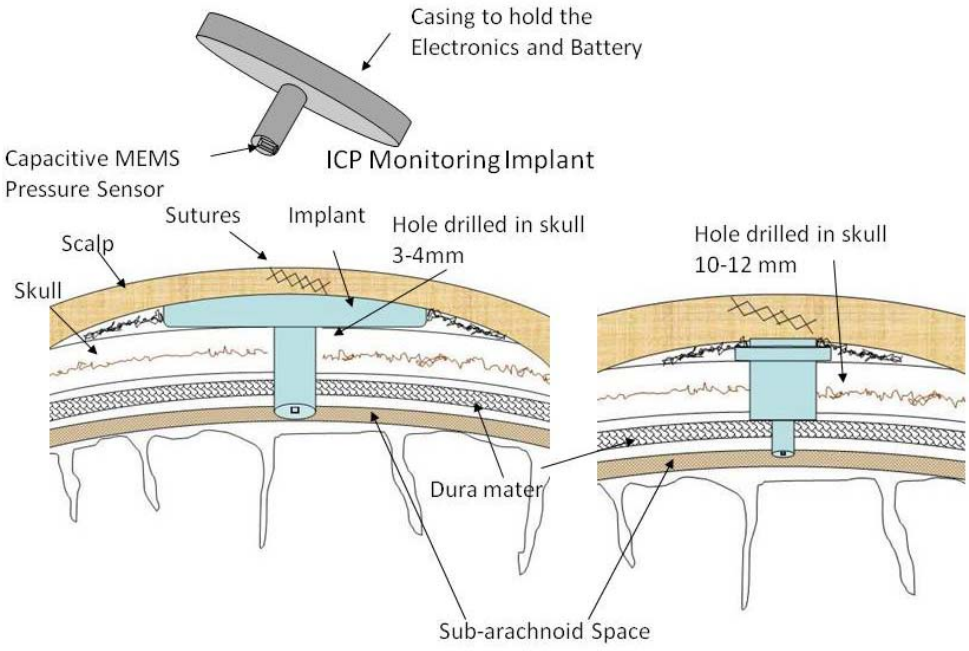

Figure 4.5. Implantation of sub-dural implants in a small (S) and a large (L) burr hole.

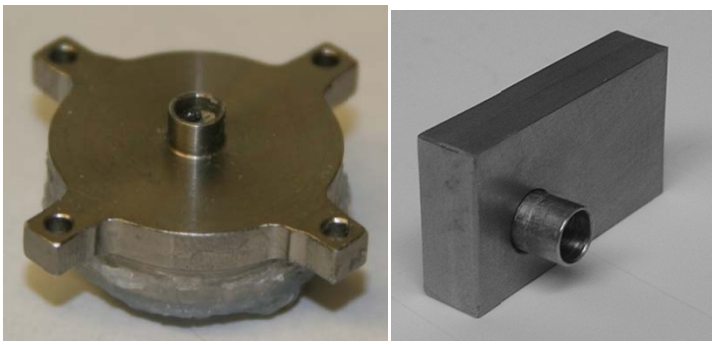

Figure 4.6. Symmetrical (C type) and asymmetrical (R type) designs for canine and rodent studies, respectively.

A classification code is described here for an ease in the identification of the various implant types. Table 4.3 lists the various codes in reference to the type of implant along with an example of the nomenclature.

Table 4.3: Nomenclature for identification of the type of an implant.

Type	Code
Piezoresistive pressure sensor	PZR
Capacitive pressure sensor	Cap
Epidural	ED
Sub-dural	SD
3-4 mm hole	S
10-12 mm hole	L
Symmetric casing	C
Asymmetric casing	R
Example	
PZR_ED_L_C	Piezoresistive sensor based epidural implant in a large hole for canine model

4.3 Evolution of implant packaging

As the implants were modified to accommodate various changes in parameters (type of sensor, type of antenna, site of pressure sensing, the nature of study), the implant packaging also changed. One of the significant changes was to physically isolate the capacitive pressure sensor from the rest of the electronics. This modification allowed performing the device implantation in a smaller burr hole. Figure 4.7 is a sketch of the sensor as a part of the main cage design and physically isolated from the main structure. The stages of prototype development are outlined in Figure 4.8.

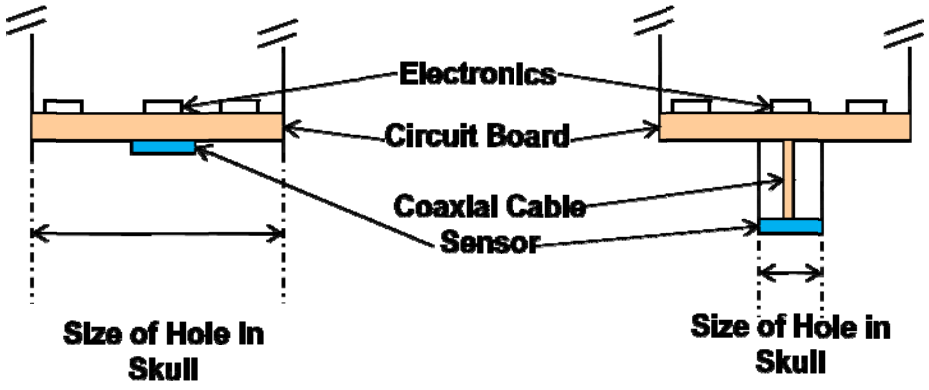

Figure 4.7. A section of Implant depicting placement of the pressure sensor (drawing not to scale).

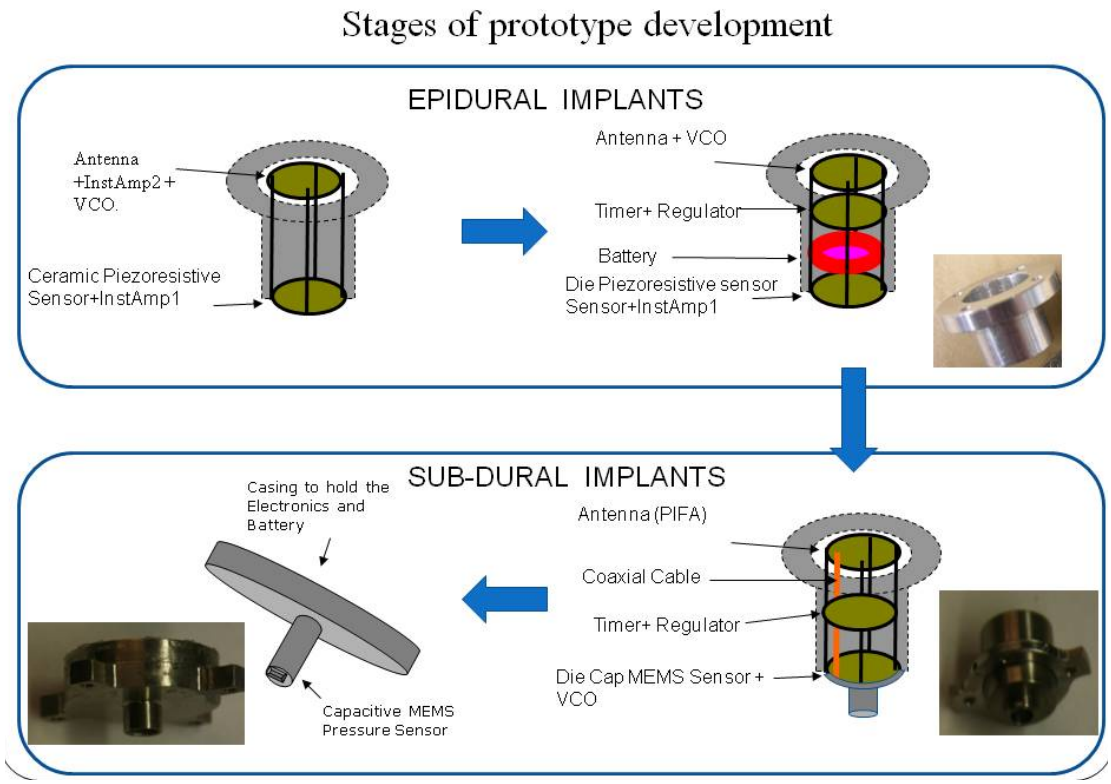

Figure 4.8. Stages of device packaging.

4.4 Concept of electronic design

The implants designs were based on a PZR pressure sensor and a capacitive pressure sensor. In each case a 2.4 GHz voltage controlled oscillator (VCO, Maxim 2753) was coupled to an antenna for wireless pressure transmission. A VCO was used to directly provide power to the device transmitter antenna. The VCO implementation was chosen, since it could conveniently provide enough power (about -20 dBm)[RThesis] for reliable signal monitoring within a range of about 1 m, for a receiver sensitivity of better than -80 dBm. The circuitry for each design is detailed here. A simple power management is employed by switching the main circuitry on and off with a period of 10 ms and for a duration of approximately 25 μs (0.25% duty cycle). The device case (10-12 mm diameter) could host an 11-mA/h rechargeable 3-V battery (ML302S). However, for the duration of our long-term experiments, it was decided that

an external 3-V battery (CR2032, 220 mAh, 20-mm diameter) be used to supply power to the device while it runs at a regulated voltage of 2.5 V. Due to the size limitations the battery would be housed in a sleeve adjoining the implant case. It is envisioned that larger size batteries could also be implanted next to the implant over the skull.

4.4.1 Based on PZR

The implant is run at a supply voltage of 2.8V. A half-closed bridge pressure sensor (absolute) in ceramic packaging is exposed to pressure variations. The full scale range of the sensor is 0-258.33 mmHg; however the device is designed for 0-100 mmHg range. An instrumentation amplifier conditions the signal from the sensor for noise elimination and scales it to a linear operating range (1.2V-1.75V) of a 2.4 GHz VCO [85]. VCO output is fed to a chip antenna. The antenna nominal bandwidth and center frequency are 120 MHz and 2.450 GHz respectively. The receiver antenna is hooked up to a spectrum analyzer to monitor the frequency shift and the strength of the signal obtained due to pressure variations [86]. Figure 4.9 shows a block diagram of the pressure sensing, transmitting and receiving mechanism.

4.4.2 Based on capacitive pressure transducer

The MEMS capacitive pressure sensor is part of an *RC* circuit of a 700-kHz (varying with the ICP) Schmitt Trigger oscillator (Figure 4.10). The Schmitt Trigger output modulates the VCO directly. In the ICP device, the VCO is set at a frequency of around 2.44 GHz. The VCO generates a burst of 700-kHz modulated pulses with a duration of 25 μs, at a duty cycle of 0.25%. Figure 4.11 shows the assembly of the implant incorporating the design described above and is depicted in Figure 4.10. At the receiving end, a receiver antenna is connected to a vector signal analyzer to record bursts of pressure dependant modulated pulses. A fast Fourier transform (FFT) of the received signal gives the frequency which is indicative of the measured pressure. Figure 4.12 is a sample of the received signal and the plot of the frequency transform.

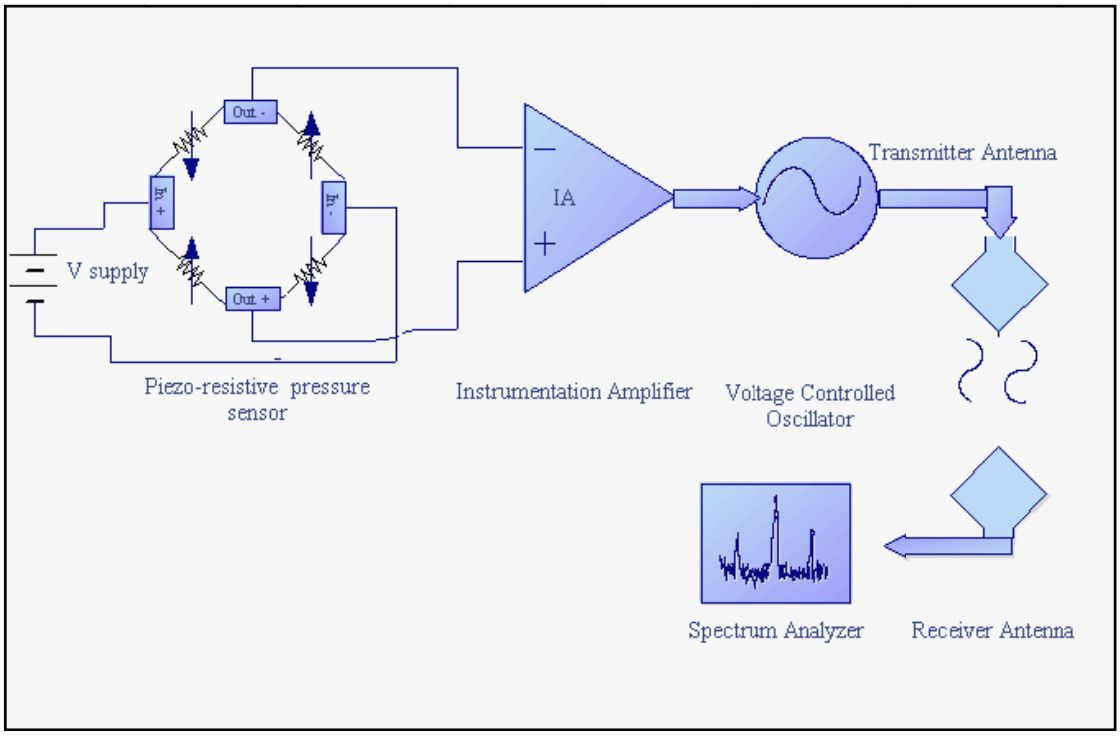

Figure 4.9. Block diagram showing the basic components of transmitter and receiver system for ICP monitoring.

Two types of implantable transmitting antennas were embedded in the implant. In the preliminary work, a commercially available linearly polarized 2.45-GHz chip antenna (AF2.4, Antenna Factor, 2.2 mm×6.5 mm2 in size, Merlin, OR) was used. The antenna was coated with a biograde silicone. However, it was observed that the biocompatible coating and the scalp phantom drastically changed the antenna resonance frequency. Thus, design and characterization of low profile planar (microstrip) implantable antennas for the ICP implant, were performed by Warty, Tofighi et al. [87]. The design specifications of the planar inverted-F antenna (PIFA) that is utilized in the ICP implant are outlined in Figure 4.13 [87]. PIFA typically consists of a rectangular planar element located above a ground plane, a short circuiting plate or pin, and a feeding mechanism for the planar element. These antennas have been characterized for ICP monitoring and elaborate details are reported in [88].

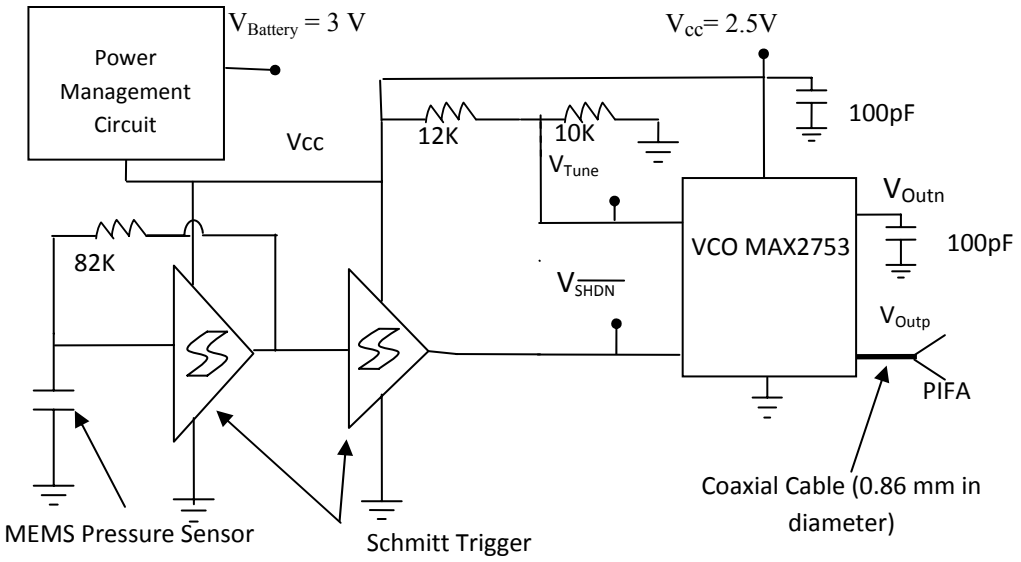

Figure 4.10. Working schematic of ICP implant with a capacitive pressure sensor. PIFA stands for Planar inverted-F antenna

4.5 Materials used in the fabrication of the implant

The materials selected for fabrication of the implants were chosen in compliance with the FDA guidelines.

4.5.1 Choice of metals

In order to make the implants robust, the casings were machined out of metals. Implant grade aluminum, stainless steel or titanium was used for the casing.

4.5.2 Choice of sealants

Cyanoacrylate and silicone rubber were used as adhesives and sealants for the implant. Silicone (Factor II Inc., Lakeside, AZ) was preferred due to the ease of doing any rework during the fabrication process. The electronics and the traces PCBs were sealed in silicone to provide electrical isolation as well as act as barrier for any moisture. This two part silicone was placed

in a vacuum chamber to expel any trapped air bubbles. The silicone was sealed parts were let alone 24 hours for the curing to complete.

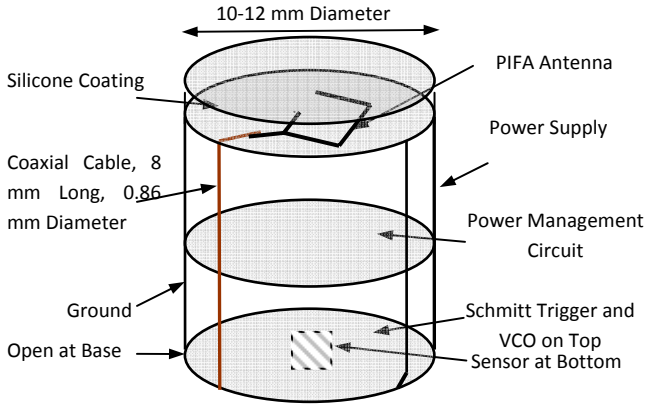

Figure 4.11. The assembly of the intracranial pressure monitoring implant incorporating the circuitry sketched in Figure 4.10.

4.5.3 Choice of superstrate for PIFA

Commercially available silicone (ε_r = 3.7, tanδ = 0.003) [90] was utilized as the biocompatible superstrate for PIFA. The optimal thickness of silicone superstrate on the antenna was determined by our team and is explained in a Master's thesis authored by Ms. Ruchi Warty [88] as well as in [87]. A detailed account of the simulations and experimentations to determine the parameters that are suitable for the use of PIFA as an implantable antenna in the ICP implant is presented in [87, 88]. It was concluded that a layer of silicone, 0.5 mm thick would be ideal for our application, with the chosen dimensions of the antenna (Figure 4.13).

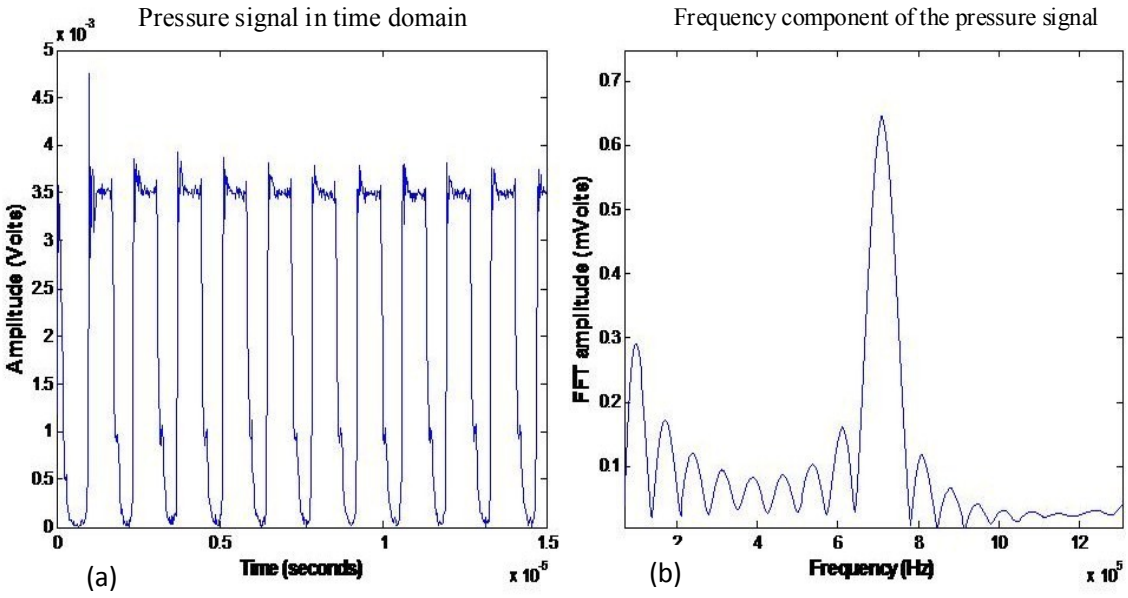

Figure 4.12. a) Time domain pressure dependant signal, b) FFT of the signal.

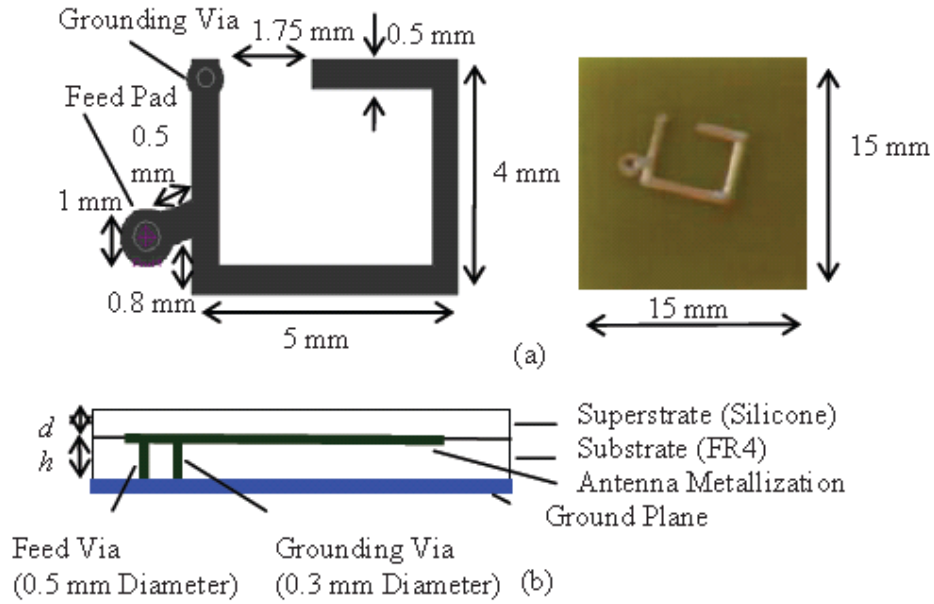

Figure 4.13. Layout of the PIFA geometry; a) top and b) side view of the PIFA metallization, feed, and grounding vias [87].

4.5.4 Choice of biocompatible coating

The biocompatibility of Parylene (polyxylylene) and its popularity in medical applications is discussed in Chapter 3. The last step in the fabrication of ICP implant is to coat the implant with Parylene. Implants coated with 2.5 µm, 5 µm, and 10 µm were evaluated for determining the desirable thickness of the coating. Thick coatings are prone to being peeled off from the surface of the implant. A 2.5 µm thick Parylene was deemed to be optimal due to its good adhesion to the surface of the implant and negligible effect on the sensitivity of the capacitive pressure sensor (discussed in Chapter 5).

4.5.4.1 Chemistry of Parylene

Parylene is a polymeric form of para-xylylene. Parylene C has a Cl atom on the benzene ring and has favourable properties for biomedical applications due to it slow permeability to moisture and corrosive solvents [91], [93]. Figure 4.14 shows the monomeric structure of Parylene, Parylene C [91], and Parylene C in its dimeric form. Parylene is stored in its dimeric form.

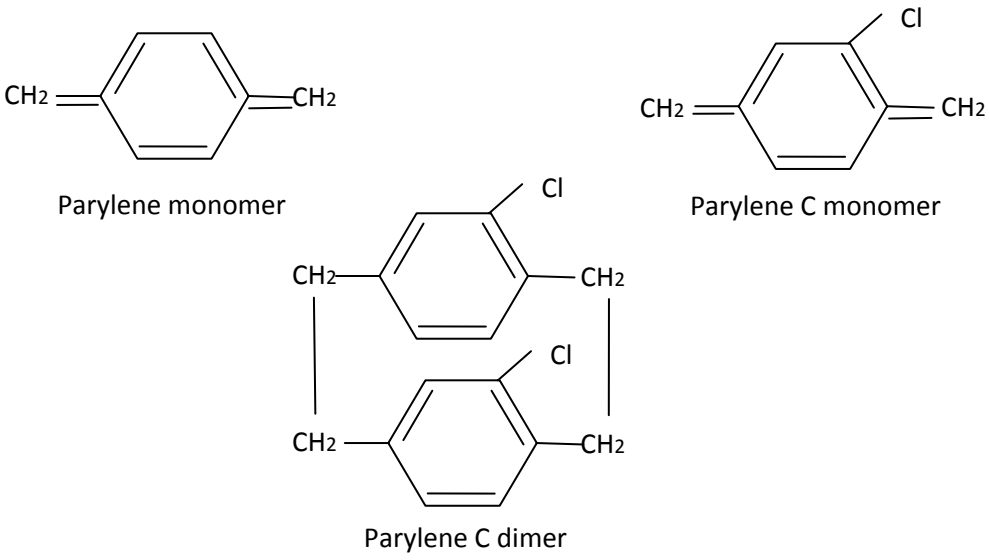

Figure 4.14. Structural formula of Parylene and Parylene C [91].

4.5.4.2 Deposition process

Parylene deposition occurs in vacuum at room temperature. The key steps (Figure 4.15) in the deposition process are:

i) Vaporization: Heating solid Parylene dimer (di-para-xylylene) until it sublimes into the gaseous state.

ii) Pyrolysis: The heating and cleaving of the gaseous Parylene dimer into a monomer (para-xylylene).

iii) Polymerization: The formation of Parylene, as a polymer (poly-para-xylylene), onto the substrate at room temperature.

iv) Condensation: Any unused monomers are trapped on a cold thimble.

Figure 4.16 shows the chemical reaction involved in the polymerization and deposition.

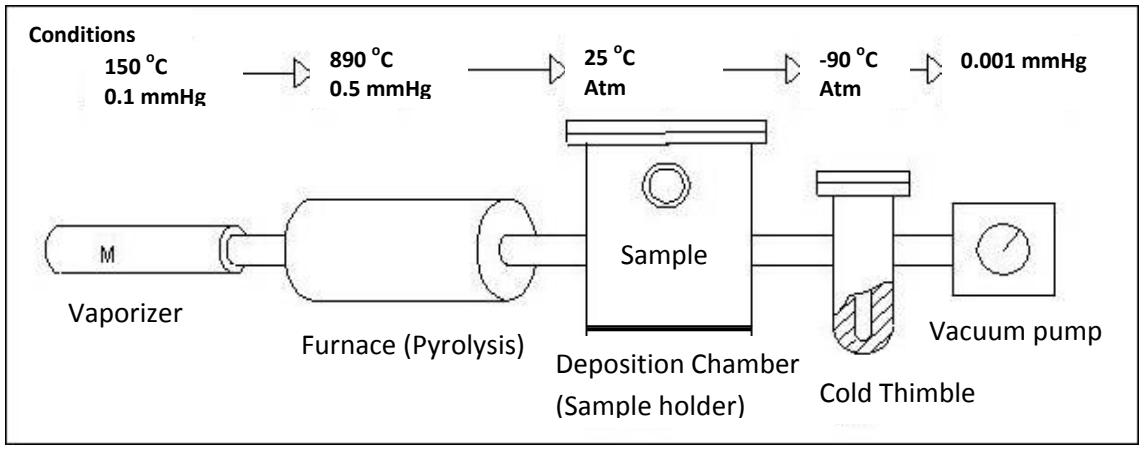

Figure 4.15 Process of Parylene deposition [91].

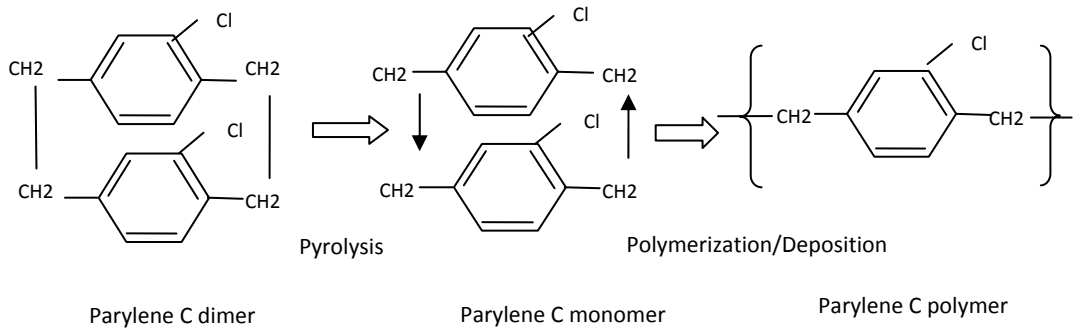

Figure 4.16. Chemical reaction involved in the deposition of Parylene [91].

5. *In-vitro* Evaluation of the Implant and its Characterization

The intracranial pressure (ICP) implants were evaluated for a number of criteria which include the sensitivity to pressure and temperature, repeatability, drift, integrity in water medium, and image artifacts on Magnetic Resonance Imaging (MRI) scans. The first section of this chapter details the materials and method that were employed to devise various test set-ups for testing and characterizing the implant in a laboratory environment. The implants were tested in an air medium, followed by tests conducted in water medium. The implants were calibrated against the current gold standard (Camino catheters) for monitoring of ICP. Thus each test set-up was made with a provision for taking parallel pressure measurements with a catheter. A test method was designed to determine the wireless range of the implant. A number of MRI experiments were done to study the effect of the metal (used to make the implant casing) on the MR images. The results and findings from the aforementioned tests are presented in the second section of the chapter. The chapter concludes with a discussion on the findings of all the experimentations that were carried out *in-vitro*.

5.1 Materials and Methods

5.1.1 Air test set-up

In-vitro tests of the fabricated devices were conducted in the presence of a Camino catheter, used as a reference. These tests were performed in order to establish a relationship between the device signal monitored by a spectrum analyzer or a vector signal analyzer and the pressure obtained by the Camino catheter. The tests were also carried out in an air pressure chamber at room temperature (19-23 ^{o}C). The dry tests were performed inside a sealed chamber based on the sphygmomanometer technique of varying and recording the pressure. Figure 5.1 illustrates the dry *in-vitro* investigational technique. The pressure chamber is connected to a bulb for altering pressure inside the chamber, while a pressure gage displays the chamber pressure. The Camino catheter is placed adjacent to the device. The device antenna (chip or

PIFA) faces a medium emulating the biological environment (polyacrylamide gel [93]). The pressure signal is picked up by a chip antenna [86], [87] followed by a low noise amplifier (ZX60-3018G, Mini-Circuits, NY, USA), before reaching the analyzer.

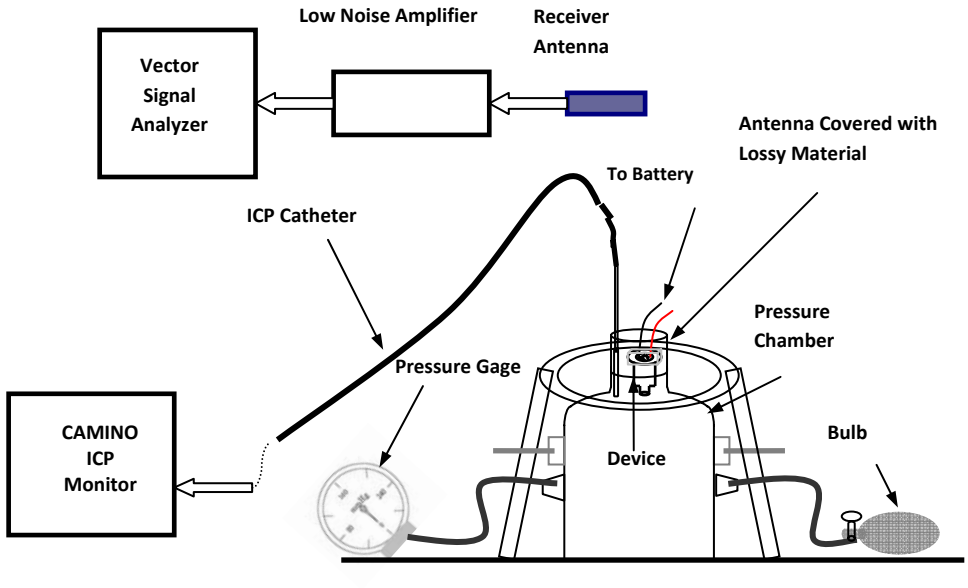

Figure 5.1. Schematic of the set-up based on sphygmomanometer technique for monitoring air pressure

For the purposes of measuring temperature sensitivity of the implants, a heat gun is used to elevate the temperature of the implant from room temperature to 60 C. The frequency as a function of temperature is recorded at atmospheric pressure.

The epidural implants were tested for pressure sensitivity in the dry set-up only. The epidural (ED) implant was soaked in a water/saline medium prior to any *in-vivo* study to determine the integrity of the implant and its readiness for the *in-vivo* study. However, the sub-dural implants with capacitive MEMS sensor (SD_C) were subjected to both dry and wet tests prior to any animal study. The next sub-section gives an account of the wet (hydrostatic) test set-up.

5.1.2 Hydrostatic test set-up

Figures 5.2 and 5.3 illustrate the photograph and the schematic of the hydrostatic pressure measurement set-up, respectively. A graduated water column is connected to a bottle, which acts as a pressure chamber. The implant is fitted in the pressure chamber which is held stationary inside a temperature controllable water bath. The implant in the water chamber is

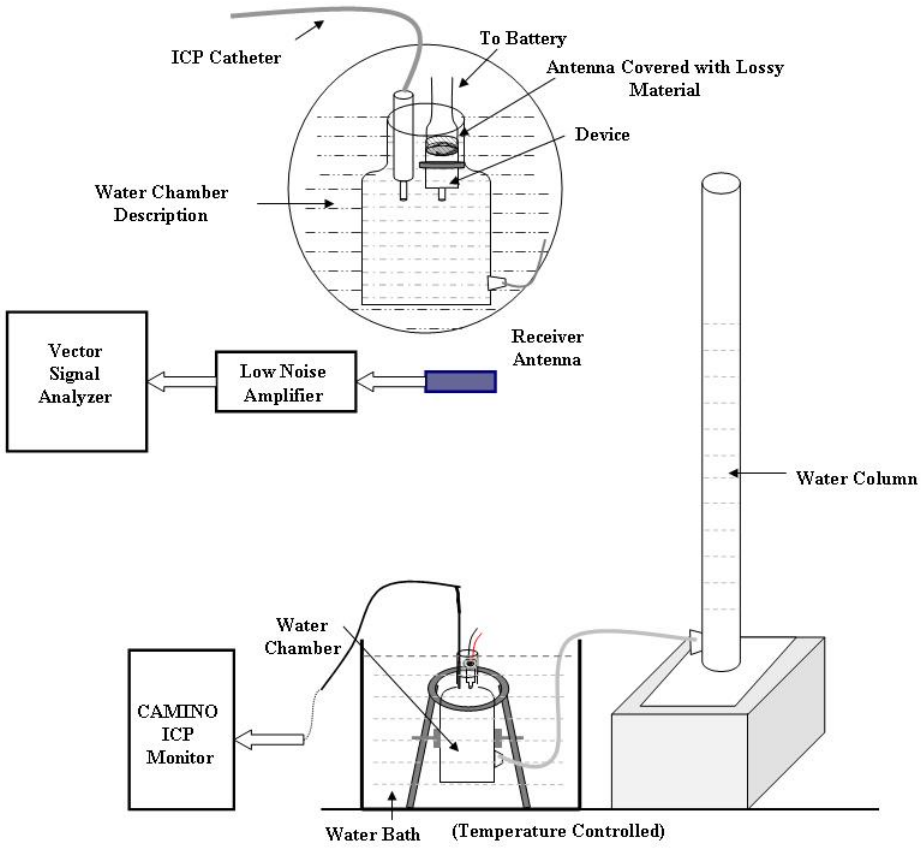

Figure 5.2. Schematic of the hydrostatic pressure measurement set-up [89].

positioned in such a way that the overlying confining surface is 1 cm away from the silicone covered embedded PIFA. This space is filled by a closely fitted polyacrylamide gel phantom [89] or water, emulating the biological environment. The pressure in the system is varied by

adjusting the height of the water in the column. The implant is tested in the pressure range 0-40 mmHg during hydrostatic tests. The pressure in the hydrostatic test set-up was not elevated beyond 40 mmHg due to a possible leakage from the water chamber. In order to determine the temperature sensitivity of the implant in a water medium, the temperature of the water bath was varied from room temperature to 40 ^{o}C. Measurements were taken while increasing and decreasing the temperature, and maintaining a fixed pressure.

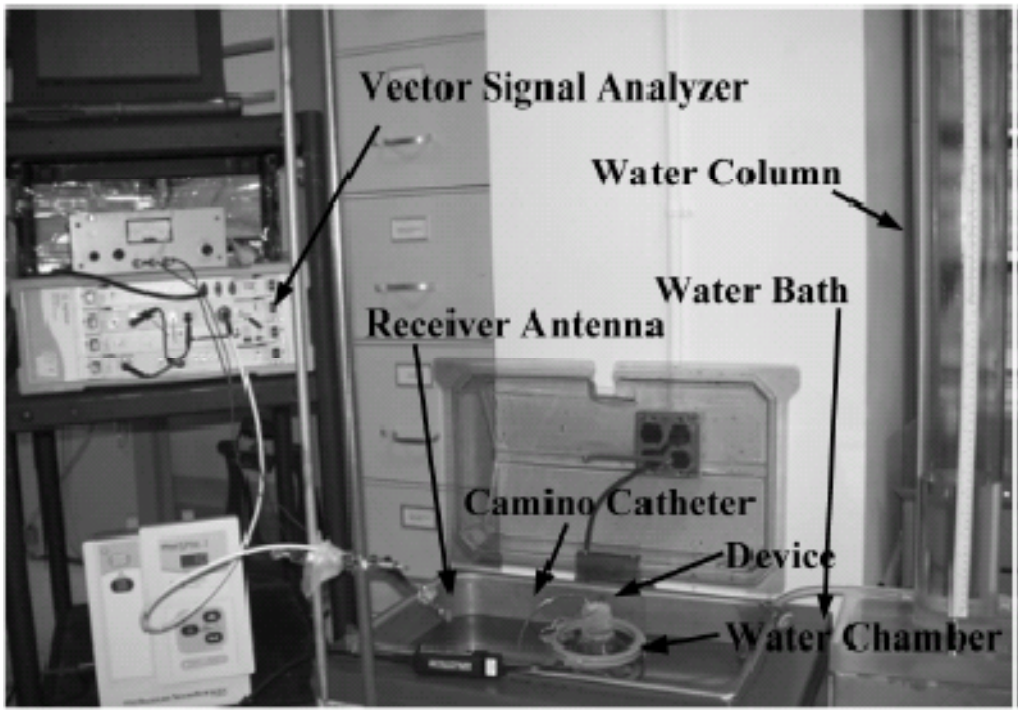

Figure 5.3. Photograph of the set-up for hydrostatic pressure measurements.

5.1.3 Microwave transmission

A study was carried out for quantifying the microwave transmission through a polyarylamide gel phantom by using the commercial chip antenna. The PIFA was extensively studied in this regard by our team [87, 88]. The details of polyacrylamide gel phantom and the set-up for performing measurements on chip antenna are presented here. The phantom electrical

property was measured by a coaxial probe to be ε_r (Permittivity) =50 and σ(Conductivity)= 2.2 S/m at 2.45 GHz.

5.1.3.1 Polyacryamide phantom

Skin phantom models are applied in simulation of the tissue behavior to microwave frequencies. For equivalence between the phantom and biological tissue three different parameters can be considered. Electrical parameters like circuit properties, power transfer, internal electromagnetic power deposition, and internal temperature distribution are the most significant. In order to have equivalent electrical property, the phantom material is required to have real and imaginary parts of permittivity (electrical/ magnetic) equal to that of the tissue material to be simulated i.e., scalp.

Polyacrylamide gel is a convenient and an effective phantom. It has noted advantages as following [91]:

i) The transparency is modifiable and is also good in the optical range. This gel can also be conveniently used to simulate optical behavior of tissue,

ii) It can be easily prepared with a wide range of reproducible electric parameters,

iii) It is solid elastic,

iv) It can be molded in any form,

v) It has convenient mechanical characteristics- self –sustaining without any physical support, soft enough to be pierced or stable insertion of needles, wires, thermocouples,

vi) The recipe ingredients are easily available, and

vii) The preparation time is 15 minutes and curing time is approximately 1 hour for volume of 50cc phantom.

The only drawback is that this phantom looses moisture over a period of time. However, if stored in an air-tight condition its properties are maintained for a longer duration.

The base material in preparation of the gel is Acryalamide (C_3H_5NO) which polymerizes after addition of water. Gel is doped with sodium chloride (NaCl) for required conductivity. Permittivity can be changed by varying the quantity of water by substituting water with other liquids like dioxane, pyridine, and ethane diol. The phantom material is cast in liquid form. Additional material can be added after polymerization by negligible mixing or subsequent diffusion to alter electrical properties.

5.1.3.2 Phantom recipe

The base formula for the preparation of polyacrylamide gel is detailed here [90, 93, 94]. Ingredients of the gel are:

i) Polymeric acrylamide (C_3H_5NO),

ii) Polymerization catalysts:

MBA (N, N'-methylene bis-acrylamide $C_7H_{10}N_2O_2$) ,

TMEDA (N,N,N',N' –tetraethyl ethylene diamine ($C_6H_{16}N_2$) ,

iii) Primer: Ammonium persulphate (AP),

iv) NaCl, and

v) Water.

Two solutions are separately made and mixed for polymerization to form the polyacrylamide gel. They are:

Solution 1: A total volume of 47 cc is made with acrylamide, MBA, TMEDA, NaCl , and water

Solution 2: 1.3% by weight solution of AP in water.

Solutions 1 and 2 are mixed to start the polymerization reaction which is an exothermic process.

For our recipe, the gel contained 9 g of acrylamide, 0.05 g of MBA, 0.25 cc of TMEDA, 0.238 g of NaCl, 3 cc of 1.3% (by weight) AP, and deionised water in a total volume of 50 cc. The measured complex permittivity within the desired range of frequency is provided in [85].

5.1.3.3 Effects of ingredients on the electric properties of the phantom

i) NaCl: Salt content is a major determinant in the conductivity values of the phantom. With no salt added, base conductivity of 0.15 S/m is obtained at room temperature at 2.4 GHz. This value is attributed to the presence of AP.

ii) AP: AP influences the conductivity. With no salt added lower conductivities are created by lowering the AP content. However, reducing AP increases the setting time of gel. The reaction can be hastened by increasing temperature. If there is no AP present , the gel has zero conductivity and the temperature has to be increased to the melting point of Acrylamide to cause polymerization to complete faster. Increasing AP and NaCl can yield all practical values of the conductivity.

iii) Acrylamide: This compound controls permittivity. By altering the monomeric quantity and accordingly varying the water content, the permittivity is changed. For example, doubling acrylamide, reducing water, and maintaining TMEDA and MBA stoichiometric ratio, causes reduction in the permittivity and a slight lowering of conductivity. This would also increase the mechanical strength of gel. An increase in the acrylamide content alters the transparency of the gel. Higher concentrations of monomer lead to highly exothermic reaction, loss of transparency due to inhomogenity, and discontinuities in the internal surfaces.

iv) Water: Water being polar in nature has an effect on the conductivity of the gel, but the extent is negligible. Reducing water content causes reduction in the permittivity.

v) Non-polar and low permittivity liquids: Water can be replaced by these liquids to alter dielectric constant of phantom. These liquids should be solvents for the compounds used in the recipe, be non-ionic to avoid any un-necessary contribution to conductivity, be miscible with water, and have high boiling temperature to tolerate the exothermic process. Some examples are dioxane, pyridine, ethylene glycol (ethane diol).Care should be taken with handling certain reagents like dioxane – a harmful chemical. It must be handled under a fumehood. It also alters transparency of phantom. Ethylene glycol on the other hand makes the material sticky [90].

5.1.3.4 Test-set up for measuring microwave transmission through scalp phantom

An *in-vitro* set-up (Figure 5.4) was arranged to emulate the actual scenario of the device embedded in a highly absorbent tissue medium. The device was sealed with a biocompatible grade silicone, covered by the gel and immersed in water up to the level of the phantom. In absence of a phantom, the water level was sufficiently decreased to avoid overflowing the gel. It should be mentioned that the received signal strength is highly dependent on the polarization mismatch and the multipath environment. The receiving antenna was first oriented for the best polarization match and then the distance measurement was performed.

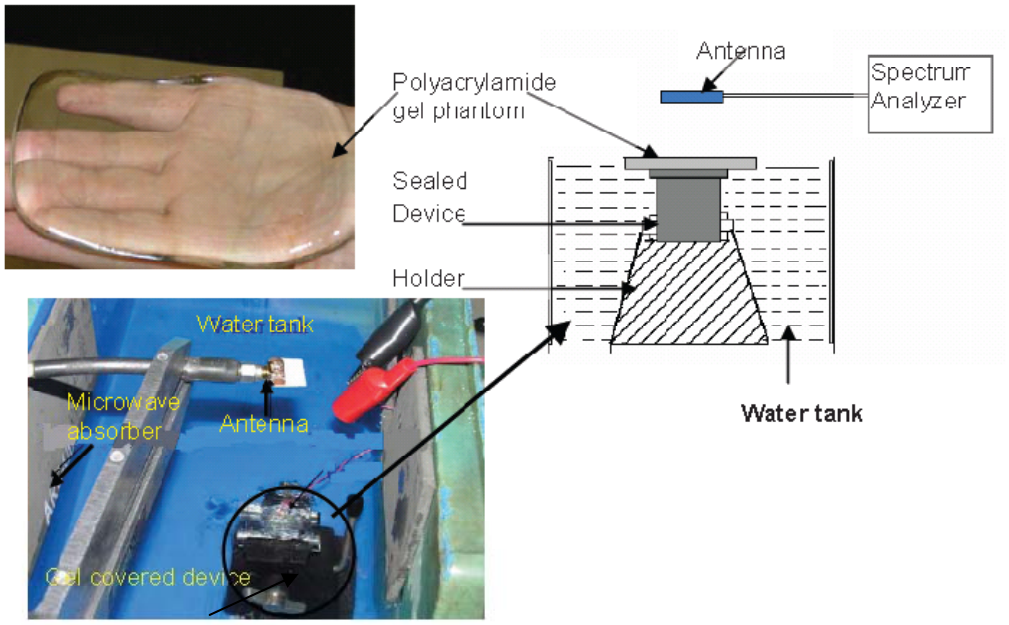

Figure 5.4. Set-up for measuring microwave transmission through a scalp phantom. Microwave carbon absorbers are used to avoid multi-path.

5.1.4 Stability of Parylene coating

In addition to testing the 2.5 µm thick Parylene coating on a complete ICP implant, the coating was also tested in a simplified assembly. The simplified assembly made of only the RC Schmitt Trigger configuration. Note that Schmitt Trigger oscillator (for capacitive MEMS implant) generates an approximately 700 kHz signal, whose frequency varies with the pressure. The simplified assembly was enclosed by silicone and coated with Parylene before being immersed in 0.9% saline. In a complete implant configuration the implant and hence the effectiveness of the coating was monitored for a maximum period of 14 days. The simplified assembly was immersed and left undisturbed in saline for a duration of 18 months (see section 5.2.4).

5.1.5 MRI compatibility test

Three different designs of the ICP implants, as shown in Figure 5.5, were tested. Firstly, the devices were tested to see how strongly they experienced force and torque in the MR

environment. The cases were made of stainless steel, aluminum, and titanium for implants #1, #2, and #3 (Figure 5.5), respectively. Secondly, general gradient-echo (GRE) and spin-echo (SE) images were acquired to observe how the device distorts the magnetic field due to magnetic susceptibility ($\chi_m/10^{-6}$ cc/mol). A conductive agar-gel phantom (7g/liter agar, 170mM NaCl, 6.3mM $CuSO_4$) was prepared for temperature measurements as well as GRE and SE scanning, as shown in Figure 5.6(a). Each device was placed in the agar-gel phantom as depicted in Figure 5.6(b). Finally, temperature changes near the probe were monitored with thermo-optic probes while RF pulses with a time average power of 16.65W were delivered to the coil over a period of 2 minutes [96],[97]. The placement of four optical probes (Ch 1- Ch 4), for measuring the temperature is also indicated in Figure 5.6.Two temperature probes (Ch 3 in the front and Ch 4 on the top of this device) were positioned close to the device and two other probes (Ch 1 and Ch 2) were placed far from it. The near and the far probes were placed symmetrically in the cuboid gel phantom as indicated in Figure 5.6. The results of these tests are presenting in section 5.2.5.

Figure 5.5 The casing material of ICP devices. The casing material of the implant #1(Type SD_Cap_C), #2 (Type ED_Cap_C), and #3 (Type SD_Cap_C) was stainless-steel, aluminum, and titanium, respectively.

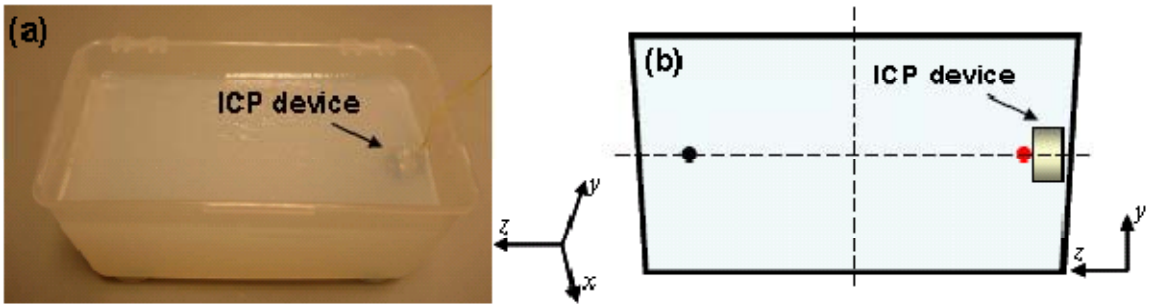

Figure 5.6. (a) Conductive agar-gel phantom. (width×height×depth=15×7×8.5cm3) (b) One thermal sensor (red spot) was placed in front of the device and the other sensor (black spot) was placed at the opposite location.

The MRI compatibility tests were conducted by Dr. Sukhoon Oh in the Department of Radiology, College of Medicine, Pennsylvania State University, Hershey, PA.

The next section is a compilation of results that were obtained from various experimentations conducted on the ICP implants in environments and set-ups described here.

5.2 Results

5.2.1 PZR epidural ICP implant (PZR_ED_C)

The performance of two implant prototypes that were tested in air is presented here. Figure 5.7 is a plot of frequency versus pressure. Figure 5.10 shows the performance of the implants with a variation in temperature and supply voltage. The results are tabulated in Table 5.1.

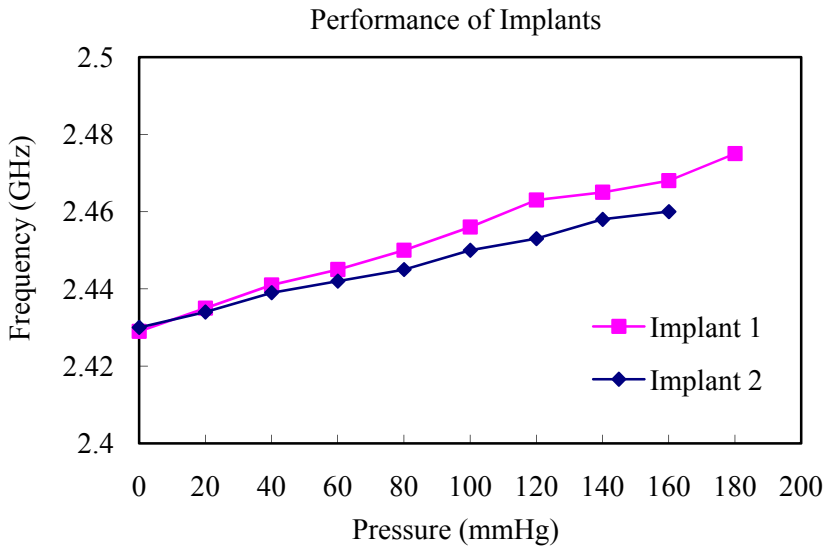

Figure 5.7. The variation in transmitted frequency as a function of pressure. Tests were conducted at room temperature in air [86].

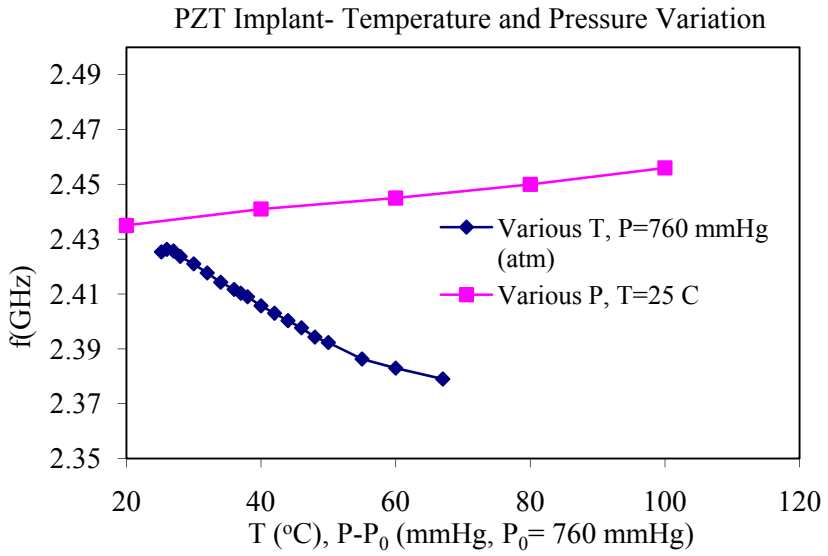

Figure 5.8. The effect of temperature and supply voltage on the transmission frequency of implant. Tests were conducted at atmospheric pressure.

Table 5.1. Measured performance of PZR_ED implant in terms of the frequency (f), received power (P_{Rec}), and frequency sensitivity, i.e., the rate of change of frequency with pressure ($\delta f/\delta(\Delta P)$), temperature ($\delta f/\delta T$), and supply voltage ($\delta f/\delta V_{cc}$) changes [86]. $\Delta P = P - P_o$, where P_o = 760 mmHg. d is the separation between the implant and the receiver antenna.

Parameter	Test conditions	Value
$\delta f/\delta(\Delta P)$,	T = 25°C, V_{cc}= 2.8 V	0.30 (MHz/mmHg)
$\delta f/\delta T$	T = 37°C, ΔP=0, V_{cc}= 2.8 V	-1.35 (MHz/°C)
$\Delta f/V_{cc}$	T = 37°C, ΔP=0	18 (MHz/V)
f	T = 25°C, ΔP=0, V_{cc}= 2.8 V	2.429 (GHz)
f	T = 37°C, ΔP=0, V_{cc}= 2.8 V	2.410 (GHz)
P_{Rec}	T = 25°C, d= 10 cm, ΔP=0, V_{cc}= 2.8 V	-60±3 (dBm)

5.2.2 Capacitive MEMS ICP implant

In total 20 implants based on the capacitive pressure sensor were tested and calibrated in an *in-vitro* setting. Two versions of pressure sensing elements were provided by the manufacturer (VTI Technology, Finland) over the course of time. The earlier versions exhibited unpredictable behavior in the presence of humidity. Thus a modified version of the sensor was later developed by the manufacturer. Out of the 20 devices that were fabricated, 15 were designed for large burr holes (10-12 mm, Cap_ED_L_C or Cap_SD_L_C) and 5 were designed for small burr holes (3-4 mm, Cap_SD_S_C).The older version of the sensor was used in 9 Cap_SD_L_C implants and the rest were built with the improved version. These implants were characterized in air and water. A sample time domain signal picked up from the device as captured by the VSA is shown in Figure 5.9. To measure the pressure, fast Fourier transform is applied to the raw time domain data to determine the Schmitt trigger frequency which is directly related to the pressure. The sensitivity (frequency as a function of pressure) varied between implants, but was fixed for a single implant. For the sake of conciseness, results from a single

implant are presented. It must be noted that the trend of results for all the implants remained essentially the same. For example, the sensitivity of the implants over the pressure range of 0-100 mmHg was -0.377 kHz/mmHg ± 0.028 (average± standard deviation). As an example, one of the Cap_SD_L_C implants is presented here [89].

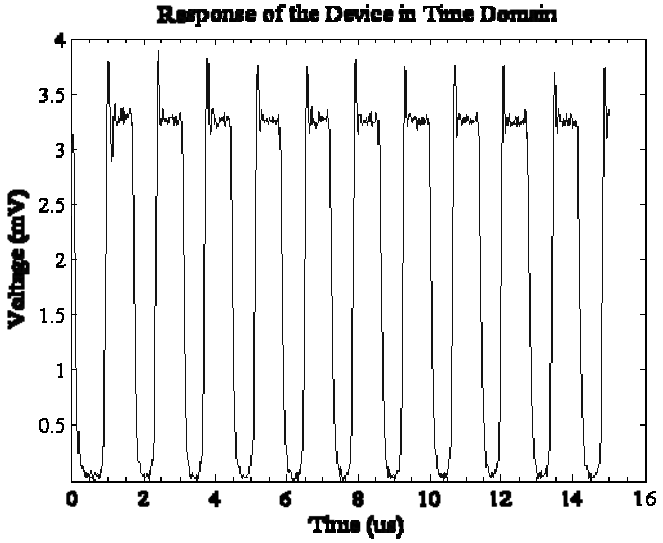

Figure 5.9. A typical time domain signal containing the pressure information, as captured by the VSA [89].

5.2.2.1 Temperature sensitivity

Temperature variability tests were performed in the range of 22-45 °C in water to determine the effect of temperature on the device performance. The implant exhibited an average temperature sensitivity of -0.325 kHz/^{o}C (corresponding to 0.87 mmHg/^{o}C pressure reading drift for this implant), obtained by hydrostatic measurements at a pressure of 0 mmHg.

5.2.2.2 Sensitivity and the effect of Parylene coating

The implant was tested after being coated with Parylene, over the range of 0-100 mmHg, in the air pressure set-up, at room temperature, and over a period of 5 days. Figure 5.11 shows the graph of the results obtained for the repeated trials (one trial before Parylene coating

and five trials after Parylene coating). The zero pressure sensitivity of the implant in air prior to the coating was -0.362 kHz/mmHg, which changed to -0.336 kHz/mmHg after Parylene coating. A frequency shift of 7.48 ± 0.09 kHz (mean ± standard deviation) was observed as a result of the Parylene coating (Figure 5.10).

5.2.2.3 Repeatability in air tests

At zero pressure, the device demonstrated a standard deviation of ±0.951 kHz which corresponds to ±2.6 mmHg zero pressure drift.

5.2.2.4 Repeatability in hydrostatic tests

The implant was also tested in the hydrostatic set-up for its integrity and performance under variable hydrostatic pressure at a fixed temperature. An average shift of 22.90 kHz from the performance in air tests was seen. However, the sensitivity of -0.373 kHz/mmHg was not significantly different from the air tests. The mean frequency at 0 mmHg was 710.73 kHz with a standard deviation of ±0.713 kHz, which corresponds to ±1.91 mmHg zero pressure drift. Figure 5.10 also shows the performance of the Parylene coated implant in different trials (twelve trials for the hydrostatic set-up). It should be emphasized that the implant was kept immersed in the hydrostatic set-up for the entire measurement period (twelve days), while the data was being collected.

The Cap_SD_S_C , i.e., sub-dural for small burr holes (see Figures 4.4 and 4.7, Chapter 4) implants were also studied in air and water. As an example, one of the implants exhibited a sensitivity of -0.401 kHz/mmHg in air and -0.399 kHz/mmHg in water.

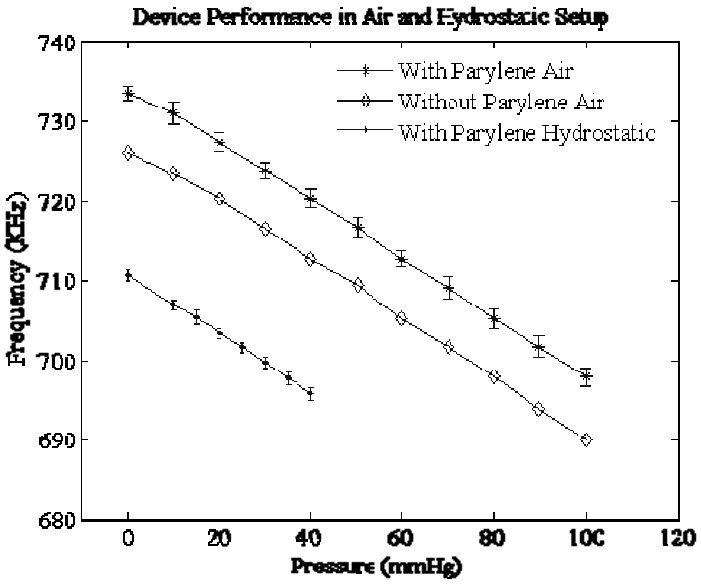

Figure 5.10. The performance of implant in the air pressure before Parylene coating and over repeated (five trials) measurements for five days after Parylene coating compared with the performance of the Parylene coated implant over repeated measurements (twelve trials) in the hydrostatic pressure set-up for twelve days. Error bars indicate measurements' standard deviation [89].

5.2.3 Microwave transmission

A preliminary microwave transmission experiment was conducted on our PZR implant with a chip antenna (Figure 5.4). With the device covered by a scalp phantom, the detected signal, received by an identical chip antenna, was only about 8-13 dB below the case without the phantom [85], [86] (Figure 5.11), for measurements up to a distance of 1 m. The scalp insertion loss was about 10.5 dB on average. This measurement was done within a multipath environment. The chip antenna was later replaced by PIFA. Therefore, comprehensive studies were carried out for microwave transmission in a dedicated microwave chamber set-up [87]. An understanding of effective isotropic radiated power (EIRP) or effective radiated power (ERP) from a transmitting antenna is useful in comparing the radiation against the regulatory limits that are put forth by FCC. The EIRP for 2.4 GHz ISM-band short range communication is -1.25 dBm [87]. The EIRP value is same as the antenna gain, with respect to an isotropic source, for

1W of power that is delivered to the antenna. As it is described in [87], three PIFAs labeled as Antenna_I3, Antenna_II1, and Antenna_I4 were used to evaluate ERP per 1W delivered to the PIFA, denoted as E_{1W}. The E_{1W} for the given PIFAs over a range of frequency (2.2 -2.8 GHz), with a separation of 27.9 cm between the transmitting (PIFA) and receiving (chip antenna) antenna, is shown in Figure 5.12.

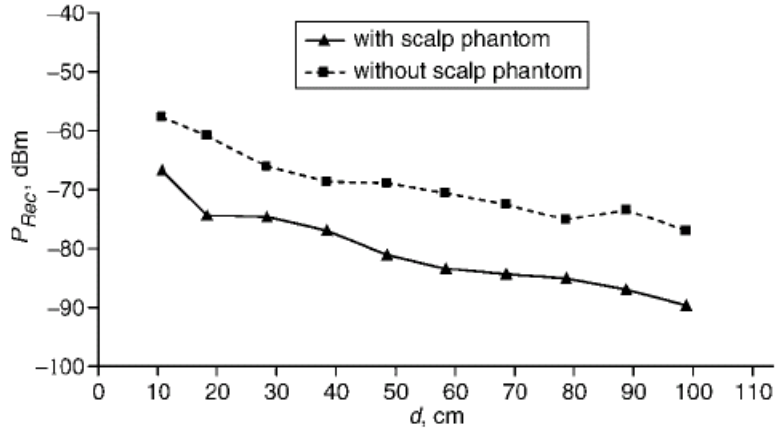

Figure 5.11. Received power (P_{Rec}) against distance (d), with and without scalp phantom [85]. Measurements performed with a chip transmitting antenna at room temperature, atmospheric pressure, and 2.8 V supply voltage to implant.

The low values of the evaluated E_{1W} that are obtained here suggest that (as could be expected) a medical implant requires a large amount of power delivered to the antenna before

ERP becomes an issue. Therefore, the SAR limit dictates the maximum device power rather than the regulatory ERP (EIRP) value. We have performed finite-element simulation for evaluating the SAR, which demonstrates that for the present level of output power (10μW) from the ICP implant [85]–[88], the peak SAR level is approximately 4 mW/kg, which is far below the regulatory limit of 1.6 W/kg. This implies that this maximum SAR would be reached with

dBm (for CW operation). This value corresponds to an EIRP of 0.013 mW (-18.8 dBm),which is far less than the EIRP limit of -1.25 dBm at 2.45 GHz.

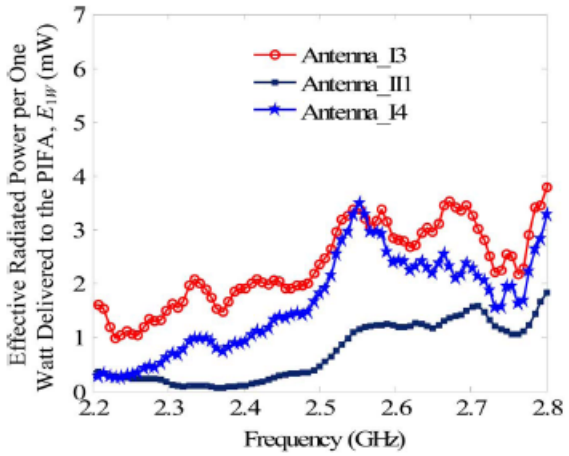

Figure 5.12. ERP per 1W delivered to the PIFA (E_{1W}) versus frequency for a separation of 27.9 cm between transmitter and receiver antennas for three PIFAs [87].

5.2.4 Effectiveness of Parylene coating

The efficacy of 2.5 µm Parylene coating was studied on a simplified assembly composed of the capacitive MEMS sensor, 82 KΩ resistor (forming RC), Schmitt Trigger, and a power management circuit. Three wires were drawn out from this assembly for power supply and probing the Schmitt Trigger for the pressure dependant modulating frequency. These assemblies were continuously monitored for a period of days, following which the power was disconnected, and the assemblies were immersed in 0.9 % saline for approximately 18 months. The frequency at the output of the Schmitt Trigger was recorded to be 698.91 ± 0.0128 kHz (mean ± standard deviation) and 777.66 ± 0.048 kHz (mean ± standard deviation) for the two assemblies. The above standard deviations for the two assemblies correspond to ±0.033 mmHg and ±0.127 mmHg respectively, a drift that is considered to be negligible. After 18 months a

stable signal was observed at the Schmitt Trigger from both the assemblies. The measurements were taken for a period of one hour. The frequency was recorded to be 699.69 ± 0.833 kHz (mean ± standard deviation) and 776.42 ± 0.456 kHz (mean ± standard deviation) for the two assemblies. The average drift over the period of 18 months was recorded to be 2.1 mmHg and 3.2 mmHg, respectively.

5.2.5 MRI compatibility studies

Implant #1 experienced significant force and torque near the 3.0T magnet, as a consequence of that, it could not be held stationary in a gelatin phantom, therefore, further experiments were not performed with that implant. Implant #2 (Al) and implant #3 (Ti) experienced very little and no discernable force, respectively. Therefore, implant #2 and #3 were suitable for further testing. Significant precipitation was observed on implant #2 during phantom preparation, apparently due to interaction between the aluminum casing and the copper sulfate in solution (used to shorten T1 relaxation time). When the copper sulfate solution was replaced with a 1% gadolinium solution, there was no precipitation. In GRE images, significant image distortions were observed near both implant #2 and #3, due to the relatively large difference in the magnetic susceptibility of the materials and the medium (agar-gel). The image distortions could not be compensated even by using SE sequence as shown in Figure 5.13. The magnetic susceptibilities of aluminum, titanium, and water are +16, +151, and -1.04, respectively, though the values for aluminum and titanium depend somewhat on how they are alloyed [98]. The image distortions precluded the use of MR thermography to measure temperature changes near the device during RF heating with methods demonstrated recently [96]. Therefore, the temperature changes were recorded using fiber optic thermal sensors (OpSens, Canada) near the ICP implant and at a location opposite to the implant (in the absence of the implant SAR and temperature change at these two locations would be identical). The rate of temperature change near implant #2 was 0.100°C/min compared to 0.040°C/min at the opposite location, as shown in Figure 5.14(a). Implant #3 (of smaller diameter and titanium

casing) showed a very similar temperature change rate (0.045°C/min) to the opposite location (0.040°C/min), as shown in Figure 5.14(b).

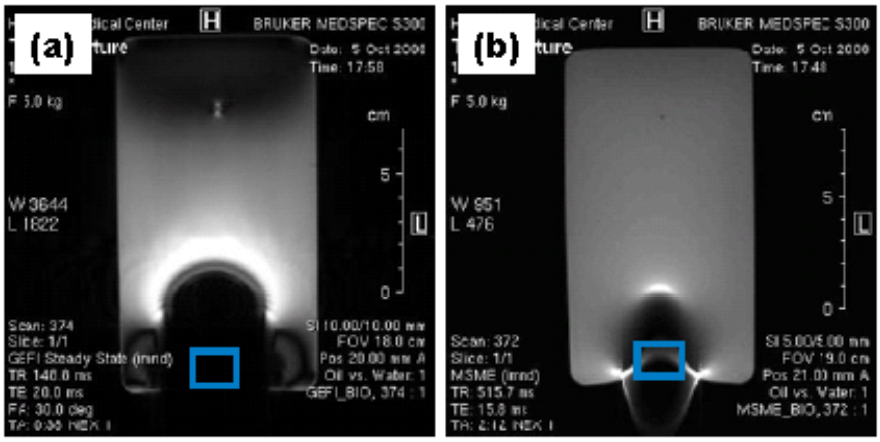

Figure 5.13. (a) Gradient-echo and (b) spin-echo image of implant #2. Similar image distortion was observed for implant #3 (not shown here). Blue rectangle indicates the position of ICP implant.

5.3 Conclusions and discussions

The MEMS capacitive pressure sensors exhibit better performance than the PZR sensors. However, the capacitive sensors of desired characteristics were not available at the start of this work. The initial prototypes of the implant were built with PZR sensors. These implants were used in conducting the preliminary studies to prove the concept of a wireless embedded ICP monitoring.

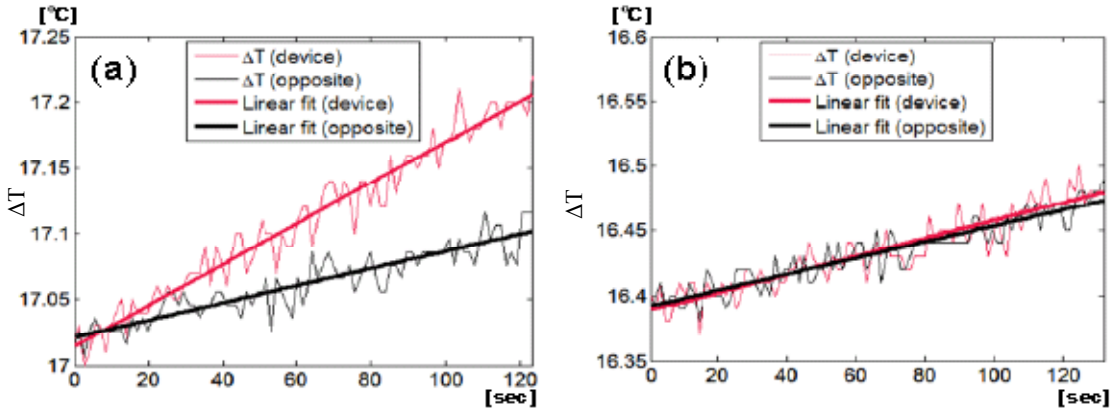

Figure 5.14. (a) Temperature changes (ΔT) near the ICP device #2 (aluminum casing) and (b) device #3 (titanium casing). In each figure, red and black lines correspond to red and black spots in Figure 5.6 (b).

The MEMS capacitive pressure sensors, subsequently acquired from a commercial source, exhibited erroneous behavior when tested in an animal (discussed in Chapter 6). The performance of the sensors was sensitive to the changes in humidity. However, the new improved sensors, which were believed to be stable under varying conditions of humidity, were tested over time in an *in-vitro* water medium (mimicking the biological environment). The reliability of these sensors in the *in-vitro* experiments was established. The sensors demonstrated a corresponding pressure drift (uncertainty) of better than ±0.13 mmHg and ±1.9 mmHg when tested as part of the Schmitt Trigger (for a period of 11 days) and the complete device (for a period of 12 days), respectively. The device drift can be improved by further modification and the integration of implant circuitry.

Parylene coating was determined to be reliable in maintaining the integrity of the implant in saline and in *in-vivo* environment (discussed in Chapter 6).

6. *In-vivo* Evaluation of the Implant

In the development of a medical device it is required to show equivalence of response between the standard method and any new method developed. For this reason, animal studies were conducted with the intracranial pressure (ICP) implant. The overall goal of performing *in-vivo* experimentation was to establish a correlation between measurements acquired from the gold standard and the ICP implant, and biocompatibility assessment of the implant. This chapter describes the protocol for performing animal studies, the choice of animal model, types of measurements, and the findings from each animal study. In general, the goal was to implant the ICP implant and Camino ICP catheter on the contralateral sides of the frontal bone. Concurrent measurements were taken from both techniques for a short duration of time. ICP catheter was removed and the implant was monitored for a predetermined duration. All the *in-vivo* studies are individually described here which includes the findings from each study. Under normal circumstances, limited variation in ICP is expected in an animal. As a result, a method was devised to induce intracranial hypertension (ICH) at the end of one animal study. This enabled a comparison between the two methods over a wide range of pressure.

6.1 Choice of animal model

The choice of an experimental animal is critical in predicting the outcome of a study in human trials. The cranial size of large animal models, such as swine is comparable to that of human cranium and can accommodate the ICP implant device as well as the commercial pressure monitor. The first animal of choice was a miniature Yorkshire pig due to the fact that pigs share many physiological and anatomical similarities with humans [99], [100]. However, the presence of large pneumatic cavities in the frontal region [101] of pigs is not favorable of ICP evaluation. Consequently, only one *in-vivo* study was conducted in a pig and further experiments were conducted in canine models [56], [102-105]. There is a large body of data available in the literature on the use of beagle dogs in ICP and head injury experimentation. In

addition to the size of head, large animals were chosen instead of small animals like rodents or rabbits due to a higher probability of reproducing the results from animal studies in humans.

6.2 Number of animals

A power based assessment for determining the sample size is considered. The important factors to be taken into account are significance criteria (Type I error or α i.e., false positive), power = 1-β (where β is the probability of Type II error, i.e., false negative), and effect size (d). In this experimental design, no prior knowledge on the long term performance of the ICP implant in animals is available. The values for α, which are considered to be practical are in the range of 0.05 – 0.1, but not greater than 0.1[106], [107]. As per the available literature on the design of animal experiments, the acceptable values of power are from 0.7 to 0.9 [107]. The values of α and power recommended by most researchers are 0.05 and 0.8 respectively [106], [107]. A discussion on the selection of population effect size is found in [108].

With the desired values of α, power, and d, the power tables in [109] can be used to determine the size of the sample for an experimental design. For our study, we consider d= 0.80, α = 0.05, power= 0.80, sample size= 20 (from the power tables in [109]). Thus selecting a sample size of 20 animals gives an adequate combination of significance criteria, desired power, and effect size for the overall goal of translating this work from animal studies to clinical trials in future. However completion of animal studies on 20 animals is beyond the scope of this thesis. Consequently, 7 animal studies were conducted as a part of this work. With this sample size the power of the study reduces to 0.7 (from the power tables in [109]).

The animal studies were conducted in compliance with the Institutional Animal Care and Use Committee (IACUC) guidelines. An IACUC approved protocol was adhered to while conducting the studies.

6.3 Pre-surgical preparation of animal

The animal was allowed to get acclimatized for a period of at least one week prior to the study. It was ensured that the animal is exhibiting a normal behavior to avoid any unpredictable influence on the study. The food intake, excretion, and weight were monitored during the acclimatization phase. Food was withheld for 12 hours prior to anesthesia.

6.4 Anesthesia protocol

A dose of atropine 1ml (intramuscular) was injected followed by thiopental (5mg/Kg, IV). Thiopental caused unconsciousness within 30-45 seconds. An endotracheal tube was inserted and the dog was put on a ventilator. Anesthesia was maintained by continuous isofluorane (1-2%) inhalation. Buprenorphine was given preemptively at 0.01 mg/kg (intramuscular) prior to the surgical procedure.

6.5 Surgical procedure

The surgical procedures were carried out by Dr. Francis Kralick, Department of Neurosurgery, Drexel University College of Medicine, with assistance from Ms. Kimberly Wasko, Department of Surgery, Drexel University College of Medicine. Anesthesia was administered as outlined previously. The scalp was shaved and prepped using betadine scrub. Betadine paint was then used and incisions were demarcated using a sterile skin marking pen. A 4 cm incision was made on the left side of the scalp, 1 cm from midline and centered 1cm posterior to the coronal suture. Subcutaneous tissues were dissected using unipolar electrocautery. A self-retaining retractor was placed. A cutting burr was used on a high speed drill to trephine the skull in a circular fashion. The dura mater beneath the bony opening was left intact for epidural studies and punctured for access to the sub-dural space for sub-dural studies. Figure 6.1 shows a large burr hole drilled in the skull with intact dura mater for an epidural study. Figure 6.2 shows a small burr hole for a sub-dural implant. These figures also present a comparison between the two sizes of burr holes. It is worthwhile to mention that the

efficacy of the implantation procedure increases many times in the second case, owing to the ease and rapidness of drilling a small burr hole.

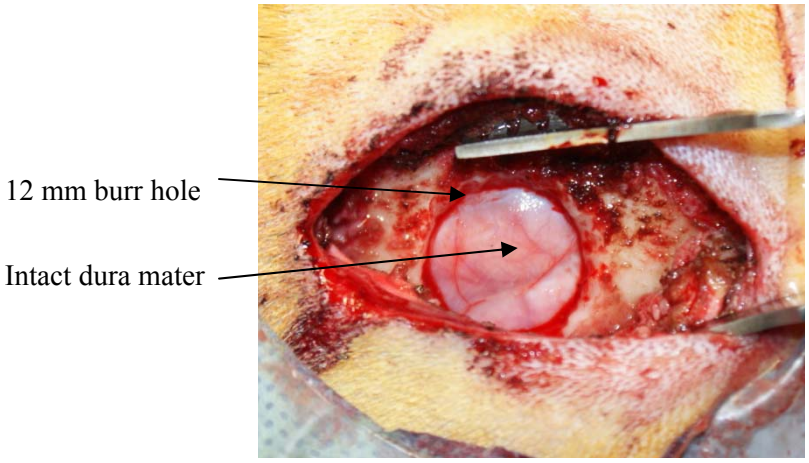

Figure 6.1. Photograph showing a section of intact dura mater as a site of epidural pressure sensing.

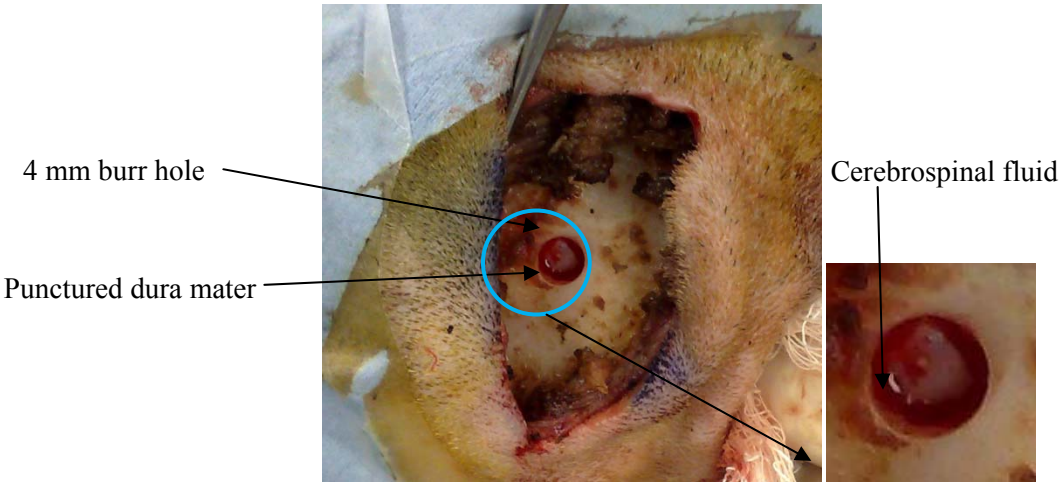

Figure 6.2. Photograph showing a section of pnctured dura mater for aceess to sub-arachnoid space in the case of sub-dural pressure sensing. CSF can be seen in the sub-section of the picture shown to the right.

An adjustable collar that was provided with implants for large burr-holes was set to the proper depth dictated by the thickness of the skull. Set-screw were tightened to maintain proper depth. The device was then fixed to the skull with 4 self-drilling, self-tapping 8 mm screws. The set-screws for fixing the level of flange are seen in Figure 6.3. Figure 6.4 shows the self-tapping screws that fix the implant to skull, and an unsutured incision above the implant that is positioned in skull. The scalp was closed using interrupted silk sutures with power leads tunneled through the incision for external power supply to the implant. In later studies, the implant package housed a battery for power supply. Attention was then turned to the implantation of the Camino subarachnoid 'bolt". The "bolt" was implanted in prescribed fashion. In one of the studies the external fiberoptic cable of the Camino "bolt" was placed within a specially designed collar. The purpose of the collar was to contain the fiberoptic cable when not in use and protect the monitor from being dislodged.

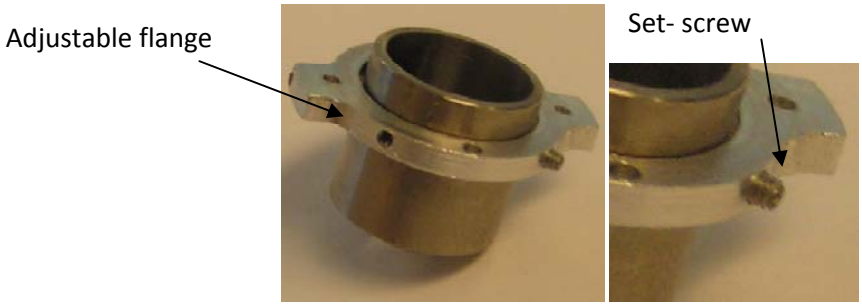

Figure 6.3. An empty casing with the adjustable flange. Set-screw to adjust the level of flange for variable skull thicknesses can be seen in the exploded view.

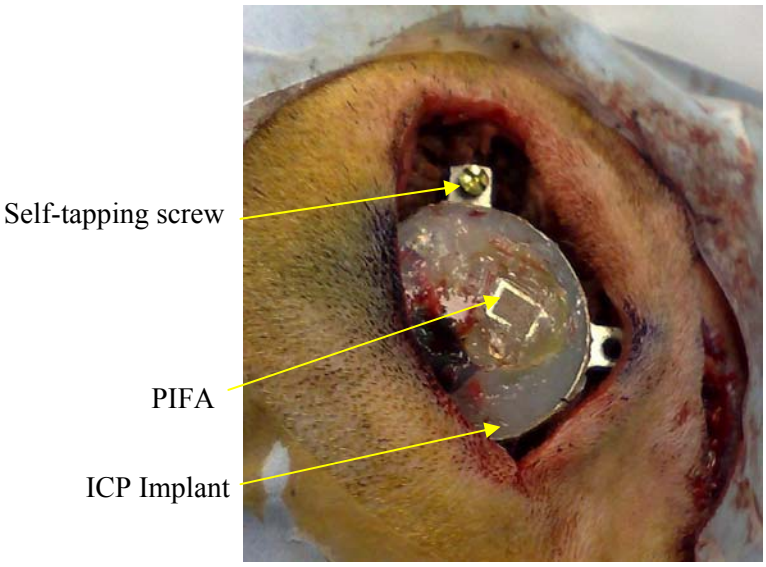

Figure 6.4. Placement of an implant under the scalp. The implant is fixed to skull by self-tapping screws. Note that this picture shows a sub-dural implant for a small burr hole.

While the animal was under anesthesia both monitors were tested and provided expected data. Moderate alterations in ventilation rate to produce hypo and hyperventilation were made. Hyperventilation causes cerebral vasoconstriction, reduction in the cerebral blood flow, and as a result a reduction in ICP is produced. Hypoventilation has a reverse effect leading to vasodilatation and a consequent increase in ICP. Under normal circumstances, the variations in ICP are limited and altering the rate of ventilation has a very modest effect on ICP. Moreover, the ventilation rates are only altered within safe limits so that the effects are not detrimental to animal. Prolonged hyperventilation can cause cerebral ischemia and sustained hypoventilation may lead to brain damage by increasing ICP. Thus, the respiratory rate was changed over a range of 2-18 breaths per minute. Each rate was maintained for a period of approximately 5 minutes while the vital parameters of the animal were also being monitored. Jugular venous occlusion was also performed to increase ICP. Measurements were taken from

both monitors and recorded. Figure 6.5 is a photograph that was taken while simultaneous measurements were acquired from the two ICP measuring methods.

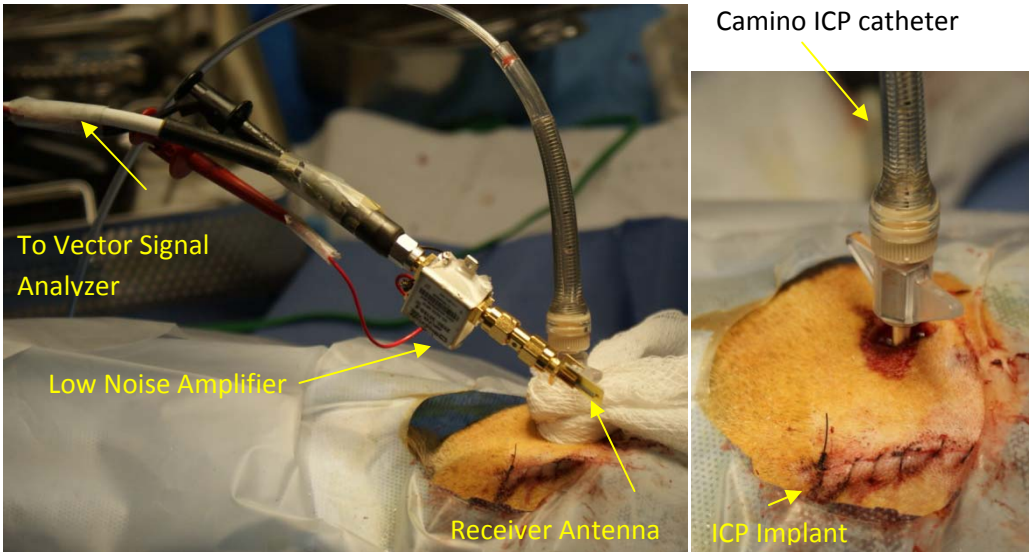

Figure 6.5. Simultaneous measurements being taken from ICP implant and Camino monitor in an anesthetized animal.

The animal was then allowed to emerge from anesthesia and taken to the recovery area. Further measurements from the ICP implant were taken daily for the duration of the study. At the end the animal was euthanized by an overdose of Pentobarbital (5mg/Kg in 5ml) administered intravenously. The implant was recovered; samples of tissue (Figure 6.12) were extracted from the site of implantation for toxicity study.

6.6 Post-surgical medication

The post-surgical regimen of medication was prepared to counter any risks of infection and alleviate distress or pain exhibited by animal. In order to avoid infection, antibiotics (Baytril) were administered for a period of 14 days. For pain management Metacam, Tremadol,

and Buperenorphine were prescribed for mild to severe signs of distress. The site of incision was periodically inspected for any fluid discharge.

6.7 Induced intracranial hypertension

For the purposes of evaluating the performance of the ICP implant over a wide range of pressure, ICH was induced in the animal. In order to achieve this, sterile, pyrogen free saline (mock CSF) injections were administered into the brain of an anesthetized dog. A cisternal needle was inserted into the brain to allow infusion of mock CSF to produce a range of ICP. For each session, more fluid was injected into the brain to produce a range of ICP between the normal level and approximately 80 mmHg (Figure 6.6). For each ICP level, the Camino pressure was recorded and compared with the simultaneous reading of the ICP implant. At the end of this session, the cisternal needle was retracted. It must be noted that this procedure was carried out only once for a single animal study as higher levels of pressure can cause irreversible damages to the brain. Thus, it was conducted at the end of a study after which the animal was sacrificed.

A summary of the process involved in conducting an animal study is presented in Figure 6.7.

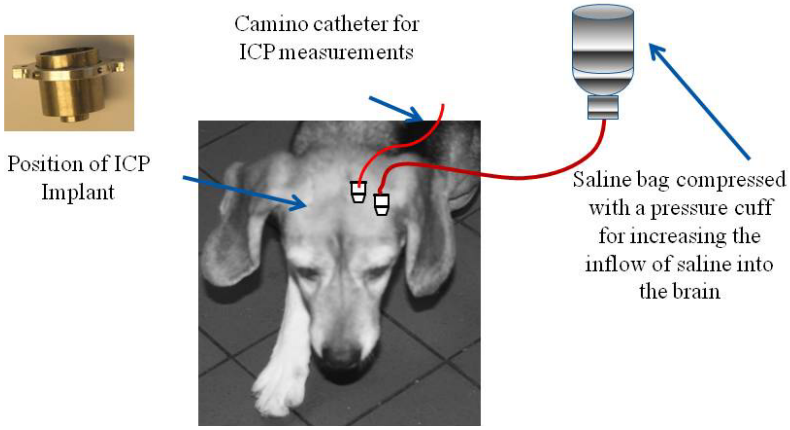

Figure 6.6. Scheme for infusing saline into the brain for inducing intracranial hypertension by increasing the amount of saline that is injected into the brain.

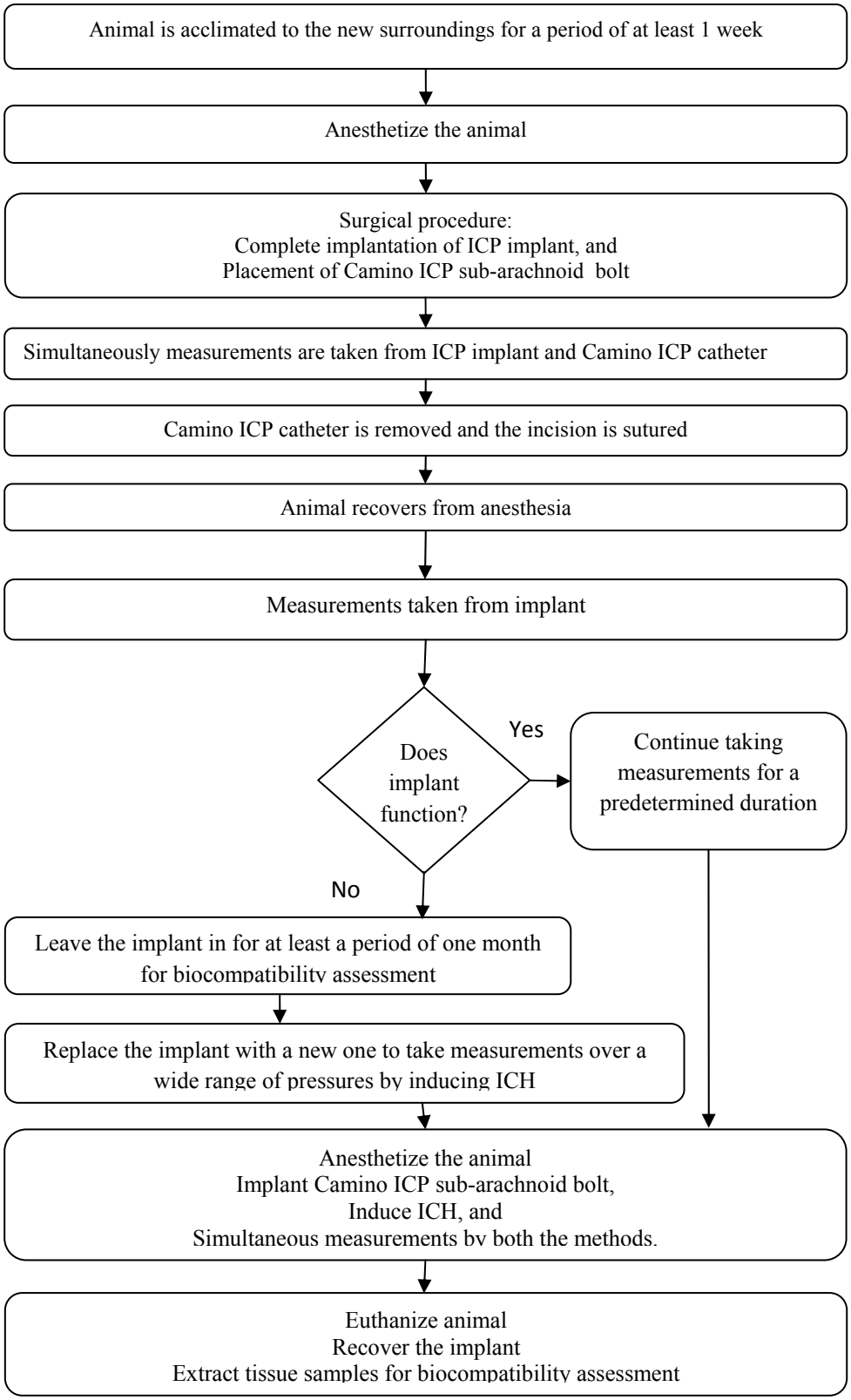

Figure 6.7. Flowchart describing the sequence of events while conducting an animal study.

6.8 Duration and key findings of animal studies

A total number of 7 out of 20 animal studies (as determined by statistical analysis, section 6.2) were conducted. One study was carried out in a pig and six were performed in dogs. The key details of all the animal studies including duration of each study are tabulated in Table 6.1.

Table 6.1: Details of animal studies including key findings from each study.

Animal Model	Type of Sensor	Type of Implant	Duration of Study	Key Findings
Pig 1	PZR	E_L	4 hours	• Feasibility of microwave transmission through scalp • Pressure as a function of ventilation rate
Dog				
1	PZR	E_L	5 weeks	• Integrity of Implant • Biocompatibility assessment
2	PZR	E_L	24 hours	• Correlation between Camino catheter and implant
3	C	Cap_L	24 hours	• Correlation between Camino catheter and implant
4	C	Cap_L	2 months	• Implant performance over a wide range of pressure • Integrity of Implant
5	C	Cap_L	20 days	• Correlation between Camino catheter and implant
6	C	Cap_S	27 days	• Longevity study • Feasibility of using a small burr hole

Key: PZR: Piezoresistive, Cap: Capacitive MEMS, E: Epidural, S: Sub-dural, L: large burr hole, S: Small burr hole.

The findings from each animal study were critical in improving and designing the course of next *in-vivo* experiment in terms of its goals and desired outcomes. The findings from each animal study and their influence on the next are presented here.

6.8.1 Pig Study

The aim of this study was to determine the feasibility of microwave transmission through scalp [85]. This study was conducted with a PZR_ED_L model for duration of 4 hours. At the time of this study, the Camino ICP monitor was not available to us. Figure 6.8 shows the implantation in a pig model. Methyl-methacrylate cement was used to hold the implant steady in the burr hole. It must be noted that this implant had an external power supply instead of an embedded battery. The pressure variations as a function of respiratory rate were recorded and plotted (Figure 6.9). Power measurements as function of separation between the scalp and receiver antenna were recorded to determine the wireless range of the implant (Figure 6.10).

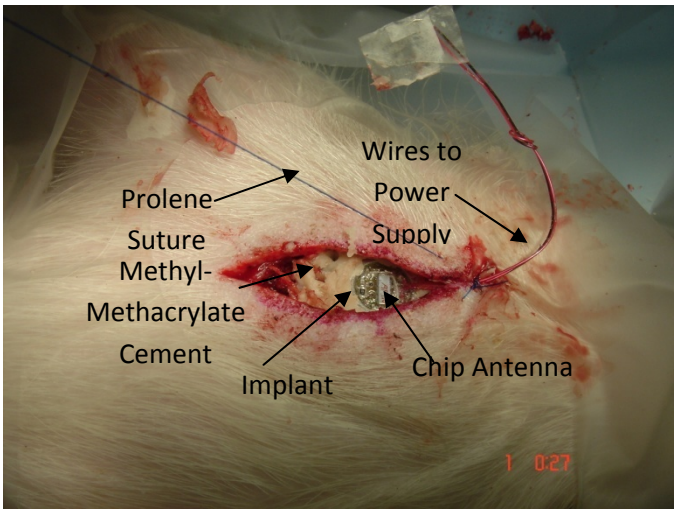

Figure 6.8. Implantation in a pig.

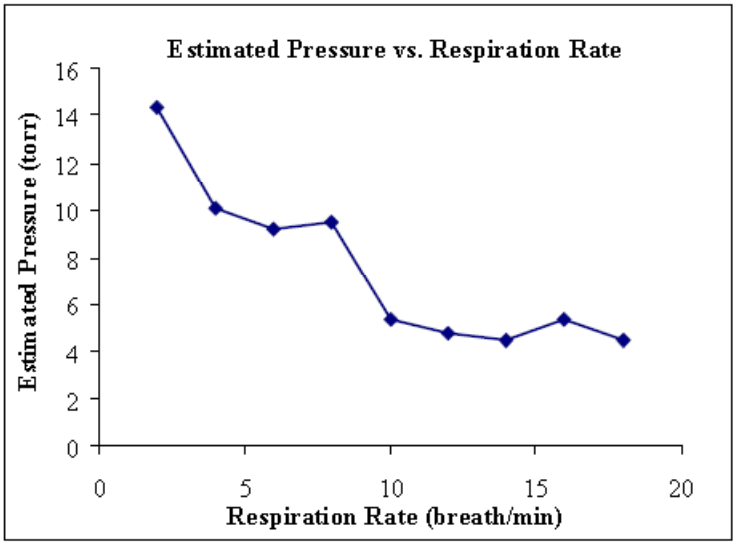

Figure 6. 9. Estimated ICP as a function of respiratory rate [85].

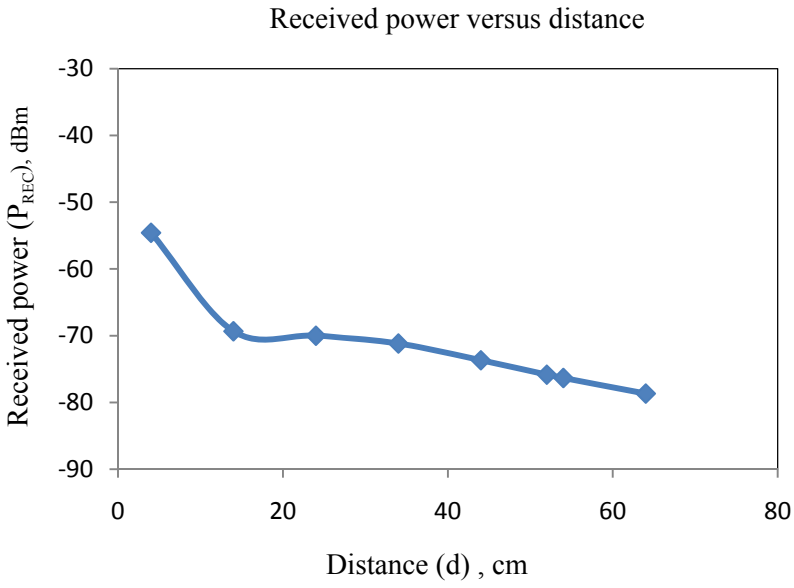

Figure 6.10. Power received from the implant as a function of the distance [85].

The ICP varied inversely with the rate of respiration, as expected. The effect of hypoventilation is seen as an increase in the pressure. However, at lower values of pressure, the pressure curve (Figure 6.9) depicts an overall insensitivity of the device in low pressures. This can be due to the contraction of dura at low pressures. Moreover, the pressure sensor surface was not in direct contact with the dura because of the ceramic packaging of the pressure sensor. This can also lead to the insensitivity of the frequency to ICP.

6.8.2 Dog 1

In the subsequent study, the implant previously used in a swine was reused and implanted in a canine model for a period of five weeks. A good healing of the scalp overlying the implant was observed. Figure 6.11 shows a small protrusion on the dog's head at the site of implantation after one week. It should be noted that with the healing of the scalp and the growth of hair at the site of incision, the position of the implant or battery is hardly discernible for any aesthetic concerns.

The subject was euthanized and three specimens (Figure 6.12) were obtained for histo-pathological examination. The specimens were:

i) *Specimen #1*: This specimen was from the tissue overlying the implanted implant and shows reactive 'scar tissue formation'. There were abundant lymphocytes (colorless cells that are cellular mediators of immunity) within a fibrous matrix.

ii) *Specimen # 2:* This specimen was from brain beneath the implant and shows no abnormality. It shows normal cortical architecture devoid of reactive fibrotic tissue. There are no abnormal cells or necrosis present.

iii) *Specimen # 3:* This specimen was from dura mater. One end of the specimen was taken from beneath the implanted device. This is contiguous with dura mater sample remote from the device under normal skull. The specimen demonstrates significant thickening and fibrosis of the area beneath the device. There are many lymphocytes in a fibrous matrix as

well as plasma cells (that secrete antibodies) representative of an inflammatory reaction. A slide picture of specimen # 3 recovered after the canine study is presented in Figure 6.13.

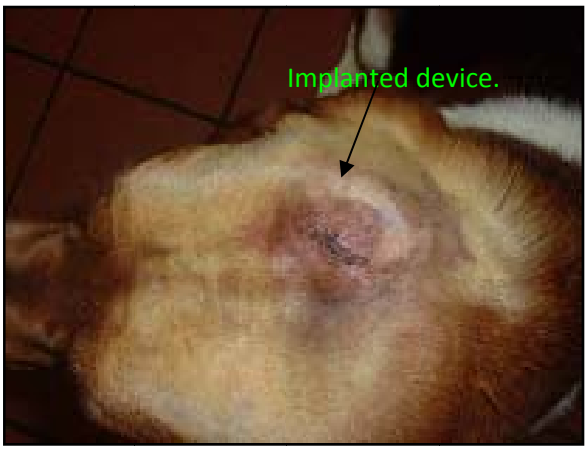

Figure 6.11.Appearance of protrusion at the implantation site.

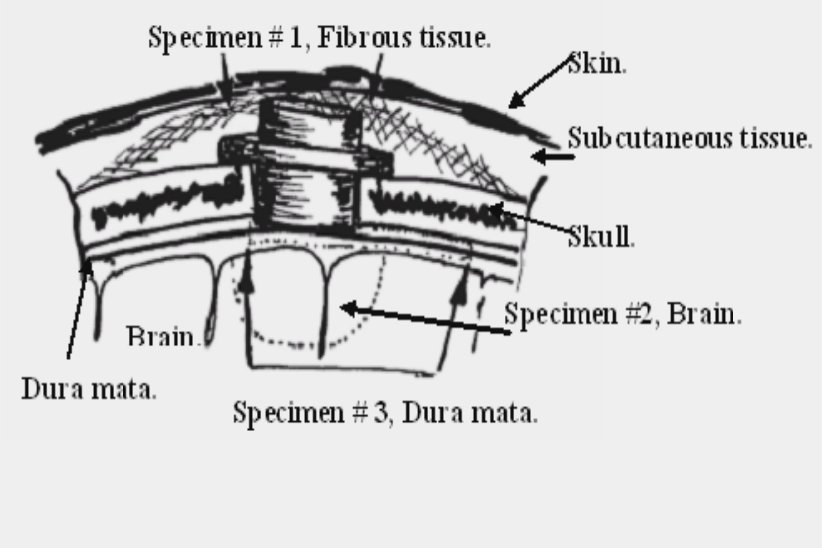

Figure 6.12. Sketch of an epidural device placement and the recovered specimens.

This implant showed aberrant performance after the study period. No electrical/signal testing was performed during this experiment. However, alterations to the design of the implant casing were made as a result of this study.

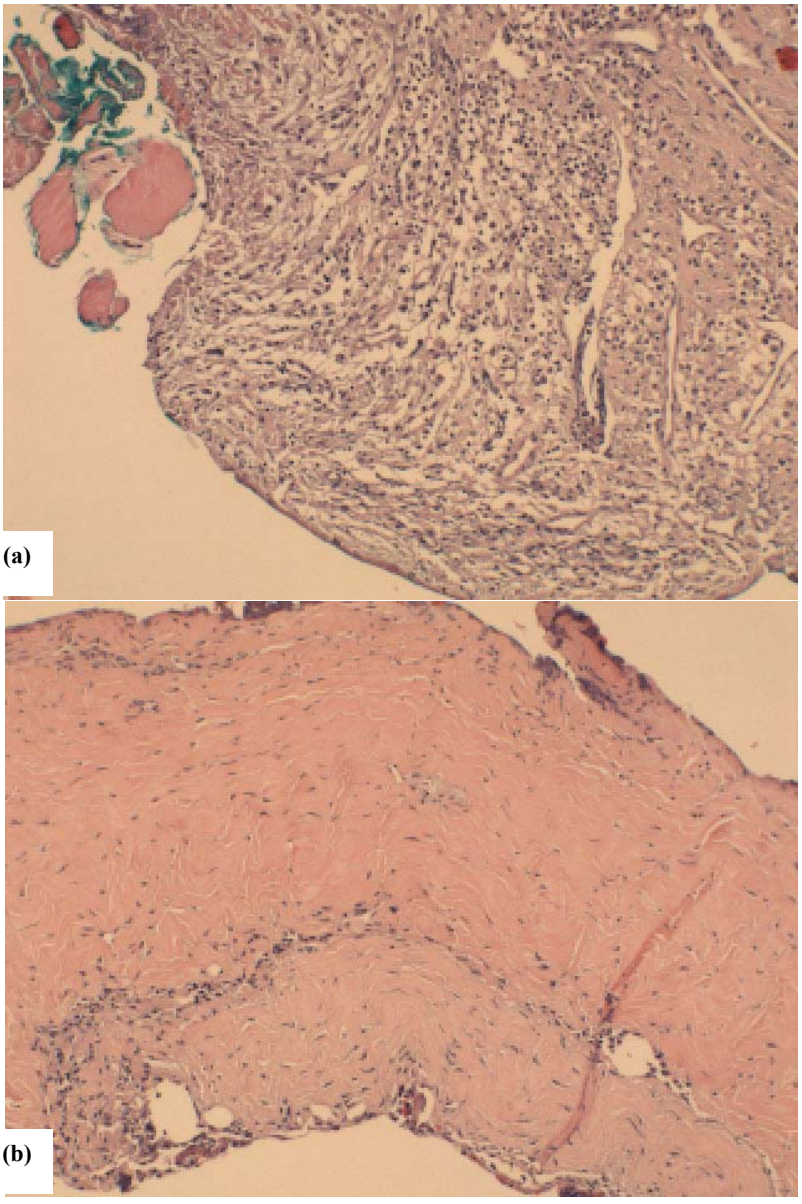

Figure 6.13. Specimen # 3 showing thickening of dura mater under the implant due to fibrosis and lymphatic innervations. a) thick dura mater appearance of fibrous matrix, b) normal dura mater distal to the implant.

6.8.3 Dog 2

The modified epidural implant (including PIFA antenna and a die PZR sensor) was implanted in a dog for a period of 24 hours. A standard ICP monitoring catheter was placed on the other side of the midline for rapid and continuous ICP measurements, and comparison with the wireless measurement. For this particular study a pressure variation in the range of 11-22 mmHg was achieved by altering the rate of respiration. Readings were taken while the dog was anesthetized and being weaned of the ventilator. An r-squared correlation of 0.88 between Camino catheter and ICP implant was determined. A plot of Camino pressure versus the pressure measured by ICP implant is shown in Figure 6.14. The measurements are less erroneous in the pressure range of 10 to 20 mmHg (±2 mmHg) and show a slightly higher variation at elevated pressures. High pressures may lead to a forceful dural contact with the sensor. This could be the reason for erroneous response of the device at >20 mmHg, since this sensor is not a touch mode sensor.

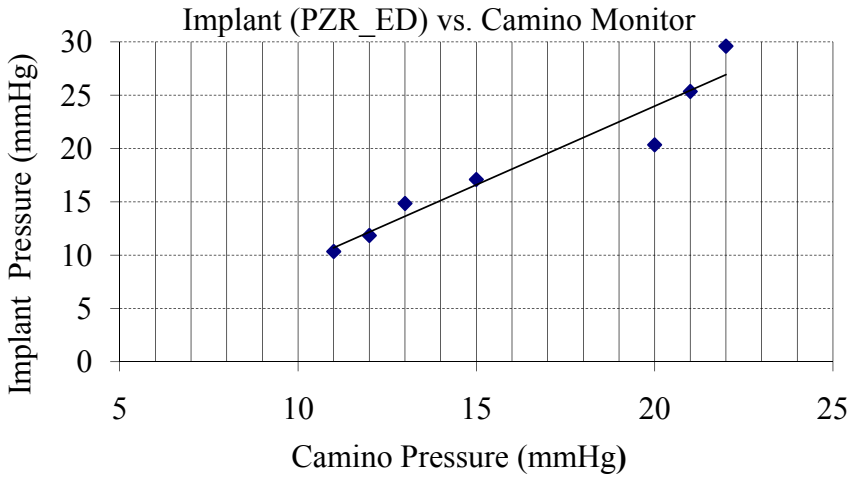

Figure 6.14. Performance of the implant as compared to Camino catheter for dog 2.

6.8.4 Dog 3

In a follow up canine study, an epidural configuration with capacitive MEMS was used for a one-week study. The results obtained relative to the in-vitro tests and in comparison to the Camino catheter pressure monitoring showed a great degree of inconsistency between the in-vitro and in-vivo implant readings. Moreover, the implant readings were not repeatable for different measurement sessions, for which the study was conducted. This was attributed to the unstable capacitor response in wet environment. However, a new MEMS capacitive sensor, modified to resolve the humidity issue (verified by the manufacturer) was made available to us. This new sensor was utilized in conducting further studies. On the other hand, because of further issues with the epidural device placement (as indicated by histo-pathological findings), the MEMS based epidural device was not studied again.

The preliminary work on the PZR design paved the way for a better approach in designing the system with a MEMS capacitive pressure sensor, while issues like biocompatibility, integrity of the device and feasibility of microwave transmission through scalp were addressed. The growth of fibrous tissue underneath the device in epidural measurements and the variability in the thickness of dura mater led to the decision to move to a more reliable sub-dural measurement technique.

The implants in used the next three dog studies were of capacitive MEMS subdural type.

6.8.5 Dog 4

The total duration of this study was two months during which two implants were used. The first implant functioned for 13 days after implantation. Moderate changes in ICP were achieved in an anesthetized animal and the pressure measurements were taken from the implant and the catheter at the onset of this experiment. Figure 6.15 is a plot comparing the two measurement techniques. A correlation coefficient of 0.98 (r-squared value of 0.96) was established between the two techniques. A maximum error of 1 mmHg was determined when

the implant measurements were compared to the Camino measurements. The later measurements were taken only from the implant for 13 days after which no signal could be received. The ICP that was recorded from the implant only, from the second day to thirteenth day was in the range of 9-10 mmHg. The malfunction of this implant was attributed to the failure of the battery. This implant was left undisturbed till the end of 2 months in the animal for biocompatibility assessment. A second implant was implanted right before terminating the study. The goal of this procedure was to gage the *in-vivo* performance of the implant when compared with the catheter over a wide range of pressure as shown in Figure 6.16. A pressure range of 10-84 mmHg by inducing ICH as described in section 6.7. A correlation coefficient of 0.998 (r-squared value of 0.996) was established between the two techniques. A maximum error of 2.25 mmHg was determined when the implant measurements were compared to the Camino measurements.

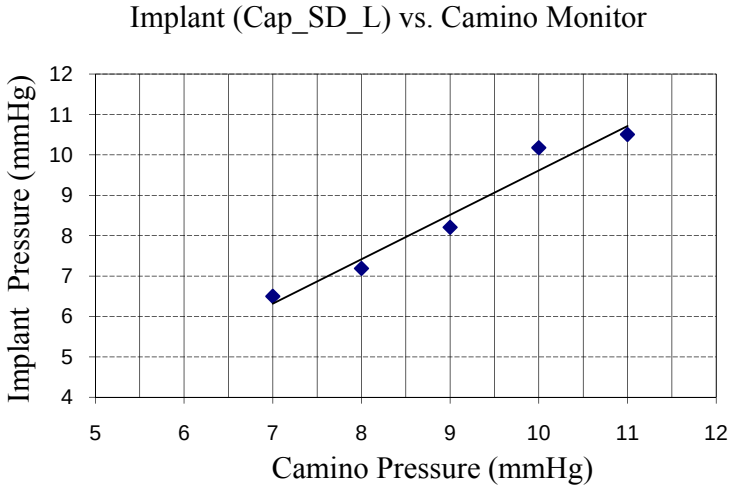

Figure 6.15. Comparison of Cap_SD_L Implant with Camino catheter for dog 4.

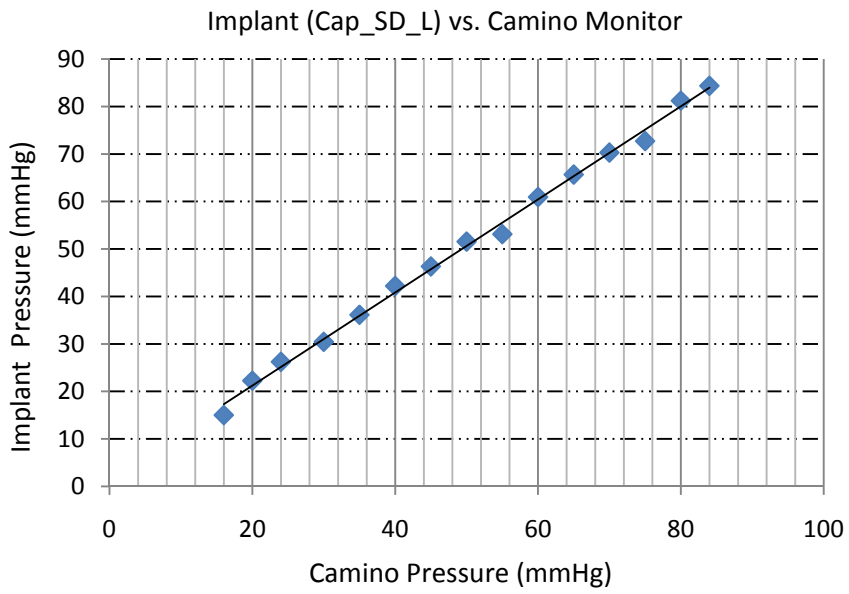

Figure 6.16. Comparison of Cap_SD_L Implant with Camino catheter for dog 4.

Tissue specimens from this study were examined for any abnormalities. An abundance of fibrous tissue matrix was found as expected.

6.8.6 Dog 5

This study was conducted with a Cap_SD_L implant. Measurements were taken from this implant for 13 days. This animal developed complications due to infection at the site of implantation. Serous fluid accumulation due to bacterial infection was also resulted. The animal had to be euthanized due to the complications. Figure 6.17 presents a plot of pressure values from implant versus pressure measured by catheter on the day of surgery. A maximum error of 1.34 mmHg was determined when the implant measurements were compared to the Camino measurements. A correlation coefficient of 0.98 (r-squared value of 0.97) was established between the two techniques. The ICP that was recorded from the implant only, from the second day to thirteenth day were in the range of 8-11 mmHg.

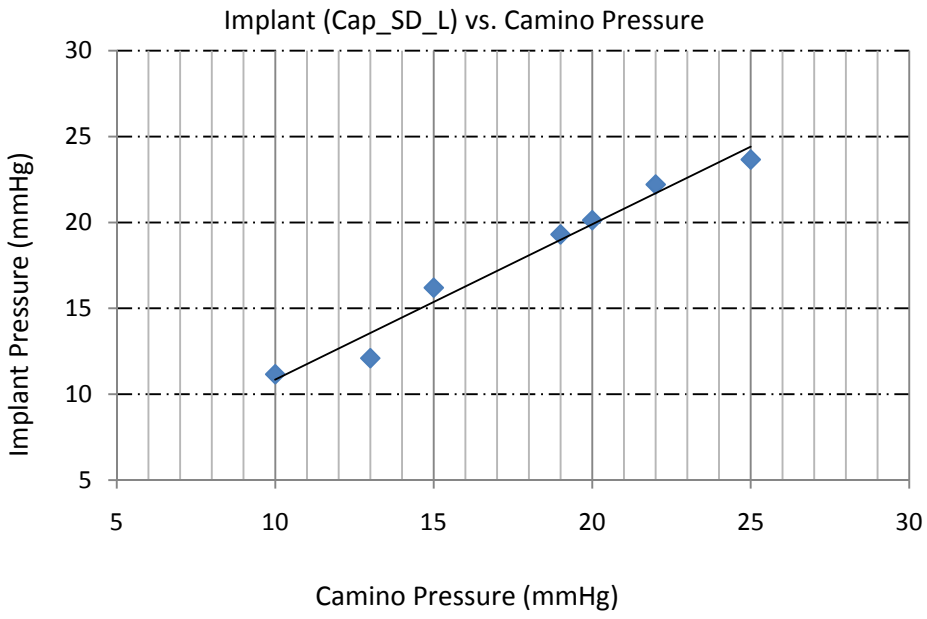

Figure 6.17. Comparison of Cap_SD_L Implant with Camino catheter for dog 5.

6.8.7 Dog 6

The last animal study was conducted with an implant (Cap_SD_S) that is designed for a small burr hole. The measurements from ICP implant were in good agreement with the Camino measurements with a correlation coefficient of 0.988 (Figure 6.18). A maximum error of 1.2 mmHg was determined when the implant measurements were compared to the Camino measurements. Data was collected from the implant on a regular basis for 45 days. The ICP values in a normal active dog were in the range of 8-12 mmHg as shown in Figure 6.19. During this period, blood samples were also collected from the dog to test for complete blood count, sedimentation rate, and C-reactive protein. The results hence obtained, did not indicate any immunological reaction or organ dysfunction.

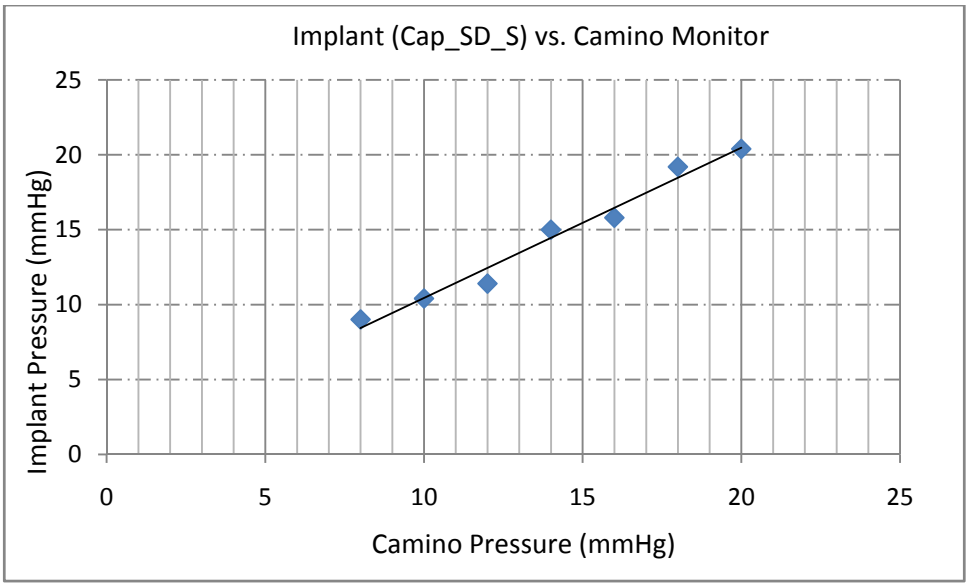

Figure 6.18. Comparison of Cap_SD_S Implant with Camino catheter for dog 6.

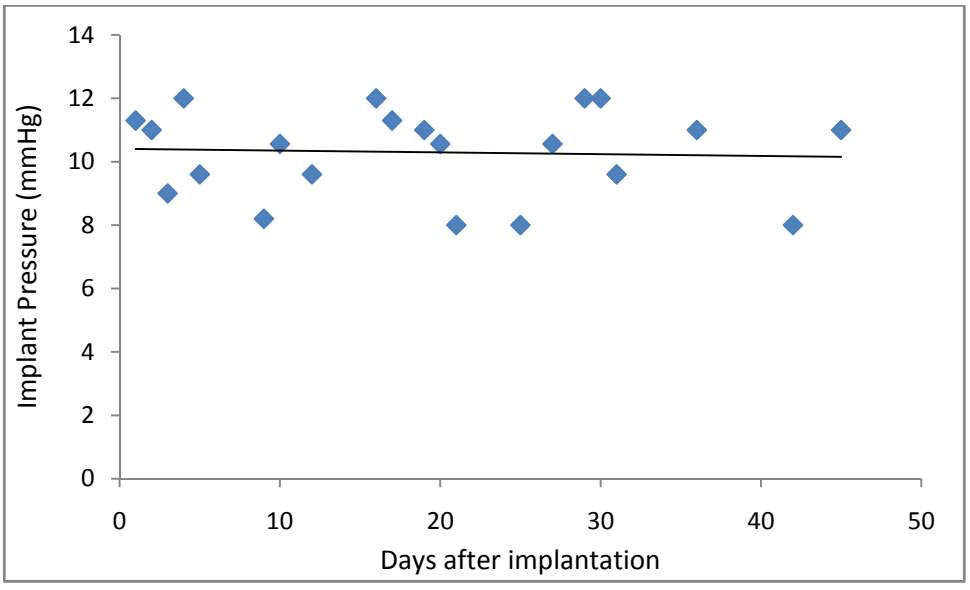

Figure 6.19. ICP measurements taken by the implant over a period of 45 days while embedded in dog 6.

The healing of scalp is shown in Figure 6.20. This photograph was taken on day 30 after the surgery.

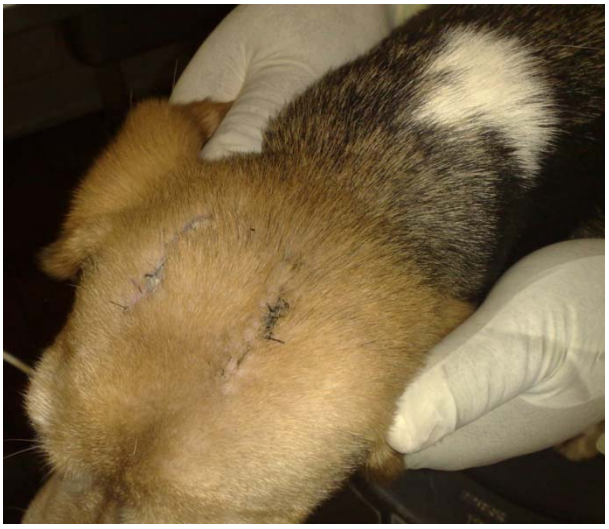

Figure 6.20. Photograph of dog showing the healing of scalp after 30 days of surgery.

6.9 Test of Correlation

In order to determine the significance of the correlation coefficients between the two modes of measurements that were determined for the animal studies, a two-tailed hypothesis test was performed. Consider a null and alternative hypothesis as follows:

Ho: r =0 (i.e. there is no significant correlation between the paired data)

Ha: r ≠ 0 (i.e. a significant correlation between the paired data exists)

The formulae for calculating the test statistics are given by:

$$T\ statistics\ test = r\sqrt{\frac{n-2}{1-r^2}} \tag{6.1}$$

$$p - value = tdist(T, df, 2) \quad (6.2)$$

where, n is the number of paired data points and df is degrees of freedom and equals (n-2).

If the p-value is less than the significance criteria, α then the null hypothesis is rejected and the alternate hypothesis holds good.

The T and p-values for all the animal studies are reported in Table 6.2. With α=0.05 (section 6.2), all the p-values were below the significance criteria. Therefore, alternate hypothesis is accepted and a significant correlation is found between the measurements taken from the ICP implant and Camino catheter.

6.10 Sources of error in ICP measurements

A number of sources that can potentially introduce an error in the measurement of ICP by the implant are identified and enumerated below. The error estimates that are presented here are in reference to the implant that is described in section 5.2.2

i) *Averaging error:* A number of measurements (three or four) are acquired for each pressure point. The mean value of the measurements is considered to be the true value of pressure for a given pressure point. For example, the pressure values were in the range of 0.1 mmHg from the mean pressure.

ii) *Resolution of Camino catheter:* The Camino monitor offers a limited resolution of 1 mmHg. In a complete study, the pressure measurements from the ICP implant are taken in two steps, i.e., *in-vitro* and *in-vivo*. In each step measurements from the implant are compared with the Camino catheter. The implant is characterized in reference to the Camino catheter in the *in-vitro* tests. A mathematical function that describes the dependence of frequency on the pressure is determined from these tests. Since the catheters do not resolve the pressure to a fraction of 1mmHg, an error of ±0.5 mmHg is introduced at the time of *in-vitro* characterization of the implant. Similarly, the implant is compared with the catheter at the

time of conducting *in-vivo* studies, when a maximum error of ±0.5 mmHg is possibly introduced into the pressure measurements from the implant. Since the *in-vitro* and the *in-vivo* measurements are taken at separate instances, the errors at each instance are cumulative in the overall two-step ICP measurement process. Thus, a possible maximum error of ± 1 mmHg could be expected in a complete ICP measurement study that comprises of the *in-vitro* and the *in-vivo* experimentations.

iii) Temperature uncertainty: In the two-step ICP measurement process, an error could be caused due to the fact that the pressure dependant frequency varies with temperature fluctuations. However, the temperature uncertainty had a small effect on the overall error in the ICP measurements. For example, the temperature sensitivity of one of the implants in the *in-vitro* tests is 0.87 mmHg/^{o}C. The body temperature of an anesthetized animal varied by ± 0.2 ^{o}C in our *in-vivo* studies. This corresponds to an error of ± 0.17 mmHg, which is a small in magnitude in comparison to the error that is introduced due to the limited resolution of the Camino catheter.

iv) Site of pressure sensing: The fluctuations of ICP that occur internally within the skull contribute to the overall certainty with which an ICP monitoring system can measure the pressure. However, quantifying the variations in ICP is beyond the scope of this work. In addition, the error in ICP measurements by the implant is estimated in relation to Camino catheter. Since both the techniques measure ICP in the frontal region, the effects of the site of pressure sensing can be ignored.

The sources of error described above are independent of each other. Thus, the maximum error in the measurement of ICP by the implant would be the sum of individual errors. In this case, the maximum error due to averaging, limited resolution of Camino catheters, and temperature uncertainty is 1.27 mmHg.

6.11 Conclusions

The evaluation of ICP implants in the *in-vivo* settings provided vital details that validate the applicability of this implant in the monitoring of ICP. The practicability of microwave transmission through swine and canine scalp is established. It must be noted that dogs have a thick temporalis muscle beneath their scalp. In some instances the thickness of temporalis-scalp

Table 6.2: Correlation coefficients and p-values for animal studies.

Dog number	ICP range (mmHg)	Correlation	df	T	p-value (two-tailed)
2	11-22	0.94	5	6.161	0.0016
4	7-11	0.978	3	8.20	0.0038
4	16-84	0.998	13	59.20	0.0001
5	10-30	0.987	6	16.52	0.0001
6	8-20	0.988	5	15.84	0.0001

complex can be greater than the thickness of scalp in humans. Thus, the implant could possibility have a longer wireless readability range than 0.8 meters that was determined from the animal studies. The long duration studies on the implant proved its integrity and wholeness in corrosive biological environment. Parylene coatings on various implants were impermeable to the body fluids and were critical in maintaining the proper performance of the implant. A 2.5µm thick coating did not have any effect on the sensitivity of the implant.

Various models of the implant were evaluated and a preference of their use was derived from these studies. The thickening of dura mater at the site where the pressure sensor made contact with dura was suggestive of a compromise in the overall accuracy of the implant over an extended period of ICP measurement. These histo-pathological findings from a five week study

in dog 1 underscored the need for sub-dural method of pressure sensing. A reduction in the size of burr hole required for an ease of implantation, possibly at the bed-side, was also achieved. Thus, a sub-dural ICP implant that requires a small burr hole has a preferred combination of implant properties.

The performance of ICP implant in relation to Camino catheter was determined. A correlation coefficient of 0.94 or better was estimated. It is also worthwhile to mention that the epidural mode of pressure sensing produced the lowest value of correlation. Thus corroborating with the earlier finding that the sub-dural mode of pressure measurement provides a more accurate result than the epidural mode. Although the readings from the implant were not compared to that of the catheter during long-term studies, yet the implants exhibited a consistency in their performance over the duration of pressure monitoring. The pressure values for each study were within ±2 mmHg of the normal pressure for a particular animal as was recorded by Camino catheter on the first day of the study. Thus it can be inferred that the implants did not present any significant drift over the course of measurements.

The ICP implants invoked a normal immunological reaction by the body to any foreign object. A microscopic study of the specimens that were collected from the animals after a long-term implantation showed the presence of lymphocytes and did not indicate any toxicity due to the metal, silicone, or parylene used in the fabrication of implants. The study conducted in dog 6 with the preferred configuration of the implant (SD_S) produced vital results that could be a driving factor for conducting any long-term study with these implants. This particular study had a power source (battery) embedded in the packaging of the implant. The effectiveness of the packaging proved to be pivotal in preventing any battery leakage and also ensured longevity of the implant. The equivalence of ICP implants to the gold standard for monitoring of ICP was established as a consequence of *in-vivo* evaluation of these implants. The concept of an embedded microwave ICP monitoring implant at 2.4 GHz ISM band was demonstrated and substantiated by a body of data gathered from conducting animal studies.

The thickening of dura mater and its effect on the sensitivity of the implant provided an impetus to simulate the relationship between the thickness of dura and the degree of deflection caused by certain amount of intracranial pressure that is exerted on dura mater. The details of simulations are elucidated in chapter 7.

7. Simulations on Dura Mater

The formation of scar tissue is part of the healing process after a severe external injury, is found around implants in biological tissue, and it accumulates internally after injury or surgery. The *in-vivo* studies that were conducted on the epidural ICP implant (described in chapter 6) showed the growth of scar tissue around the implant in addition to the thickening of dura mater. The thickening of dura mater can be attributed to fibrosis as a reaction to the presence of a foreign body (implant) [110]. The build-up of scar tissue can affect the sensitivity and accuracy of an epidural pressure measurement system since the pressure is measured as a function of the deflection of dura mater due to ICP. In this chapter, some preliminary simulations are shown to quantify the effect of dural thickness on its deflection. In order to conduct any simulations, it is important to know the mechanical properties of dura mater and scar tissue. The mechanical properties of dura mater have been extensively studied by various researchers [111-114]. However little is known about the mechanical properties of the dura and scar tissue complex. A few details of the mechanical properties of dura mater and scar tissue are presented here. It should be noted that the work presented here is in its preliminary stages and will serve as an opening for a more detailed work in the future.

7.1 Mechanical properties of dura mater and scar tissue

Dura mater is a viscoelastic material that possesses viscosity (the relative resistance to the ease of flow) and elasticity (the tendency of the material to return to its original form after a force is applied to it) at the same time. Anatomically, dura is made up of connective tissue –collagen and elastin fibers. The collagen fibres in the inner portion of the dura are almost perpendicular to fibers in the outer region [114]. The Young's modulus and Poisson's ratio for cranial dura mater have been reported to be

30-40 MPa and 0.45-0.5, respectively [115] – [116]. Scar tissue is known to have greater elasticity that normal tissue [117]. The growth of scar tissue is a dynamic process and its mechanical properties change with time. The mechanical properties are also dependant on the site of fibrosis due to its adhesion with the parent tissue or foreign object. Due to a lack of information on the mechanical properties of scar tissue that grows on dura mater, scar tissue is considered to be a part of the parent dura for simulations purposes. It is also believed that considering dura and scar to be a continuous membrane is an acceptable assumption over long duration of fibrosis.

A finite element model of the dura-scar tissue complex is defined in the next section.

7.2 Finite element modeling of dura-scar tissue complex

A simplified model for simulating the effect of the thickness of dura-scar tissue complex is outlined here. The simulations are performed on ABAQUS version 6.6, student version. A square section of dura mater (5cm X 5cm) is modeled here. Since skull has a curved geometry, a radius of curvature of 15 cm is assigned to the modeled section of dura mater [118]. A uniform pressure of 10 mmHg is applied over 25 cm^2 area of dura since the normal range of ICP is 0-15 mmHg. For boundary conditions, the perimeter of the model is assumed to be fixed. The normal thickness of dura alone is 0.3-1mm. The histo-pathology results from an in-vivo study (Chapter 6) indicated up to a threefold increase in the thickness of dura mater when a sample of dura mater was excised and examined after 5 weeks of implant placement in the skull. For simulations, the thickness of dura was varied between 0.5 and 3 mm. Figure 7.1 is a diagrammatic representation of the simplified model that is outlined above.

The entire segment of the dural model is divided into four sections and each section has 196 elements making a total of 784 elements for the segment. An eight node, linear brick element with reduced integration and a seed size of 0.0035 is used. It must be noted that the student version of ABAQUS only allows processing of a total of 1000 elements. For this reason, a linear brick element with small seed size was selected over a quadratic hex element of the same size.

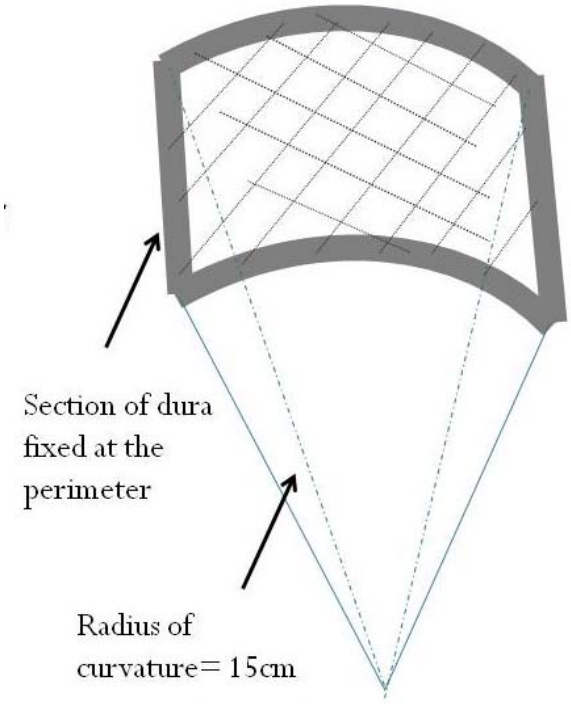

Figure 7.1. A simplifed model of dura mater.

7.3 Results and conclusions

The epidural implants were housed in a cylindrical case that was 10-12 mm in diameter (Chapter 3). It is assumed that the device is positioned at the center of the

dural section that is under consideration here. Therefore, attention is diverted to the middle section of the finite element model of the dural section. The stress pattern due to ICP of 10 mmHg that is applied uniformly to dura, is shown in Figure 7.2. The deflection of 0.5 mm thick dura due to the ICP is shown in Figure 7.3.

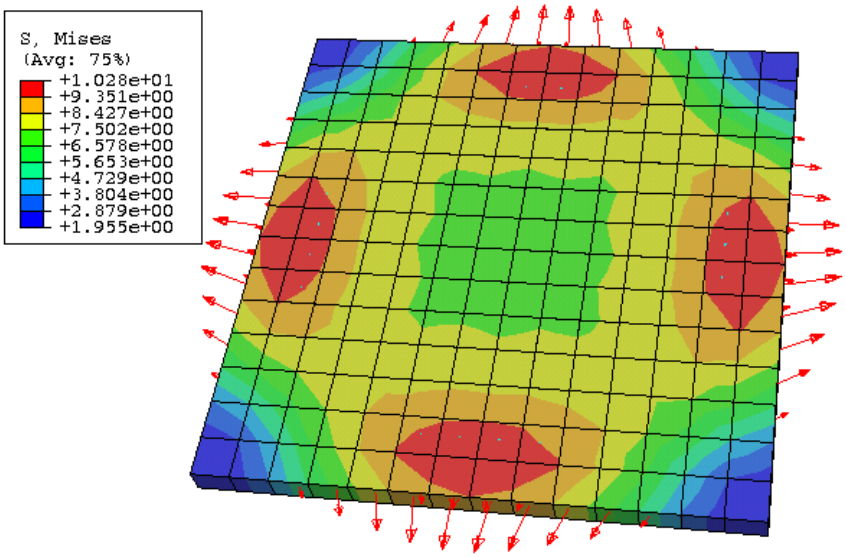

Figure 7.2. Contour plot showing the pattern of stress as a result of a uniform ICP.

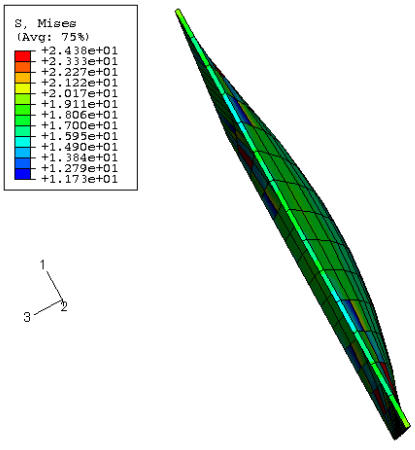

Figure 7.3. Contour plot showing the deflection of dura as a result of a uniform ICP.

The deflection of the dura-scar complex for various thicknesses as a function of constant and uniform ICP is plotted in Figure 7.4.

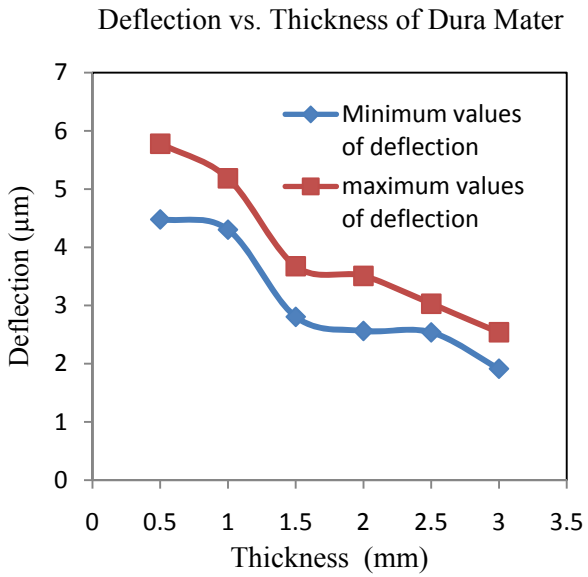

Figure 7.4. The change in the deflection as a function of the thickness of dura-scar tissue complex.

Since dura is a viscoelastic material, it is not possible to derive a linear relation between the deflection and the thickness of the dura-scar complex. In general, an increase in the thickness of dura-scar complex would lead to a reduction in the amount of deflection that would be caused by a certain amount of pressure. In other words, a build-up of scar tissue would affect the accuracy and sensitivity of an epidural ICP monitoring system. Thus further confirming the need to measure ICP in a sub-dural space as discussed in Chapter 6.

8. Conclusions and Future Work

The technology of ICP monitoring in the research arena has been receiving constant attention for decades and significant advancements have been made by various investigators. The contributions from researchers from various disciplines that include, but are not limited to, sensor technology, wireless technology, biomaterials, have built a rich pool of background information that has been cardinal in designing our research work. These contributions have been detailed in Chapter 3 of this thesis. This chapter presents the uniqueness of our work and a summary of the tasks that have been accomplished while developing our ICP monitoring technology. In addition, an account of the recommendations for future work is also outlined here.

8.1 Contribution of this thesis

The significant contribution of our work is emphasized by its uniqueness and the success in conducting animal studies that have answered the concerns that are relevant to the development of a medical implant.

8.1.1 Uniqueness of this work

The singularity of our work lies in the fact that our ICP implant has been designed to operate in the Industrial-Scientific-Medical band of 2.4 GHz. The wireless ICP implants that have been reported so far are designed at lower frequencies, for example in the MHz range as in [119]-[122]. Moreover, our selection of frequency for wireless communication was also recently confirmed by Poon and his co-workers who have theoretically demonstrated that the optimal frequency for power transmission in biological media is in the GHz range [41].

8.1.2 Summary of the achievements

Throughout the duration of this research the ICP implant was constantly modified to meet the challenges in designing and achieving an optimal combination of the implant features.

Few of the challenges were ensuring biocompatibility, longevity of the implant in an animal model, repeatability of performance, minimizing the contact area between the sensor and the tissue, reducing the size of the burr hole to be drilled in the skull for an ease in the implantation procedure etc. The implants were immersed in a hydrostatic pressure chamber for determining their integrity in a water medium in the *in-vitro* environment after being coated by a 2.5µm thick Parylene. Parylene coating proved to be a reliable interface between the implant and the biological medium. It was tested for a duration of 18 months in 0.9% saline solution and 5 weeks in an animal model. It was efficient in isolating the implant from the corrosive fluids in the body and at the same time protected the MEMS sensor from degrading in wet conditions. The performance of the ICP implant was monitored for 12 days in water and up to one month in animal studies. In water medium, the drift was less than 2 mmHg. In animal studies, the pressure was compared to the gold standard only on day 1 of the study; a correlation of 0.94 and better was determined (from four dog studies) between the implant and the Camino catheter (gold standard for ICP measurements). A sense of normal pressure for a particular animal was gained on this day of the study while simultaneous measurements were obtained from the implant and the Camino catheter. In the following days, during the course of an animal study, the implant pressure was monitored on a regular basis. The values of ICP were in the normal range for a particular animal as was determined on the first day of the study.

The design of the implant evolved from an epidural to the sub-dural type. It was determined from our study and is also reported in the literature that a sub-dural pressure monitoring system is a more accurate method of pressure measurement than an epidural system. A measure of intra-ventricular pressure has been reported to be the most desirable way to quantify ICP. However, a sub-dural method provides a good compromise between the site of pressure sensing and the degree of invasion into the brain. In our technique, the pressure sensor is placed in sub-arachnoid space where it measures the cerebrospinal fluid (CSF) pressure. In addition, no damage is caused to the brain tissue as the pia mater remains intact.

In an alternative step of design advancement, the size of the burr hole that is required to implant the system was reduced from 10-12mm diameter to 3-4 mm diameter. This resulted in a considerable reduction in the amount of time that was spent in the implantation procedure. The ultimate goal would be to miniaturize the implant to allow for a bed-side implantation method that would be at par with the Camino catheters. The Camino catheters have to be implanted in a sterile condition, but do not necessarily demand a sterile operating room environment. They can be easily implanted at the bed-side in an ICU.

It should be emphasized that our latest animal study was conducted with a sub-dural implant that required a 3.6 mm burr hole to be drilled in the skull. On the first day of the study, the ICP was measured with both the Camino catheter and our implant, and a correlation coefficient of 0.988 was calculated between the two measurements. The normal ICP for the dog was in the range of 8-12 mmHg. The catheter was then removed and the scalp was sutured. This implant continued to perform for a period of 45 days and the pressure recordings were in the normal range for this animal.

This latest study opens up the possibility of ICP monitoring in ambulatory conditions which is beyond the horizon of catheter based systems. It also supports the use of our ICP implant in conditions where it is desirable to monitor the pressure for longer periods than practically realizable by catheters. An understanding of the ICP trends over a duration of time in patients that are recovering from traumatic brain injury, cerebral hemorrhages, or brain tumors while they are not restricted to hospitals, would aid in defining their regimen of therapy and would also lead to a significant improvement in the outcome. Furthermore, the capability of wireless monitoring will facilitate advancement in home health care system and decentralization of medicine.

8.2 Recommendations for future work

This ICP implant strictly produces a number that represents the CSF pressure inside the cranium. The implant has been successfully tested for up to a period of one month which does

not necessarily promise its applicability to hydrocephalic conditions. It will be for the benefit of a larger population to increase the ambits of our ICP implant applications. A few of the possibilities along with directional examples are enumerated here.

8.2.1 Long-term studies

In case of chronic conditions like hydrocephalus, an ICP implant that can be left inside the cranium as an adjunct to the shunt systems can dramatically influence the course of treatment. It can be either incorporated with an existing shunt system or used as an independent device to function as a shunt check. In either case, the failure of a shunting mechanism will lead to a buildup of ICP which will be detected by the implant and can raise an alarm demanding an intervention. The durability of Parylene in an *in-vivo* environment for one month was established as a result of our work. However, that does not warrant its durability for hydrocephalic conditions and remains to be determined. Animal studies should be designed to investigate the possibility of extending the application of our implant in the realm of hydrocephalus.

8.2.2 Power management

For long-term applications an efficient power management scheme should be introduced into the design of our implant. One possibility is to integrate a rechargeable battery with a recharging mechanism using optical energy. In a different scheme a low power MOSFET could be activated by optical energy and would act as a switch to turn on the implant when desired.

8.2.3 Scar tissue prevention

Protein adsorption on the implant surface is the first step in the series of events which lead to scar formation, thus being detrimental to the performance and longevity of the implant. The probability of fibrosis can be reduced by hindering the protein adhesion properties of fibrin to the implant surface. Non-fouling PEG (poly ethylene glycol) coatings are protein repellant and can be easily immobilized on a titanium oxide surface [123]. A class of co-polymers based

on poly (L-lysine)-g-poly (ethylene glycol), PLL-g-PEG adsorbs spontaneously onto the titanium oxide layer from an aqueous solution. PEG is immobilized onto surfaces by coupling it with functional groups having affinity towards the target surface. Adhesion of PEG is due to electrostatic interactions between PEG ions and the oxide layer, thus physiologic pH and ion concentration play a significant part. These conditions are fairly constant in CSF and therefore the sensor area.

8.2.4 ICP monitoring and treatment of excessive CSF

In present clinical practice, the monitoring of ICP and treatment of excessive CSF are being conducted as two independent routines. An integrated system that would have an ICP monitoring technique in conjunction with a method of treatment will improve the management of the underlying cause of the disorder. For example, merging of ICP implant with a CSF shunting mechanism. Another application can be based on a combination of ICP implant and a reservoir system (for example, Ommaya reservoir) [124]. An elastic expandable reservoir with a one way valve in a conduit that tunnels from sub-arachnoid space to the reservoir can be implanted under the scalp. An elevation of ICP would cause the reservoir to fill up and the patient will suffer from the symptoms of intracranial hypertension. At that time, as the implant detects higher levels of ICP, the reservoir can be accessed by a needle to withdraw CSF and reduce the pressure. In a more advanced method our ICP implant could be coupled with upcoming techniques like “microfabricated arachnoid villi” [125] that mimic the function of arachnoid villi found in the sub-arachnoid space. The microfabricated arachnoid villi are one way microvalves that control the flow of CSF based on pressure differential.

8.2.5 Blast injury studies

It is widely believed that the shock waves produced due to explosions have detrimental effects on the central nervous system. However the relation between ICP and a blast injury is not clearly defined. A good understanding of the ICP trends during and after the blast will aid in determining the thresholds of blast intensity for various levels of blast injury. Chavko et al.,

have observed that a direct measurement of the pressure wave inside the brain during an exposure to blast has not been reported [126]. They have also reported a direct measurement of ICP by a miniature fiber optic probe in rats that were exposed to a blast. In the same publication, the limitations to the use of the probe have been indicated which include a risk of infection due to prolonged implantation of the probe. These studies were limited to 3 days owing to a limited applicability of the pressure sensing probe. Our ICP implant can be an excellent replacement for these probes for a number of reasons. Firstly, it is a completely implantable system with no open incision which reduces the risk of getting infected. Secondly, studies can be conducted for a longer duration of time. Thirdly, experiments could be conducted on larger animal models that can better relate to humans than rats. In addition, this is a tether-less system, thus adding to an overall ease of the experimental procedure.

List of References

[1] B. Mokri , “The Monro-Kellie hypothesis,” *Historical Neurology,* vol. 56, pp. 1746-1748, February 2001.

[2] N. Lundberg, “The saga of Monro-Kellie doctrine in intracranial pressure,” *Proceedings of the fifth International Symposium on Intracranial Pressure*, May-June 1982, Tokyo, Japan.

[3] F. W. Stahnisch, “Instrument transfer as knowledge transfer in neurophysiology: Francois Magendie's (1783-1855) early attempts to measure cerebrospinal fluid pressure,” *J. History of the Neurosciences*, vol. 17, no.1 , pp. 72-99 ,January 2008

[4] D. Greitz, “Cerebrospinal fluid circulation and associated intracranial dynamics. A radiologic investigation using MR imaging and radionuclide cisternograp,” *Acta Radiol. Suppl.,* vol. 386, pp. 1-2, 1993.

[5] R. Round and J. R. Keane," The minor symptoms of increased intracranial pressure-101 patients with benign intracranial hypertension,” Neurology, vol. 38, no. 1461, 1998.

[6] A. R. Crossman and D. Neary “*Neuroanatomy*,” 2nd ed, Edinburg, NY: Churchill Livingstone, 1995.

[7] Marieb, “*Human Anatomy and Physiology,”* 5th ed., San Francisco: Benjamin Cummings, 2001.

[8] W. E. Ganong, “*Review of Medical Physiology*,” 17th ed., Norwalk, Connecticut: Appleton and Lange.

[9] G. F. Fliesher, S. Ludwig, and B. K. Silverman, “*Synopsis of Pediatric Emergency Medicine,”* Rev. ed., Philadelphia, PA: Lippincott Williams & Wilkins, 2002, pp. 475.

[10] A. R. Tunkel and W.M. Scheld, “Pathogenesis and pathophysiology of bacterial meningitis,” *Clin. Microbiol. Rev.*, vol. 6, pp. 118-136, 1993.

[11] M. Shakeri, P. Vahedi, and I. Lotfinia, “A review of hydrocephalus history, etiologies, diagnosis, and treatment,” *Neurosurg. Quarterly*, vol. 18, no. 3, pp. 216-220.

[12] J. Punt, P. H. Schurr, and C. E. Polkey, " Principles of CSF diversion and alternative treatment," In: , eds. Hydrocephalus, New York: Oxford, 1993, pp. 139-160.

[13] R. Katzman, "Low pressure hydrocephaly*,"* In: Wells CE, ed. Dementia. Philadelphia: F. A. Davis, 1997.

[14] W. R. Gowers, "*A Manual of Diseases of the Nervous System*," Philadelphia: P. Blakiston, Son & Co, 1895.

[15] R. D. Adams, C. M. Fisher, S. Hakim, et al, "Symptomatic occult hydrocephalus with normal cerebrospinal fluid pressure. A treatable syndrome," *N Engl. J. Med.*, vol. 273, pp. 117–126, 1965.

[16] M. S. Huckman, "Normal pressure hydrocephalus; evaluation of diagnostic and prognostic tests," *Am. J. Neuroradiol.,* vol. 2, pp. 385-395, 1981.

[17] J. L. Antunes, K. M. Louis, and S. R. Granti, "Colloid cysts of the third ventricle," *Neurosurg.*, vol. 7, pp. 450-455, 1980.

[18] P. C. Ferrera, and L. E. Kass**, "**Third ventricle colloid cyst," *Am. J. Emer. Med*., vol.15, no. 2, March 1997.

[19] A. C. Mamourian, L. D. Cromwell, and R. E. Harbaugh, **"**Colloid cyst of the third ventricle: sometimes more conspicuous on CT than MR**,"** *Am. J. Neuroradiol.,* vol. 19, pp. 875–878, May 1998.

[20] R. G. Geocadin, P. N. Varelas , D. Rigamonti, and M. A. Williams, "Continuous intracranial pressure monitoring via the shunt reservoir to assess suspected shunt malfunction in adults with hydrocephalus," *Neurosurg. Focus*, vol. 22, no.4:E10, 2007.

[21] D. J. Bohn, W.D. Biggar, C.R. Smith, A.W. Conn, and G.A. Barker, "Influence of hypothermia, barbiturate therapy, and intracranial pressure monitoring on morbidity and mortality after near-drowning," *Crit. Care Med.*, vol.14, no.6, pp. 529-34, 1986.

[22] C. S Chi, K. L. Law, T. T.Wong , G. Y. Su,and N. Lin "Continuous monitoring of intracranial pressure in Reye's syndrome--5 years experience," *Acta Paediatr. J.,* vol. 32, no. 4, pp. 426-434, 1990.

[23] K. Nakanishi, H. Hirasawa, S. Oda, et al, ”Intracranial pressure monitoring in patients with fulminant hepatic failure treated with plasma exchange and continuous hemodiafiltration,” *Blood Purif.*, vol. 23, no. 2, pp. 113-118, 2005.

[24] C. Hamani, M. V. Zanetti, F. C. Pinto, A. F. Andrade, O. Ciquini, Jr., and R. Marino, Jr., “Intraventricular pressure monitoring in patients with thalamic and ganglionic hemorrhages,” *Arq Neuropsiquiatr*; vol. 61, no. 2B, pp. 376-380, 2003.

[25] Y. Carvi, M. Nievas, S. Toktamis, H. G.Hollerhage, and E. Haas, “Hyperacute measurement of brain-tissue oxygen, carbon dioxide, pH, and intracranial pressure before, during, and after cerebral angiography in patients with aneurysmatic subarachnoid hemorrhage in poor condition,” *Surg. Neuro.l*, vol. 64, no. 4, pp. 362-367, discussion 7, 2005.

[26] A. Valentin ,T. Lang , R. Karnik, H. P. Ammerer, J. Ploder, and J, Slany, “Intracranial pressure monitoring and case mix-adjusted mortality in intracranial hemorrhage,” *Crit. Care Med.* , vol.31, no. 5, pp.1539-1542, 2003.

[27] K. D. Petersen, U. Landsfeldt, G. E. Cold, et al, “Intracranial pressure and cerebral hemodynamic in patients with cerebral tumors: a randomized prospective study of patients subjected to craniotomy in propofol-fentanyl, isoflurane-fentanyl, or sevoflurane-fentanyl anesthesia,” *Anesthesiology*, vol. 98, no. 2, pp. 329-336, 2003.

[28] Y. C. Chen, L. M. Tang, C.J. Chen, S. M. Jung, and S. T. Chen, “Intracranial hypertension as an initial manifestation of spinal neuroectodermal tumor,”*Clinical Neurol. and Neurosurg.,* vol. 109, no. 5, pp. 408 - 411, 2005.

[29] R. V. Patwardhan and A. Nanda, “Implanted ventricular shunts in the United States: the billion-dollar-a-year cost of hydrocephalus treatment,” *Neurosurg.* ,vol. 56, no. 1, pp. 139-144; discussion 44-5, 2005.

[30] A. Pacult, “Cerebral aneurysms, subarachnoid hemorrhage: an overview of incidence, location, presentation, diagnosis and therapy,” *J S C Med. Assoc*, vol. 90, no. 1, pp. 6-10, 1994.

[31] J. D. Sussman, N. Sarkies, and J. D. Pickard, “Benign intracranial hypertension. Pseudotumour cerebri: idiopathic intracranial hypertension,” *Adv. Tech. Stand. Neurosurg.*, vol. 24, pp. 261-305, 1998.

[32] M. Biaha, D. Lazar, “Traumatic brain injury and haemorrhagic complications after intracranial pressure monitoring,” J. *Neurol. Neurosurg. Psychaitr.* , vol. 76, pp. 147, 2005.

[33] "Traumatic Brain Injury in the United States, Emergency Department Visits, Hospitalizations and Deaths," Center for Disease Control, Figure 1, pg. 7, 2006.

[34] D. Warden, "Military TBI during the Iraq and Afghanistan wars," *J. Head Trauma Rehabil.,* vol. 21, no. 5, pp. 398-402, August 23, 2006.

[35] E. Singer, "Brain Trauma in Iraq," *Technology Review*, April/May 2008.

[36] A. Rosen, M. A. Stuchly, and A. Vander Vorst, "Applications of RF/Microwave in medicine," *IEEE Trans. Microwave Theory and Tech.*, vol. 50, no. 3, pp. 963-974, March 2002.

[37] R. W. Y. Habash, and H. T. Alhafid, "Key developments in therapeutic applications of RF/Microwaves," *Int. J. Sci. Res.,* vol. 16, pp. 451-455, 2006.

[38] A. Vander Vorst, A. Rosen, and Y. Kotsuka*, RF/Microwave Interaction with Biological Tissues*, Hoboken, New Jersey: Wiley, 2006.

[39] R. Schlierf, U. Horst, M. Ruhl, T. Schmitz-Rode, W. Mokwa, and U. Schnakenberg, "A fast telemetric pressure and temperature sensor system for medical applications," *J. Micromech. Microeng.,* vol. 17, pp. S98-S102, 2007.

[40] J. Kim, and Y. Rahmat-Samii, "Implanted antenna inside a human body: simulations, designs, and characterizations," *IEEE Trans. Microwave Theory and Tech.*, vol. 52, no. 8, pp. 1934-1943, August 2004.

[41] A. Y. Poon, S. O'Driscoll, and T. H. Meng. "Optimal operating frequency in wireless power transmission for implantable devices," P*roceedings of the 29th Annu. Intl. Conf. IEEE EMBS*, pp. 5673-5678, August 2007.

[42] K. Gosalia, G. Lazzi, and M. Humayun, "Investigation of a microwave data telemetry link for a retinal prosthesis," *IEEE Trans. Microwave Theory and Tech.*, vol. 52, no. 8, pp. 1925-1933, August 2004.

[43] O.B-Lubecke and V.M.Lubecke, "Wireless house calls: using communications technology for health care and monitoring," *IEEE Microwave Mag.*, vol. 3, no. 3, pp. 43-48, September 2002.

[44] J. Schepps, and A. Rosen, "Microwave industry outlook- wireless communications in health care," *IEEE Trans. Microwave Theory and Tech.,* vol. 50, no. 3, pp. 1044-1045, March 2002.

[45] Y. H. Lin, I-C. Jan, P. C-I Ko, Y-Y. Chen, J-M. Wong, and G-J. Jan, "A wireless PDA-based patient monitoring system for patient transport," *IEEE Trans. Information Tech. in Biomed*., vol. 8, no. 4, pp. 440-447, December 2004.

[46] C. S. Pattichis, E. Kyriaccou, S. Voskarides, M. S. Pattichis, R. Istepanian, and C. N. Schizas, "Wireless telemedicine system: an overview," *IEEE Antennas Propag. Mag.,* vol. 44, pp. 143-153, April 2002.

[47] A. DeHennis and K. D. Wise, "A double-sided single-chip wireless pressure sensor," *Digest of IEEE Conference on MicroElectroMech. Sys.,* pp. 252-255, Jan. 2002.

[48] R. N. Simons, D. G. Hall, and F. A. Miranda, "RF telemetry system for an implantable bio-MEMS sensor," *Digest of 2004 IEEE International Microwave Symposium*, vol. 3, pp. 1433–1436, June 6–11, 2004, Fort Worth, TX.

[49] P. Marik, K. Chen, J. Varon, R. Fromm, Jr., and G. L. Sternbach, "Management of increased intracranial pressure: A review for clinicians," *The J. Emergency Medicine*, vol. 17, no. 4, pp. 711-719, 1999.

[50] D. P. Becker, J. D. Miller, and J. D. Ward, "The outcome from severe head injury with early diagnosis and intensive management," *J. Neurosurg.,* vol. 49, pp. 491-502, 1977.

[51] J. D. Miller, J. F. Butterworth, S. K. Gudeman, J. E. Faulkner, S. C. Choi, J. B. Selhorst, J. W. Harbinson, H. Lutz, H. F. Young, and D. P. Becker, "Further experience in the management of severe head injury," *J. Neurosurg.*, vol. 54, pp. 289-299, 1981.

[52] J.A. Boockvar, W. Loudon, and L.N. Sutton, "Development of the Spitz-Holter Valve in Philadelphia," *J. Neurosurg.*, vol. 95, pp. 145-147, 2001.

[53] K. B. Sahay, R. Mehrotra, U. Sachdeva, and A. K. Banerji, "Relation between epidural and ventricular pressures in canine brain: an experimental study," *J. Neurosurg.*, vol. 5, no. 4, pp. 379-386, 1991.

[54] M. Brock, and N. H. Ishii, *ICP Revisited.* Tokyo: Springer-Verlag, pp. 3-7, 1983.

[55] J. M. Bland and D. G. Altman, "Statistical methods for assessing agreement between two methods of clinical measurement", *The Lancet*, vol. 327, no. 8476, pp. 307-310, February 1986.

[56] M. P. Powell and H. A. Crockard, "Behavior of an extradural pressure monitor in clinical use. Comparison of extradural with intraventricular pressure in patients with acute and chronically raised intracranial pressure," *J. Neurosurg.*, vol. 63, pp. 745-749, 1985.

[57] A. Raabe, R. Totzauer, O. Meyer, R. Stockel, D. Hohrien, and J. Schoche, "Reliability of epidural pressure measurement in clinical practice: behavior of three modern sensors during simultaneous ipsilateral intraventricular or intraparenchymal pressure measurement," *Neurosurg. Online*, vol. 43, no. 2, pp. 306-311, August 1998.

[58] H. Nornes, and F. Serk-Hansen, "Simultaneous recording of the ventricular fluid pressure and the epidural pressure," *Euro. Neurol.*, vol. 7, pp.364-372, 1972.

[59] W. D. Newman, A. S. Hollman, G. N. Dutton, and R. Carachi, "Measurement of optic nerve sheath diameter by ultrasound: a means of detecting acute raised intracranial pressure in hydrocephalus," *British J. Opthalmology*, vol. 86, pp. 1109-1113, 2002.

[60] L. Lin, G. Li, S. Xiang, and J. Sun, "Research on non-invasive intracranial pressure measurement using near-infrared light, " in *Proceedings of SPIE*, vol. 4916, 2002.

[61] G.C. Steinbach, W.T. Yost, B. Macias, J. Iyengar, T. Nguyen, D. O'Leary, J. H. Cantrell, and A. R. Hargens, "Noninvasive intracranial diameter/pressure measurements using ultrasounds: in-vitro characterization and in-vivo application during 30 days bedrest," *Bioastronautics Investigators' Workshop*, Division of Space Life Sciences, Universities Space Research Association, January 17-19, 2001,Galveston,TX. [Online] Available: http://www.dsls.usra.edu/meetings/bio2001/pdf/151p.pdf

[62] T. Ueno, B.R. Macias, and A. R. Hargens, "Pulsed phase lock loop technique to measure intracranial pressure non-invasively," *Proceeding of 2003 IEEE Ultrasonics Symposium*, Honolulu, October 5-8.

[63] J. H. Piatt Jr, "Clinical recognition of CSF shunt failure," *American Academy of Pediatricians Grand Rounds*, vol. 5, no. 6, pp. 56-58, June 2001.

[64] J. S. Crutchfield, R. K Narayan, C. S. Robertson, and L.H. Michael, "Evaluation of fiberoptic intracranial pressure monitor," *J. Neurosurg.*, vol. 72, pp. 482-487, 1990.

[65] M. Gelabert-Gonzales, V. Ginesta-Galan, R. Sernamito-Garcia, A. G. Allut, J. Bandin-Dieguez, and R. M. Rumbo, "The Camino intracranial pressure device in clinical practice. Assessment in a 1000 cases," *Acta Neurochirurgica*, vol. 148, pp. 435-441, 2006.

[66] R. C. Ostrup, T. G. Luerssen, L. F. arshall, and M. H. Zornow, "Continuous monitoring of intracranial pressure with a miniaturized fiberoptic device," *J. Neurosurg.*, vol. 67, pp. 206-209, 1987.

[67] N. Bruder, P. N'Zoghe, N. Graziani, D. Pelissier, F. Grisoli, and G. Francois, "A comparison of extradural and intraparenchymatous intracranial pressures in head injured patients," *Intensive Care Medicine*, vol. 21, no. 10, pp. 850-852, 1995.

[68] Catalog of Integra Life Sciences products, pp.13, NJ. [Online] Available: www.integra-ls.com/PDFs/catalogs/NeuromonitoringCatalog.pdf

[69] NIH Technology Assessment Conference on implants, 10-12 January 2000, Bethesda, MD.

[70] J.R. Davis, *Handbook of materials for medical devices*, Materials Park, OH: ASM International, c2003.

[71] ASTM F732-82, "Reciprocating pin-on-flat evaluation of friction and wear properties of polymeric materials for use in total joint prosthesis", in: *Annual book of ASTM standards*, *Medical Devices and Services*, Section 13, ASTM International, Philadelphia, PA, 1997, pp. 227-232.

[72] D. C. Mears, "Metals in medicine and surgery," *Int. Met.. Rev.* , vol. 22, pp. 119-155, June 1977.

[73] J. M. Courtney and T. Gilchrist, "Silicone rubber and natural rubber as biomaterials," *Med. Biol. Eng. Comput.* , vol. 18, pp. 538-540, 1980.

[74] D. C. Smith, B. D. Ratner, A. S. Hoffman, and J. E. Lemons, "Adhesives and sealants,"in: *Biomaterials science: an introduction to materials in medicine*, 2nd ed. , NY: Academic Press, 1996.

[75] G.W. Ritter, "Using adhesives effectively in medical devices," *Med. Dev. Diagnost. Ind*., pp. 52, Nov 2000.

[76] L. Woglemuth, "Assessing the performance and sustainability of Parylene coating," *Med. Dev. Diagnost. Ind.*, pp. 42, Aug 2000.

[77] P. Chen, D. C. Rodger, S. Saati, M. S. Humayun, and Y. Tai, "Microfabricated implantable Parylene-based wireless passive intraocular pressure sensors," *J. Microelectromech. Sys.,* vol. 17, no. 6, pp. 1342-1351, December 2008.

[78] R.C. Wasielewski, D. G. Galat, and R. D. Komistek, "An intra-operative pressure measuring device used in total knee arthoplasties and its kinematic correlations," *Clinical Orthopedics and Related Res.*, no. 427, pp. 171-178, 2002.

[79] D. J. Edell, J. Kuzma, and D. Petratitis, "Implantable electronic systems of tomorrow," *Proceedings of the 18th Annual International Conference of the IEEE EMBS*, M9: Minisymposium, 1996, Amsterdam.

[80] H. Lee, and J. Cho, "Development of conformal PDMS and Parylene coatings for microelectronics and MEMS packaging," *Proceedings of ASME International Mechanical Engineering Congress and Exposition*, November 5-11, 2005, Orlando, FL.

[81] R. Cooper and A. Hulme, "Intracranial pressure and related phenomena during sleep," *J. Neurol. Neurosurg. Psychiat.*, vol. 92, no. 6, pp. 564-570, 1966.

[82] Report number ANSI/AAMI NS28:1998/(R), 1993.

[83] A. J. Jacobs-Cook, "MEMS versus MOMS from a systems point of view," *J. Micromech. Microeng.* vol. 6, pp. 148-156, 1996.

[84] Datasheet SCB10H series 1.2 Bar capacitive pressure sensor, VTI Technologies, Finland.

[85] M. R. Tofighi, U. Kawoos, F. A. Kralick, and A. Rosen, "Wireless intracranial pressure monitoring through scalp at microwave frequencies; preliminary animal study," *Digest of 2006 IEEE International Microwave Symposium*, June 2006.

[86] M. R. Tofighi, U. Kawoos, S. Neff, and A. Rosen, "Wireless intracranial pressure monitoring through scalp at microwave frequencies," *Elec. Letteres*, vol. 42, no. 3, pp. 148-150, Feb. 2006.

[87] R. Warty, M. R. Tofighi, U. Kawoos, and A. Rosen, "Characterization of implantable antennas: reflection by and transmission through a scalp phantom," *IEEE Trans. Microwave Theory Tech.*, vol. 56, no. 10, pp. 2366-2376, October 2008.

[88] R. V. Warty, "ISM-band antenna scattering from scalp phantom for intracranial pressure monitoring implants," Drexel University, Philadelphia, PA, December 2007.

[89] U. Kawoos, M. R.Tofighi, R. Warty, F. A. Kralick, and A. Rosen, "*In-vitro* and *in-vivo* trans-scalp evaluation of intracranial pressure monitoring implant at 2.4 GHz," *IEEE Trans. Microwave Theory Tech.*, vol. 56, no. 10, pp. 2356-2365, October 2008.

[90] P.S. Neelkanta, "*Handbook of Electromagnetic Materials: Monolithic and Composite Versions and Their Applications*", New York: CRC Press, 1995, pp. 65-68.

[91] T. Stieglitz, M. Schuetter, and K.P. Koch, "Implantable biomedical microsystems for neural prosthesis," *IEEE Engineering in Medicine and Biology Mag.,* vol. 24, no. 5, pp. 58-65, Sep.-Oct. 2005.

[92] P. Kramer, A. K. Sharma, E. E. Hennecke, and H. Yasuda, "Polymerization of para-xylylene derivatives (parylene polymerization) and deposition kinetics for Parylene N and Parylene C″. *J Polymer Science: Polymer Chemistry,* Edition 22, no. 2, pp. 475–491, 2003.

[93] D. Andreuccetti, M. Bini, A. Ignesti, R. Olmi, N. Rubino, and R. Vanni, 'Use of polyacrylamide as a tissue-equivalent material in the microwave range', *IEEE Trans. Biomed. Eng.*, vol. 35, no. BME-4, pp. 275–277, 1998.

[94] M. G. Bini, A. Ignesti, L. Milanta, "Polyacrylamide for electromagnetic hyperthermia studies", *IEEE Trans. of Biomed. Eng.*, vol. BME-31, no. 3, March 1984.

[95] A. W. Guy, "Analysis of electromagnetic field induced in biological tissues by thermographic studies on equivalent phantom models," *IEEE Trans. on Microwave Theory Tech.*, vol. 5, pp.205-215, Feb 1971.

[96] S. Oh, and C. M. Collins ,"Specific absorption rate mapping using MR thermometry in a transmit-receive head coil at 3.0T," *Proceedings of the 16th International Society for Magnetic Resonance in Medicine,* pp. 79, 2008, Toronto, Canada.

[97] S. Oh, U. Kawoos, M. R. Tofighi, A. Rosen, and C. M. Collins, "Current challenges for creating a wireless MR-compatible intracranial pressure monitor," *International Society for Magnetic Resonance in Medicine, 17th Scientific Meeting and Exhibition,* pp. 310, 2009, Hawaii, USA.

[98] Lide *et al.* "86th CRC handbook of chemistry and physics", CRC, 2006.

[99] P. Vodicka , K. Smetana Jr, B. Dvoránková, T. Emerick, Y. Z. Xu, J. Ourednik, V. Ourednik , Motlí, "Miniature pig as an animal model in biomedical research," *Ann. N Y Acad. Sci*., no. 1049, pp. 161-171, May 2005.

[100] G. A. Simon and H. I. Maibach, "The Pig as an experimental animal model of percutaneous permeation in man: qualitative and quantitative observations - an overview," *J. Pharmocological and Biophysiological Research*, vol. 13, no. 5, pp. 229-234, 2000.

[101] J. F. O'Malley, "Evolution of the nasal cavities and sinuses in relation to function," *J. Laryngology & Otology*, vol. 39, pp. 57-64, 1924.

[102] H. Shimazu, H. Ito, T. Hashimoto, K. Yamakoshi, M. Gondoh, T. Tamai, S. Nakamura, and I. Ohtaka, "Collapsing technique- The indirect measurement of intracranial pressure," *Proceedings of the 12th Annual International Conference of the IEEE Engineering in Medicine and Biology Society*, November 1-4, 1990, Philadelphia, PA.

[103] A. B. Butler, J. D. Rosenthal, N. H. Bass, and R. N. Johnson, "Multiport device for the assessment of cerebrospinal fluid dynamics under conditions of elevated intracranial pressure in man and experimental animals," *Medical and Biological Engineering and Computing*, vol. 16, no. 5, pp. 601-602, September 1978.

[104] J. S. Kroin, R. J. McCarthy, L. Stylos, K. Miesel, A. D Ivankovich, and R. D. Penn, "Long-term testing of an intracranial monitoring device," *J. Neurosurg.,* vol. 93, pp. 852-858, 2000.

[105] K.B. Sahay, R. Mehrotra, U. Sachdeva, and A.K. Banerji, "Relation between epidural and ventricular pressures in canine brain: an experimental study," *British J. Neurosurg.*, vol. 5, pp. 379-386, 1991.

[106] M. D. Mann, D. A. Crouse, and E. D. Prentice, "Appropriate animal numbers in biomedical research in light of animal welfare consideration," *Lab. Animal Sci.*, vol. 41, no. 1, January 1991.

[107] D. A. Crouse, M. D. Mann, and E. D. Prentice, "The logical determination of N in animal experimentation," *Current Issues and New Frontiers in Animal Research: Proceedings of the Conference sponsored by the Scientists Center for Animal Welfare*, University of Texas Health Science Center at San Antonio in Texas, December 8-9, 1994.

[108] H. J. Khamis, "Statistics and the issue of animal numbers in research," *Contemporary Topics in Laboratory Animal Science*, vol. 56, no. 2, March 1997.

[109] J. Cohen, *Statistical Power Analysis for the Behavioral Sciences*, 2nd Ed., Hillsdale, NJ: LEA Publishers, 1988.

[110] B. D. Ratner, “Reducing capsular thickness and enhancing angiogenisis around implant drug release system,” *J. Controlled Release*, vol. 78, pp. 211-218, 2002.

[111] R. Van Noort, T.R. Martin and M.M. Black, "The mechanical properties of human dura mater and the effects of storage media," *Clin. Phys. Physiol. Meas.*, vol. 2, no. 3, pp. 197–203, 1981.

[112] W.Y. Sayad, S.C. Harvey, and C. Samuel, "Regeneration of the Meninges: Dura Mater," *Ann Surg*, vol. 77, no. 2, pp. 129–142, 1923.

[113] T. Lodygowski, W. Kakol, and M. Wierszycki, “Three-dimensional nonlinear finite element model of human lumbar spine segment,” *Acta of Bioeng. and Biomech.,* vol. 7, no. 2, 2005.

[114] M. G. Dunn and F. H. Silver, “Viscoelastic behavior of human connective tissues: relative contributions of viscous and elastic components,” *Connective Tissue Res.*, vol. 12, pp. 50-07, 1983.

[115] L. Voo, S. Kumaresan, F. A. Pintar, N. Yoganandan, and A. Sances, Jr. , “ Finite-element models of the human head,” *Med. and Biol. Eng. and Computing*, pp. 375-381, September 1996.

[116] C.C. Ward, “Finite element models of head and their use in brain injury,” *Proceedings of the 26th Strap Car Crash Conf. Society of Automotive Engineers,* pp. 71-85, 1982*,* Ann Arbor, Michigan,.

[117] Y. Zhang, D. B. Goldgof, S. Sarkar, and L. V. Tsap. “A modeling approach for burn scar assessment using natural features and elastic property,” *IEEE Trans. Medical Imaging*, vol. 23, 2004.

[118] N. Inou, K. Michihiko, and K. Maki, "Patient specific finite element modeling of human skull," *Advances in Sci. and Tech*., vol. 49, pp. 227-234, 2006.

[119] K. A. Miesel, and L. Stylos, “Intracranial monitoring and therapy delivery control device, system and method,” *Patent no.* 6,248,080 B1*,* June 19, 2001.

[120] W. h. Ko, and A. M. Leung, “Pressure telemetry implant,” *Patent no*. 4,519,401, May 1985.

[121] M. N. Ericson, T. E. McKnight, S. F. Smith, and J. O. Hylton, "Implantable device and in-vivo intracranial and cerebrospinal fluid pressure monitoring," Patent no. 6,533,733, March 18, 2003.

[122] C. A. Rich, Y. Zhang, N. Najafi, M. Z. Straayer, and S. Massoud-Ansari, "Wireless MEMS capacitive sensor for physiological parameter measurement," *Patent no*. 6,926,670 B2, August 9, 2005.

[123] G. L. Kenausis and J. Voros, "Poly(L-lysine)-g-Poly (ethylene glycol) layers on metal oxide surfaces: Attachment mechanism and effects of polymer architecture on resistance to protein adsorption," *J. Phys. Chem B,* vol. 104, pp. 3298-3309, 2000.

[124] P.H. Gutin, W. M. Klemme, R. L. Lagger, A. R. MacKay, L. H. Pitts, and Y. Hosobuchi, "Management of the unresectable cystic craniopharyngioma by aspiration through an Ommaya reservoir drainage system," *J. Neurosurg.,* vol. 52, no. 1, pp. 36-40, January 1980.

[125] M. Emam, Y. Abashiya, B. Chareunsack, J. Skordos, J. Oh, Y. Choi, F. Kralick, and H. Noh, "A novel microdevice for the treatment of hydrocephalus: design and fabrication of an array of microvalves and microneedles,"*J. Microsys Tech,* vol. 14, no. 3, pp. 371-378, March 2008.

[126] M. Chavko, W. A. Koller, W. K. Prusaczyk, R. M. McCarron, "Measurement of blast wave by a miniature fiber optic pressure transducer in the rat brain," *J. Neurosc. Meth.,* vol. 159, pp. 277-281, July 2007

Appendix A: List of Acronyms

ANSI: American National Standard Institute

CMOS: Complementary Metal Oxide Semiconductor

CNS: Central Nervous System

CSF: Cerebrospinal Fluid

CT: Computer Tomography

ED: Epidural

EIRP: Effective Isotropic Radiated Power

ERP: Effective Radiated Power

FCC: Federal Communications Commission

FDA: Food and Drug Administration

FFT: Fast Fourier Transform

GRE: Gradient Echo

IACUC: Institutional Animal Care and Use Committee

ICH: Intracranial Hypertension

ICP: Intracranial Pressure

ICU: Intensive Care Unit

ISM: Industrial Scientific Medical

MRI: Magnetic Resonance Imaging

MEMS: Micro Electro Mechanical Systems

NIH: National Institutes of Health

NIRS: Near-Infrared Spectroscopy

PEG: Poly Ethylene Glycol

PIFA: Planar Inverted-F Antenna

PTSD: Post Traumatic Stress Disorder

PZR: Piezoresistive

RF: Radio Frequency

SAR: Specific Absorption Rate

SAS: Sub-arachnoid Space

SD: Sub-dural

SE: Spin Echo

VCO: Voltage Controlled Oscillator

Vita

Usmah Kawoos

Education

Ph.D., Biomedical Engineering, Drexel University, June 2009.
M.S., Biomedical Engineering, Drexel University, June 2007.
B.E., Medical Electronics, Vishveshwariah Technological University, India, July 2002.

Professional experiences

Ph.D. Research Assistant, Drexel University. (November 2004 - June 2009).
Teaching Assistant, Department of Physics, Drexel University, (September 2004 - June 2006).
Graduate Teaching Assistant, School of biomedical Engineering, Drexel University, (January 2007- March 2008).

Honors

IEEE MTT Fellowship for Medical Applications (2007-08).
Lee Smith Fellow at Drexel University (Academic Year 2006-07).
Recipient of Best Student Poster Award, Research Day, Drexel University College of Medicine (October 2005).
Dean's Fellow, Drexel University, (September 2003- November 2005).

Publications

1. *In progress:* **U. Kawoos**, H. Maragah, M. Tofighi, A.Rosen, "Statistical Validation of the Performance of Intracranial Pressure monitoring Implant in reference to Camino Catheters."
2. S.Oh, **U. Kawoos**, M.R. Tofighi, A. Rosen, and C. M. Collins, "Current Challenges for Creating a Wireless MR-Compatible Intracranial Pressure Monitor, " *International Society for Magnetic Resonance in Medicine, 17th Scientific Meeting and Exhibition,* Honolulu, April 2009.
3. ***Invited Paper*: U. Kawoos**, R.Warty, M. R. Tofighi, F. A. Kralick, D. Yoo, T. Neal, and A. Rosen, "Embedded Microwave System for Monitoring of Intracranial Pressure," accepted to *IEEE Radio Wireless Symposium,* January 2008.
4. **U. Kawoos**, R.Warty, M.R. Tofighi, F. A. Kralick and A.Rosen, "*In-vitro* and *in-vivo* Trans-scalp Evaluation of an Intracranial Pressure Monitoring Implant at 2.4 GHz," *IEEE Transactions on Microwave Theory and Techniques*, Vol. 56, No. 10, pp.2356-2365 , October 2008.
5. R. Warty, M. R. Tofighi, **U. Kawoos**, and A.Rosen, "Characterization of Implantable Antennas: Reflection by and Transmission through a Scalp Phantom," *IEEE Transactions on Microwave Theory and Techniques*, Vol. 56, No. 10, pp. 2366-2376, October 2008.
6. **U. Kawoos**, R. V. Warty, F. A. Kralick, M. R. Tofighi and A. Rosen. "Issues in Wireless Intracranial Pressure Monitoring at Microwave Frequencies", *Progress in Electromagnetic Research Symposium,* 2007.

7. M. R. Tofighi, **U. Kawoos**, F. A. Kralick, and A. Rosen, "Wireless Intracranial Pressure Monitoring Through Scalp at Microwave Frequencies; Preliminary Animal Study," *Digest of 2006 IEEE International Microwave Symposium*, pp. 1738-1741, June 2006.
8. M. R. Tofighi, **U. Kawoos**, S. Neff, and A. Rosen, "Wireless Interacranial Pressure Monitoring Through Scalp at Microwave Frequencies," *Electronics Letteres*, Vol. 42, No. 3, pp. 148-150, Feb. 2006.
9. **U. Kawoos**, M. R. Tofighi, S. Neff, and A. Rosen. **"**A Permanently Implantable Intracranial Pressure Monitor", Abstract published in the digest of *Biomedical Engineering Society, BMES 2005 Annual Fall Meeting*, MD, September 2005.
10. **U. Kawoos**, G. K. Mugalodi, M. R. Tofighi, S. Neff, and A. Rosen. **"**A Permanently Implantable Intracranial Pressure Monitor" *Proceedings of the IEEE 31st Annual Northeast Bioengineering Conference,* pp. 17–19, April 2005.